Dynamics

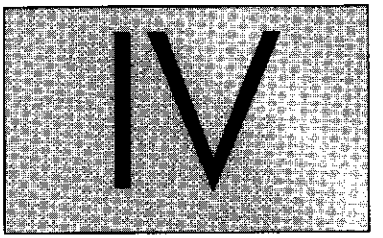

This page is intentionally left blank

Unentangled polymer dynamics

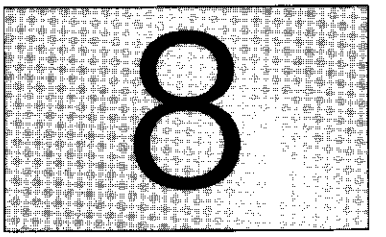

A small colloidal particle in any liquid diffuses due to the fluctuations of the number of molecules hitting it randomly from different directions. Colloidal particles are significantly larger than the molecules in the liquid, but small enough that collisions with molecules noticeably move the particle.[1] The trajectory of the particle, shown in Fig. 8.1, is another example of a random walk. The three-dimensional mean-square displacement of the colloidal particle during time t is proportional to t, with the coefficient of proportionality related to the **diffusion coefficient** D:

$$\langle[\vec{r}(t) - \vec{r}(0)]^2\rangle = 6Dt. \tag{8.1}$$

The average distance the particle has moved is proportional to the square root of time:

$$\langle[\vec{r}(t) - \vec{r}(0)]^2\rangle^{1/2} = (6Dt)^{1/2}. \tag{8.2}$$

Whereas the motion of the particle obeys Eq. (8.1) at all times, we shall see that the motion of monomers in a polymer is not always described by Eq. (8.1) [or Eq. (8.2)]. When the motion of a molecule obeys Eq. (8.1), it is called a simple **diffusive motion**. The random motion of small particles in a liquid was observed long ago using a microscope by a biologist named Brown and is often referred to as **Brownian motion**.

If a constant force $\vec{f}$ is applied to a small particle, pulling it through a liquid, the particle will achieve a constant velocity $\vec{v}$ in the same direction as the applied force. For a given particle and a given liquid, the coefficient relating force and velocity is the **friction coefficient** ζ:

$$\vec{f} = \zeta\vec{v}. \tag{8.3}$$

Since the constant force acting on the particle results in a constant velocity, there must be an equal and opposite viscous drag force of the liquid acting on the particle with magnitude ζv. The diffusion coefficient D and the friction coefficient ζ are related through the **Einstein relation**:

$$D = \frac{kT}{\zeta}. \tag{8.4}$$

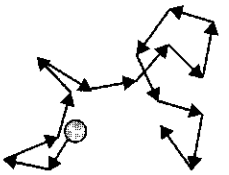

Fig. 8.1
Motion of a particle in a liquid is a random walk that results from random collisions with molecules in the liquid.

[1] Colloidal particles have sizes between 1 nm and 10 μm.

The physics behind this relation is the fluctuation–dissipation theorem: the same random kicks of the surrounding molecules cause both Brownian diffusion and the viscous dissipation leading to the frictional force. It is instructive to calculate the time scale τ required for the particle to move a distance of order of its own size R:

$$\tau \approx \frac{R^2}{D} \approx \frac{R^2 \zeta}{kT}. \tag{8.5}$$

The time scale for diffusive motion is proportional to the friction coefficient.

The mechanical properties of a liquid are fundamentally different from the solids discussed in Chapter 7. Solids have stress proportional to deformation (for small deformations). However, the stress in liquids depends only on the rate of deformation, not the total amount of deformation. If we pour water from one bucket into another bucket, there is only resistance during the flow, but there is no shear stress in the water in either bucket at rest. We describe the deformation rate of a liquid in shear by the shear rate $\dot{\gamma} = \mathrm{d}\gamma/\mathrm{d}t$ [Eq. (7.99)]. For the steady simple shear flow of Fig. 7.23, the shear rate is the same everywhere, equal to the way in which velocity changes with vertical position. The stress σ in a Newtonian liquid is proportional to this shear rate [Newton's law of viscosity Eq. (7.100), $\sigma = \eta\dot{\gamma}$], with the viscosity η being the coefficient of proportionality.

If a sphere of radius R moves in a Newtonian liquid of viscosity η, a simple dimensional argument can determine the friction coefficient of the sphere. The friction should depend only on the viscosity of the surrounding liquid and the sphere size:

$$\zeta(\eta, R). \tag{8.6}$$

The friction coefficient is the ratio of force and velocity, with units of $\mathrm{kg\,s^{-1}}$. The viscosity is the ratio of stress and shear rate, with units of $\mathrm{kg\,m^{-1}s^{-1}}$ and the sphere radius has units of length (m). The only functional form that is dimensionally correct gives a very simple relation:

$$\zeta \approx \eta R. \tag{8.7}$$

The full calculation of the slow flow of a Newtonian liquid past a sphere was published by Stokes in 1880, yielding the numerical prefactor of 6π that results in **Stokes law**:

$$\zeta = 6\pi\eta R. \tag{8.8}$$

Combining Stokes law with the Einstein relation [Eq. (8.4)] gives a simple equation for the diffusion coefficient of a spherical particle in a liquid, known as the **Stokes–Einstein relation**:

$$D = \frac{kT}{6\pi\eta R}. \tag{8.9}$$

This important relation is used to determine coil size from measured diffusion coefficient (for example, by dynamic light scattering—see Section 8.9, or by pulsed-field gradient NMR). The size determined from a measurement of diffusion coefficient is the **hydrodynamic radius**:

$$R_h \equiv \frac{kT}{6\pi\eta D}. \tag{8.10}$$

8.1 Rouse model

The first successful molecular model of polymer dynamics was developed by Rouse. The chain in the Rouse model is represented as N beads connected by springs of root-mean-square size b, as shown in Fig. 8.2. The beads in the Rouse model only interact with each other through the connecting springs. Each bead is characterized by its own independent friction with friction coefficient ζ. Solvent is assumed to be freely draining through the chain as it moves.

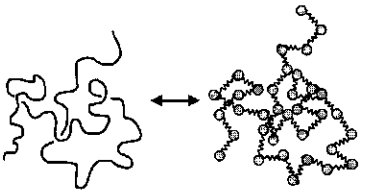

Fig. 8.2
In the Rouse model, a chain of N monomers is mapped onto a bead–spring chain of N beads connected by springs.

The total friction coefficient of the whole Rouse chain is the sum of the contributions of each of the N beads:

$$\zeta_R = N\zeta. \tag{8.11}$$

The viscous frictional force the chain experiences if it is pulled with velocity $\vec{v}$ is $\vec{f} = -N\zeta\vec{v}$. The diffusion coefficient of the Rouse chain is obtained from the Einstein relation [Eq. (8.4)].

$$D_R = \frac{kT}{\zeta_R} = \frac{kT}{N\zeta}. \tag{8.12}$$

The polymer diffuses a distance of the order of its size during a characteristic time, called the **Rouse time**, τ_R:

$$\tau_R \approx \frac{R^2}{D_R} \approx \frac{R^2}{kT/(N\zeta)} = \frac{\zeta}{kT} NR^2. \tag{8.13}$$

The Rouse time has special significance. On time scales shorter than the Rouse time, the chain exhibits viscoelastic modes that shall be described in Section 8.4. However, on time scales longer than the Rouse time, the motion of the chain is simply diffusive.

Polymers are fractal objects, with size related to the number of monomers in the chain[2] by a power law:

$$R \approx bN^{\nu} \tag{8.14}$$

The reciprocal of the fractal dimension of the polymer (see Section 1.4) is ν. For an ideal linear chain $\nu = 1/2$ and the fractal dimension is $1/\nu = 2$. The Rouse time of such a fractal chain can be written as the product of

[2] There are $N-1$ springs in the Rouse model and, for long chains, the number of springs is approximated by N.

the time scale for motion of individual beads, the **Kuhn monomer relaxation time**

$$\tau_0 \approx \frac{\zeta b^2}{kT}, \tag{8.15}$$

and a power law in the number of monomers in the chain:

$$\tau_R \approx \frac{\zeta}{kT} NR^2 = \frac{\zeta b^2}{kT} N^{1+2\nu} \approx \tau_0 N^{1+2\nu}. \tag{8.16}$$

For an ideal linear chain, $\nu = 1/2$ and the Rouse time is proportional to the square of the number of monomers in the chain:

$$\tau_R \approx \tau_0 N^2. \tag{8.17}$$

The full calculation of the relaxation time of an ideal chain was published by Rouse in 1953, with a coefficient of $1/(6\pi^2)$:

$$\tau_R = \frac{\zeta b^2}{6\pi^2 kT} N^2. \tag{8.18}$$

This Rouse stress relaxation time is half of the end-to-end vector correlation time because stress relaxation is determined from a quadratic function of the amplitudes of normal modes (see Problem 8.36).

The time scale for motion of individual monomers τ_0, is the time scale at which a monomer would diffuse a distance of order of its size b if it were not attached to the chain. In a polymer solution with solvent viscosity η_s, each monomer's friction coefficient is given by Stokes law [Eq. (8.8)]:

$$\zeta \approx \eta_s b. \tag{8.19}$$

The monomer relaxation time τ_0 and the chain relaxation time of the Rouse model τ_R can be rewritten in terms of the solvent viscosity η_s:

$$\tau_0 \approx \frac{\eta_s b^3}{kT}, \tag{8.20}$$

$$\tau_R \approx \frac{\eta_s b^3}{kT} N^2. \tag{8.21}$$

When probed on time scales smaller than τ_0, the polymer essentially does not move and exhibits elastic response. On time scales longer than τ_R, the polymer moves diffusively and exhibits the response of a simple liquid. For intermediate time scales $\tau_0 < t < \tau_R$, the chain exhibits interesting viscoelasticity discussed in Section 8.4.1.

8.2 Zimm model

The viscous resistance imparted by the solvent when a particle moves through it arises from the fact that the particle must drag some of the surrounding solvent with it. The force acting on a solvent molecule at distance r from the particle becomes smaller as r increases, but only slowly (decaying roughly as $1/r$). This long-range force acting on solvent

(and other particles) that arises from motion of one particle is called **hydrodynamic interaction**. In the case of the bead–spring model of a polymer chain, when one bead moves, there are hydrodynamic interaction forces acting on the other beads of the chain. The Rouse model ignores hydrodynamic interaction forces, and assumes the beads only interact through the springs that connect them. We shall see later that this assumption is reasonable for polymer melts, but is not correct for a polymer in a dilute solution.

In dilute solutions, hydrodynamic interactions between the monomers in the polymer chain are strong. These hydrodynamic interactions also are strong between the monomers and the solvent within the pervaded volume of the chain. When the polymer moves, it effectively drags the solvent within its pervaded volume with it. For this reason, the best model of polymer dynamics in a dilute solution is the Zimm model, which effectively treats the pervaded volume of the chain as a solid object moving through the surrounding solvent.

Assume that the chain (and any section of the chain) drags with it the solvent in its pervaded volume. Thus the chain moves as a solid object of size $R \approx bN^{\nu}$. The friction coefficient of the chain of size R being pulled through a solvent of viscosity η_s is given by Stokes law:

$$\zeta_Z \approx \eta_s R. \tag{8.22}$$

There is a coefficient 6π in Stokes law [Eq. (8.8)] for a spherical object $\zeta = 6\pi\eta_s R$, but chains are not spheres and we drop all numerical coefficients.

From the Einstein relation [Eq. (8.4)] the diffusion coefficient of a chain in the Zimm model is reciprocally proportional to its size R:

$$D_Z = \frac{kT}{\zeta_Z} \approx \frac{kT}{\eta_s R} \approx \frac{kT}{\eta_s b N^{\nu}}. \tag{8.23}$$

This is simply the Stokes–Einstein relation [Eq. (8.9)] for a polymer in dilute solution. The Zimm model predicts that the chain diffuses as a particle with volume proportional to the chain's pervaded volume in solution. In 1956, Zimm published a full calculation, where he preaveraged the hydrodynamic interactions to obtain this result with an extra coefficient of $8/(3\sqrt{6\pi^3})$ for an ideal chain:

$$D_Z = \frac{8}{3\sqrt{6\pi^3}} \frac{kT}{\eta_s R} \cong 0.196 \frac{kT}{\eta_s R}. \tag{8.24}$$

In the Zimm model, the chain diffuses a distance of order of its own size during the **Zimm time** τ_Z:

$$\tau_Z \approx \frac{R^2}{D_Z} \approx \frac{\eta_s}{kT} R^3 \approx \frac{\eta_s b^3}{kT} N^{3\nu} \approx \tau_0 N^{3\nu}. \tag{8.25}$$

The coefficient relating the relaxation time to a power of the number of monomers in the chain is once again the monomer relaxation time τ_0

[Eq. (8.20)]. Zimm's full calculation of the chain relaxation time provides an extra coefficient of $1/\sqrt{3\pi}$ for an ideal chain:

$$\tau_Z = \frac{1}{2\sqrt{3\pi}} \frac{\eta_s}{kT} R^3 \cong 0.163 \frac{\eta_s}{kT} R^3. \tag{8.26}$$

This Zimm stress relaxation time is half of the Zimm end-to-end vector correlation time.

The Zimm time is proportional to the pervaded volume of the chain. Note that the Zimm time τ_Z has a weaker dependence on chain length than the Rouse time τ_R [Eq. (8.16)].

$$3\nu < 2\nu + 1 \quad \text{for } \nu < 1. \tag{8.27}$$

Comparison of Eqs (8.16) and (8.25) reveals that the Zimm time is shorter than the Rouse time in dilute solution. In principle, a chain in dilute solution could move a distance of order of its size by Rouse motion, by Zimm motion, or some combination of the two. The chain could simply move its monomers by Rouse motion through the solvent without dragging any of the solvent molecules with it, or it could drag all of the solvent in its pervaded volume with it, thereby moving by Zimm motion. In dilute solution, Zimm motion has less frictional resistance than Rouse motion, and therefore, the faster process is Zimm motion. The chain effectively moves as though it were a solid particle with volume of order of its pervaded volume (with linear size R). The solvent within the pervaded volume of the chain is hydrodynamically coupled to the chain.[3] When the chain moves in response to its monomers being randomly hit by solvent from different directions, it effectively drags the surrounding solvent with it.

Using Eq. (3.77) for the size of the chain in a good solvent with intermediate excluded volume v in Eq. (8.25), and combining with the θ-solvent result of Eq. (8.25) with $\nu = 1/2$, yields a general expression for the Zimm time in dilute polymer solutions:

$$\tau_Z \approx \frac{\eta_s}{kT} R^3 \approx \begin{cases} \tau_0 N^{3/2} & N < b^6/\mathrm{v}^2 \\ \tau_0 (\mathrm{v}/b^3)^{6\nu-3} N^{3\nu} & N > b^6/\mathrm{v}^2 \end{cases} \tag{8.28}$$

Using $\nu = 0.588$, the Zimm relaxation time for long chains is $\tau_0 (\mathrm{v}/b^3)^{0.53} N^{1.76}$.

8.3 Intrinsic viscosity

In solution, a confusing plethora of viscosities have been defined over the years. The ratio of solution viscosity η to solvent viscosity η_s is the **relative viscosity**:

$$\eta_r \equiv \frac{\eta}{\eta_s}. \tag{8.29}$$

[3] While some solvent does move with the chain, solvent molecules diffuse into and out of the pervaded volume on a faster time scale than the diffusion of the polymer (see Problem 8.5).

The relative viscosity is the simplest dimensionless measure of solution viscosity. The difference of the relative viscosity from unity is the **specific viscosity**:

$$\eta_{sp} \equiv \eta_r - 1 = \frac{\eta - \eta_s}{\eta_s}. \tag{8.30}$$

The numerator $(\eta - \eta_s)$ is the polymer contribution to the solution viscosity, so the specific viscosity is a dimensionless measure of the polymer contribution to the solution viscosity.

The ratio of specific viscosity to polymer concentration is the **reduced viscosity**, η_{sp}/c, which has units of reciprocal concentration. In the limit of very low concentrations (far below the overlap concentration) the reduced viscosity becomes a very important material property called the intrinsic viscosity (see Section 1.7.3, and in particular Fig. 1.24):

$$[\eta] = \lim_{c \to 0} \frac{\eta_{sp}}{c}. \tag{8.31}$$

The intrinsic viscosity is the initial slope of specific viscosity as a function of concentration, and has units of reciprocal concentration [see Eq. (1.97)].

The value of the stress relaxation modulus at the relaxation time $G(\tau)$ is of the order of kT per chain in either the Rouse or Zimm models, just as the strands of a network in Chapter 7 stored of order kT of elastic energy:

$$G(\tau) \approx kT \frac{\phi}{Nb^3}. \tag{8.32}$$

The polymer contribution to the viscosity in either the Rouse or the Zimm model is proportional to $G(\tau)\tau$ [Eq. (7.120)]:

$$\eta - \eta_s \approx kT \frac{\phi}{Nb^3} \tau. \tag{8.33}$$

The typical experimental concentration used in defining intrinsic viscosity is the polymer mass per unit volume of solution, $c = \phi M_0/(b^3 \mathcal{N}_{Av})$ where M_0 is the molar mass of a Kuhn monomer [see Eq. (1.18)]. The intrinsic viscosity then follows:

$$[\eta] \approx \frac{kT\mathcal{N}_{Av}}{\eta_s M_0 N} \tau. \tag{8.34}$$

The expression for the relaxation time in the Rouse model of an ideal chain $\tau_R \approx \eta_s b^3 N^2/(kT)$ [Eq. (8.21)] leads to the Rouse prediction for the intrinsic viscosity:

$$[\eta] \approx \frac{b^3 \mathcal{N}_{Av}}{M_0} N \quad \text{Rouse model.} \tag{8.35}$$

The Rouse model predicts that the intrinsic viscosity in a θ-solvent is proportional to molar mass. However, the Rouse model assumes no

hydrodynamic interactions and is not expected to be valid in dilute solutions where intrinsic viscosity is defined.

Substituting the prediction for the relaxation time of the Zimm model $\tau_Z \approx \eta_s R^3/(kT)$ [Eq. (8.25)] into the expression for intrinsic viscosity [Eq. (8.34)] leads to the Zimm prediction for intrinsic viscosity:

$$[\eta] \approx \frac{R^3 \mathcal{N}_{Av}}{M_0 N} \approx \frac{b^3 \mathcal{N}_{Av}}{M_0} N^{3\nu-1} \quad \text{Zimm model.} \tag{8.36}$$

The Zimm model assumes that as the polymer moves it drags the solvent inside its pervaded volume with it. The Zimm model has the correct physics for the intrinsic viscosity. Equation (8.36) is more commonly written in terms of the molar mass $M = M_0 N$,

$$[\eta] = \Phi \frac{R^3}{M}, \tag{8.37}$$

where $\Phi = 0.425 \mathcal{N}_{Av} = 2.5 \times 10^{23}\,\text{mol}^{-1}$ is a universal constant for all polymer–solvent systems. This famous relation between intrinsic viscosity, coil size and molar mass is known as the Fox–Flory equation.

Equation (8.36) predicts that the intrinsic viscosity obeys a power law in molar mass. This power law was empirically recognized long ago, and is known as the Mark–Houwink equation [Eq. (1.100)]:

$$[\eta] = K M^a. \tag{8.38}$$

From the derivation of the Fox–Flory equation, based on the Zimm model, the Mark–Houwink exponent a is related to the exponent describing the molar mass dependence of coil size in solution ν:

$$a = 3\nu - 1. \tag{8.39}$$

The Mark–Houwink equation provides an indirect estimate of molar mass from a measurement of intrinsic viscosity $[\eta]$, if the two Mark–Houwink constants K and a, are known. The predictions of Mark–Houwink constants are summarized in Table 8.1. Comparison with Table 1.4 shows that the Zimm model agrees reasonably well with experimental results, as $a = 0.50$ is observed in θ-solvent and $0.7 < a < 0.8$ is usually observed in good solvents.

Using the Zimm time [Eq. (8.28)] in Eq. (8.34), yields a general expression for the intrinsic viscosity, valid for any solvent with $T \geq \theta$:

$$\begin{aligned}[\eta] &\approx \frac{kT\mathcal{N}_{Av}}{\eta_s M_0 N} \tau_Z \approx \frac{R^3 \mathcal{N}_{Av}}{M_0 N} \\ &\approx \frac{b^3 \mathcal{N}_{Av}}{M_0} \begin{cases} N^{1/2} & N < b^6/\mathrm{v}^2 \\ (\mathrm{v}/b^3)^{6\nu-3} N^{3\nu-1} & N > b^6/\mathrm{v}^2 \end{cases}\end{aligned} \tag{8.40}$$

Table 8.1 Predictions of Mark–Houwink constants

	K	a
Rouse model in θ-solvent	$b^3\mathcal{N}_{Av}/M_0^2$	1
Zimm model in θ-solvent	$b^3\mathcal{N}_{Av}/M_0^{3/2}$	$3\nu - 1 = 1/2$
Zimm model in good solvent	$b^3\mathcal{N}_{Av}/M_0^{1.764}$	$3\nu - 1 \cong 0.76$

For long chains in good solvent, $\nu = 0.588$ and the intrinsic viscosity *universally* scales as $v^{0.53}N^{0.76}$.

This relation is tested with experimental data in Fig. 8.3.[4] It is important to point out the fact that the intrinsic viscosity of polystyrene in toluene (filled squares in Fig. 8.3) crosses over to the θ-solvent result at $M \approx 30\,000$ g mol^{-1}. This provides a direct measure of the number of Kuhn monomers in a thermal blob $g_T \approx (30\,000 \text{ g mol}^{-1})/(720 \text{ g mol}^{-1}) \approx 40$ for polystyrene in toluene. The crossover between the θ-solvent and good solvent cases of Eq. (8.40) is at $N = g_T \approx (b^3/v)^2$ [Eq. (3.75)], so $g_T \approx 40$ means that the excluded volume is estimated to be $v \approx 0.16b^3$ for polystyrene in toluene. Hence, although toluene is a quite good solvent for polystyrene, it is nowhere near the athermal solvent limit, which would have even higher intrinsic viscosity that would maintain the power law with 0.76 slope to even lower molar masses. Polystyrene in methyl ethyl ketone (open circles in Fig. 8.3) has even smaller excluded volume, as $g_T \approx (100\,000 \text{ g mol}^{-1})/(720 \text{ g mol}^{-1}) \approx 140$ and $v \approx 0.08b^3$.

Figure 8.3 also shows clearly that caution is needed when using Mark–Houwink equations from the literature that have intermediate exponents in the range $0.5 < a < 0.76$. Such intermediate exponents correspond to the crossover between regimes and are only valid for the range of molar masses they were measured in.

The fact that the intrinsic viscosity measurement is simultaneously simple and precise makes it an extremely popular molecular characterization tool. Intrinsic viscosity can easily be measured to $\pm 0.1\%$ precision, which is far superior to osmotic pressure and light scattering, which have precisions of $\pm 5\%$ under the best of circumstances. Furthermore, if intrinsic viscosity and absolute molar mass are measured over a sufficiently wide range, the thermodynamic nature of the polymer solvent interaction, reflected in the excluded volume v, can be estimated using Eq. (8.40).

The temperature dependence of intrinsic viscosity enters Eq. (8.40) through the excluded volume $v \approx b^3 (T - \theta)/T$. For chains that are smaller than the thermal blob, the short chain branch of Eq. (8.40) (with $N < b^6/v^2$) applies. For such short chains, the intrinsic viscosity is independent of temperature and $[\eta]/N^{1/2}$ reduces data for different lengths of short chains to a common temperature-independent line, demonstrated in Fig. 8.4(a) for polyisobutylene in toluene with $M < 11\,000$ g mol^{-1}. On the other hand, chains with size far exceeding the thermal blob size have important excluded volume effects. The long chain branch of Eq. (8.40) (with $N > b^6/v^2$) applies to long chains and $[\eta]/N^{0.764}$ reduces data for different lengths of long chains to a common curve, as shown in Fig. 8.4(b) for polyisobutylene in toluene with $M > 400\,000$ g mol^{-1}. The curve in Fig. 8.4(b) is determined by the temperature dependence of excluded volume $(v/b^3)^{0.53} \approx (1 - \theta/T)^{0.53}$ with $\theta = 245\,K \cong -28\,^{\circ}C$ determined from the fit. Intermediate molar masses (not shown) with $M = 48\,000$ g mol^{-1} and

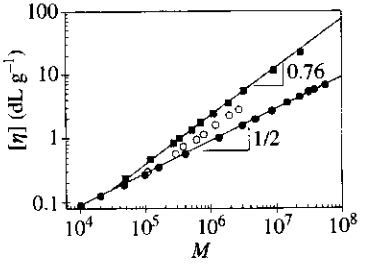

Fig. 8.3
Intrinsic viscosities of polystyrenes in three solvents. Cyclohexane is a θ-solvent ($v = 0$, filled circles, from Y. Einaga *et al.*, *J. Polym. Sci., Polym. Phys.* **17**, 2103, 1979), with Mark–Houwink exponent $a = 1/2$. Methyl ethyl ketone is a better solvent ($v \approx 0.08b^3$, open circles, from R. Okada *et al.*, *Makromol. Chem.* **59**, 137, 1963) and toluene is a good solvent ($v \approx 0.16b^3$, filled squares, from R. Kniewske and W.-M. Kulicke, *Makromol. Chem.* **184**, 2173, 1983) with $a = 0.76$.

[4] The customary units for intrinsic viscosity are dL g^{-1}, where 1 dL = 0.1 L.

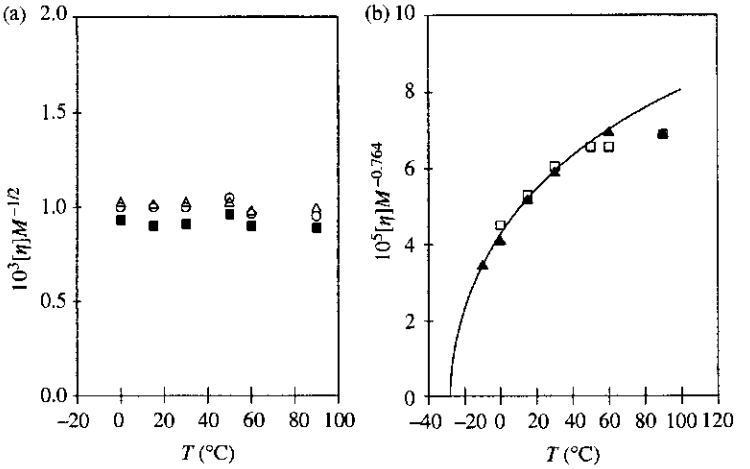

Fig. 8.4
Temperature dependence of intrinsic viscosity for polyisobutylene fractions in toluene. (a) data for the three lowest molar masses (open triangles are $M = 7080\,\mathrm{g\,mol^{-1}}$, filled squares are $M = 9550\,\mathrm{g\,mol^{-1}}$ and open circles are $M = 10\,200\,\mathrm{g\,mol^{-1}}$) that all are smaller than the thermal blob and hence have unperturbed size. The short chain branch of Eq. (8.40) reduces these data to a common temperature-independent line. (b) data for the two highest molar masses (open squares are $M = 463\,000\,\mathrm{g\,mol^{-1}}$ and filled triangles are $M = 1\,260\,000\,\mathrm{g\,mol^{-1}}$ that obey the long chain branch of Eq. (8.40). The curve is fitted to the data using Eq. (8.40) and the temperature dependence of excluded volume with $\theta = -28\,^{\circ}\mathrm{C}$ determined from the fit. The data are from T. G. Fox and P. J. Flory, *J. Phys. Chem.* **53**, 197 (1949).

$M = 110\,000\,\mathrm{g\,mol^{-1}}$ fall in the crossover between the two limiting cases of Eq. (8.40) and do not obey the scaling of either clean limit. Unfortunately, the molar mass range of $20\,000 < M < 200\,000\,\mathrm{g\,mol^{-1}}$ is the important range for commercial polymers, and it corresponds to the crossover for most good solvent/polymer solutions.

The R^3 in Eq. (8.37) comes from the relaxation time in Eq. (8.34). This Zimm time really has two size scales within it. The hydrodynamic radius R_h enters through the diffusion coefficient [Eq. (8.10)] and the radius of gyration R_g enters through the length scale that the molecule moves in its relaxation time:

$$[\eta] \approx \frac{\mathcal{R}T}{\eta_s M}\tau_Z \approx \frac{\mathcal{R}T}{\eta_s M}\frac{R_g^2}{D_Z} \approx \frac{\mathcal{N}_{Av}R_g^2 R_h}{M}. \tag{8.41}$$

Using data for polystyrene in two good solvents[5] (ethylbenzene and tetrahydrofuran) Eq. (8.41) is found to apply reasonably with

$$\frac{[\eta]M_w}{\mathcal{N}_{Av}R_g^2 R_h} \cong 7, \tag{8.42}$$

in the range $93\,000\,\mathrm{g\,mol^{-1}} \le M_w \le 4\,800\,000\,\mathrm{g\,mol^{-1}}$.

[5] K. Venkataswamy *et al.*, *Macromolecules* **19**, 124 (1986).

8.4 Relaxation modes

In Sections 8.1 and 8.2, we calculated the longest relaxation time of unentangled polymers using molecular models. The linear viscoelastic response of polymeric liquids, discussed in Section 7.6, measures the full spectrum of relaxation times. Since polymer chains are self-similar objects, they also exhibit dynamic self-similarity. *Smaller sections of a polymer chain with g monomers relax just like a whole polymer chain that has g monomers.* In all unentangled molecular models for polymer dynamics (both Rouse and Zimm and combinations thereof) the relaxations are described by N different **relaxation modes**. The modes are numbered by **mode index** $p = 1, 2, 3, \ldots, N$. These modes are analogous to the modes of a vibrating guitar string. Mode p involves coherent motion of sections of the whole chain with N/p monomers, and the corresponding relaxation time of this mode τ_p is similar to the longest relaxation time of a chain with N/p monomers. For all unentangled molecular models of flexible polymer dynamics, the shortest mode has mode index $p = N$ with relaxation time τ_0, the relaxation time of a monomer [Eq. (8.20)]. The longer modes depend on whether hydrodynamic interactions are important or not, as discussed below.

Consider a polymer liquid subjected to a unit step strain at time $t = 0$. The **equipartition principle** states that $kT/2$ of free energy is associated with each degree of freedom at equilibrium.[6] Immediately following the unit step strain, the entire chain stores of order NkT of elastic energy, since there are N independent modes that each store of order kT. To determine the time dependent viscoelastic response, we simply need to determine the relaxation time of each mode.

8.4.1 Rouse modes

In the Rouse model, the (longest) relaxation time of the ideal chain is given by Eq. (8.17):

$$\tau_R \approx \tau_0 N^2. \tag{8.43}$$

Since the pth mode involves relaxation on the scale of chain sections with N/p monomers, the relaxation time of the pth mode has a similar form to the longest mode:

$$\tau_p \approx \tau_0 \left(\frac{N}{p}\right)^2 \quad \text{for } p = 1, 2, \ldots, N. \tag{8.44}$$

The relaxation time of a monomer, τ_0 [Eq. (8.15)] is the shortest relaxation time of the Rouse model, with mode index $p = N$, making $\tau_N = \tau_0$. The mode with index $p = 1$ is the longest relaxation mode of the chain with relaxation time equal to the Rouse time $\tau_1 = \tau_R$, and corresponds to relaxation on the scale of the entire chain. The mode with index $p = 2$ corresponds to the two halves of the chain with $N/2$ monomers, each

[6] In three-dimensional space, each mode has three degrees of freedom.

relaxing independently. The mode with index p breaks the chain into p sections of N/p monomers, and each of these sections relax as independent chains of N/p monomers on the time scale τ_p.

As expected, higher index modes, involving fewer monomers, relax faster than lower index modes. Therefore, at time τ_p after a step strain, all modes with index higher than p have mostly relaxed, but modes with index lower than p have not yet relaxed.

The number of unrelaxed modes per chain at time $t = \tau_p$ is equal to the mode index p. Each unrelaxed mode contributes energy of order kT to the stress relaxation modulus. The stress relaxation modulus at time $t = \tau_p$ is proportional to the thermal energy kT and the number density of sections with N/p monomers, $\phi/(b^3 N/p)$:

$$G(\tau_p) \approx \frac{kT}{b^3}\frac{\phi}{N}p. \tag{8.45}$$

The time dependence of the mode index p for the mode that relaxes at time $t = \tau_p$ can be found from Eq. (8.44).

$$p \approx \left(\frac{\tau_p}{\tau_0}\right)^{-1/2} N. \tag{8.46}$$

Combining Eqs (8.45) and (8.46) approximates the stress relaxation modulus for the Rouse model at intermediate time scales:

$$G(t) \approx \frac{kT}{b^3}\phi\left(\frac{t}{\tau_0}\right)^{-1/2} \quad \text{for } \tau_0 < t < \tau_R. \tag{8.47}$$

This expression effectively interpolates between a modulus level of order kT per monomer at the shortest Rouse mode ($t \approx \tau_0$) to a modulus level of order kT per chain at the longest Rouse mode ($t = \tau_R \approx \tau_0 N^2$) using a power law. We already know that the stress relaxation modulus has an exponential decay beyond its longest relaxation time [Eq. (7.112)]. Therefore, an approximate description of the stress relaxation modulus of the Rouse model is the product of [Eq. (8.47)] and an exponential cutoff:

$$G(t) \approx \frac{kT}{b^3}\phi\left(\frac{t}{\tau_0}\right)^{-1/2} \exp(-t/\tau_R) \quad \text{for } t > \tau_0. \tag{8.48}$$

The Rouse time τ_R is the longest stress relaxation time [Eq. (8.18)].

For oscillatory shear, Eqs (7.149) and (7.150) allow calculation of the storage and loss moduli of a solution of linear Rouse chains (see Problem 8.14):

$$G'(\omega) \approx \frac{\phi kT}{b^3 N}\frac{(\omega\tau_R)^2}{\sqrt{[1+(\omega\tau_R)^2]\left[\sqrt{1+(\omega\tau_R)^2}+1\right]}} \quad \text{for } \omega < 1/\tau_0, \tag{8.49}$$

$$G''(\omega) \approx \frac{\phi kT}{b^3 N}\omega\tau_R \sqrt{\frac{\sqrt{1+(\omega\tau_R)^2}+1}{1+(\omega\tau_R)^2}} \quad \text{for } \omega < 1/\tau_0. \tag{8.50}$$

In the frequency range, $1/\tau_R \ll \omega \ll 1/\tau_0$, the storage and loss moduli of the Rouse model are equal to each other and scale as the square root of frequency:

$$G'(\omega) \cong G''(\omega) \sim \omega^{1/2} \quad \text{for } 1/\tau_R \ll \omega \ll 1/\tau_0. \tag{8.51}$$

For high frequencies $\omega > 1/\tau_0$, there are no relaxation modes in the Rouse model. The storage modulus becomes independent of frequency, and equal to the short time stress relaxation modulus, which is kT per monomer $G'(\omega) \approx \phi kT/b^3$. This high-frequency saturation is not included in Eqs (8.49) and (8.50). At low frequencies $\omega < 1/\tau_R$, the storage modulus is proportional to the square of frequency and the loss modulus is proportional to frequency, as is the case for the terminal response of any viscoelastic liquid.

Figure 8.5 shows that experimental data on unentangled polyelectrolyte solutions are described quite well by the Rouse model. Polyelectrolytes are charged polymers that have a wide range of concentrations where dynamics obey the Rouse model.

The viscosity of the Rouse model is obtained by integrating $G(t)$ [Eq. (7.117)]:

$$\eta = \int_0^\infty G(t)\,dt \approx \frac{kT}{b^3}\phi \int_0^\infty \left(\frac{t}{\tau_0}\right)^{-1/2} \exp(-t/\tau_R)\,dt$$
$$\approx \frac{kT}{b^3}\phi\sqrt{\tau_0\tau_R}\int_0^\infty x^{-1/2}\exp(-x)dx \approx \frac{kT}{b^3}\phi\sqrt{\tau_0\tau_R} \approx \frac{kT}{b^3}\tau_0 N\phi \approx \frac{\zeta}{b}N\phi. \tag{8.52}$$

Equation (8.52) made use of the variable transformation $x \equiv t/\tau_R$, and the integral involving x is simply a numerical coefficient. Notice that the final relation is identical to that expected by Eq. (7.120), the product of $G(\tau_R)$ [Eq. (8.32)] and τ_R [Eq. (8.17)]. The Rouse model applies to melts of short unentangled chains (for which hydrodynamic interactions are screened). The Rouse viscosity has a very simple form for an unentangled polymer melt:

$$\eta \approx \frac{\zeta}{b}N. \tag{8.53}$$

The viscosity of the Rouse model is proportional to the number of monomers in the chain. The Rouse model has been solved exactly (by Rouse), and the full calculation gives an extra coefficient of 1/36:

$$\eta = \frac{\zeta}{36b}N. \tag{8.54}$$

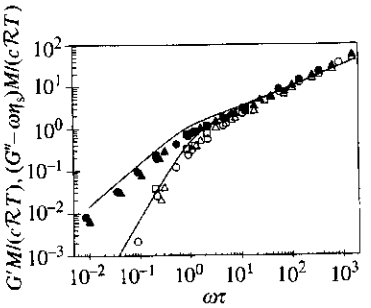

Fig. 8.5
Oscillatory shear data for solutions of poly(2-vinyl pyridine) in 0.0023 M HCl in water. Open symbols are the storage modulus G' and filled symbols are the loss modulus G''. Squares have $c = 0.5\,\text{g L}^{-1}$, triangles have $c = 1.0\,\text{g L}^{-1}$, and circles have $c = 2.0\,\text{g L}^{-1}$. The curves are the predictions of the Rouse model [Eqs (8.49) and (8.50)]. Data from D. F. Hodgson and E. J. Amis, *J. Chem. Phys.* **94**, 4581 (1991).

Rouse also derived an exact relation for the stress relaxation modulus,

$$G(t) = kT\frac{\phi}{Nb^3}\sum_{p=1}^{N}\exp(-t/\tau_p), \tag{8.55}$$

with

$$\tau_p = \frac{\zeta b^2 N^2}{6\pi^2 kTp^2}. \tag{8.56}$$

The stress relaxation times τ_p of the Rouse model are half of the correlation times of normal modes (see Problem 8.36).

This exact form demonstrates that each mode ($p = 1, 2, \ldots, N$) relaxes as a Maxwell element [Eq. (7.111)]. The exact [Eq. (8.55)] and approximate [Eq. (8.48)] Rouse predictions of the stress relaxation modulus of an unentangled polymer melt are compared in Fig. 8.6. This figure clearly shows that Eq. (8.48) is an excellent approximation of the exact Rouse result for long chains ($N \gg 1$).

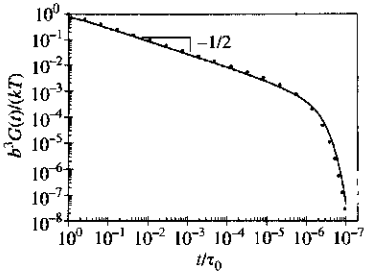

Fig. 8.6
Stress relaxation modulus predicted by the Rouse model for a melt of unentangled chains with $N = 10^3$. The solid curve is the exact Rouse result [Eq. (8.55)] and the dotted curve is the approximate Rouse result [Eq. (8.48)].

Chain sections containing N/p monomers move a distance of order of their size $b(N/p)^{1/2}$ during the mode relaxation time τ_p. The position vector of monomer j at time t is $\vec{r}_j(t)$. The mean-square displacement of monomer j during time τ_p is of the order of the mean-square size of the sections involved in coherent motion on this time scale:

$$\langle[\vec{r}_j(\tau_p) - \vec{r}_j(0)]^2\rangle \approx b^2\frac{N}{p} \approx b^2\left(\frac{\tau_p}{\tau_0}\right)^{1/2}. \tag{8.57}$$

In the final relation we used the time dependence of the mode index p [Eq. (8.46)]. The mean-square displacement of a monomer on intermediate time scales thus increases as the square root of time:

$$\langle[\vec{r}_j(t) - \vec{r}_j(0)]^2\rangle \approx b^2\left(\frac{t}{\tau_0}\right)^{1/2} \quad \text{for } \tau_0 < t < \tau_R. \tag{8.58}$$

For the motion to be diffusive, the mean-square displacement must be linear in time [see Eq. (8.1)]. Since the mean-square displacement on intermediate time scales is a weaker-than-linear power of time, the motion is referred to as **subdiffusive motion**. Individual monomers are not 'aware' that they belong to an N-mer on times shorter than the Rouse time of the chain. At each moment of time $t < \tau_R$, sections of a chain containing $g(t)$ monomers move coherently. Thus monomers only 'realize' that their chain contains at least $g(t)$ monomers at time scale $t < \tau_R$. The diffusion coefficient of these coherent sections is $D(t) \approx kT/(\zeta g)$. The number of monomers in sections that coherently participate in Rouse motion increases proportional to the square root of time $g(t) \approx (t/\tau_0)^{1/2}$ [Eq. (8.46) with $g = N/p$] and their effective diffusion coefficient decreases with time:

$$D(t) \approx \frac{kT}{\zeta g(t)} \approx \frac{kT}{\zeta}\left(\frac{t}{\tau_0}\right)^{-1/2} \quad \text{for } \tau_0 < t < \tau_R. \tag{8.59}$$

At longer times, monomers participate in collective motion of larger sections with smaller effective diffusion coefficient $D(t)$. Therefore the mean-square displacement of monomers is not a linear function of time, but instead subdiffusive:

$$\langle[\vec{r}_j(t) - \vec{r}_j(0)]^2\rangle \approx D(t)t \sim t^{1/2} \quad \text{for } \tau_0 < t < \tau_R. \tag{8.60}$$

Only on time scales longer than the Rouse time of the chain, is the motion of the chain diffusive, with mean-square displacement proportional to time [Eq. (8.1)].

8.4.2 Zimm modes

Similar scaling analysis of the mode structure can be applied to the Zimm model. The relaxation time of the pth mode is of the order of the Zimm relaxation time of the chain containing N/p monomers [Eq. (8.25)]:

$$\tau_p \approx \tau_0 \left(\frac{N}{p}\right)^{3\nu}. \tag{8.61}$$

The index p of the mode relaxing at time $t = \tau_p$ after a step strain imposed at time $t = 0$ is obtained by solving the above equation for p:

$$p \approx N\left(\frac{\tau_p}{\tau_0}\right)^{-1/(3\nu)} = N\left(\frac{t}{\tau_0}\right)^{-1/(3\nu)}. \tag{8.62}$$

The number of unrelaxed modes per chain at time $t = \tau_p$ is p. The stress relaxation modulus is proportional to the number density of chain sections with N/p monomers:

$$G(t) \approx \frac{kT\phi}{b^3}\frac{p}{N} \approx \frac{kT}{b^3}\phi\left(\frac{t}{\tau_0}\right)^{-1/(3\nu)} \quad \text{for } \tau_0 < t < \tau_Z. \tag{8.63}$$

In θ–solvents ($\nu = 1/2$), the stress relaxation modulus decays as the $-2/3$ power of time, while in good solvents ($\nu \cong 0.588$) $G(t)$ decays approximately as the -0.57 power of time. Like the stress relaxation modulus of the Rouse model [Eq. (8.47)], Eq. (8.63) crosses over from kT per monomer at the monomer relaxation time τ_0 to kT per chain at the relaxation time of the chain $\tau_Z \approx \tau_0 N^{3\nu}$ [Eq. (8.25)]. Once again, an excellent approximation to the stress relaxation modulus predicted by the Zimm model is the product of the power law of Eq. (8.63) and an exponential cutoff:

$$G(t) \approx \frac{kT}{b^3}\phi\left(\frac{t}{\tau_0}\right)^{-1/(3\nu)} \exp(-t/\tau_Z) \quad \text{for } t > \tau_0. \tag{8.64}$$

The polymer contribution to the solution viscosity is obtained by integrating $G(t)$ [Eq. (7.117)]:

$$\eta - \eta_s = \int_0^\infty G(t)\,dt \approx \frac{kT}{b^3}\phi \int_0^\infty \left(\frac{t}{\tau_0}\right)^{-1/3\nu} \exp(-t/\tau_Z)\,dt$$
$$\approx \frac{kT}{b^3}\phi\tau_Z\left(\frac{\tau_Z}{\tau_0}\right)^{-1/3\nu} \int_0^\infty x^{-1/3\nu}\exp(-x)\,dx \approx \frac{kT}{b^3}\phi\tau_0 N^{3\nu-1}$$
$$\approx \eta_s\phi N^{3\nu-1}. \tag{8.65}$$

The variable transformation $x \equiv t/\tau_Z$ was used, and the integral involving x is simply a numerical coefficient. The second-to-last relation was obtained using $\tau_Z \approx \tau_0 N^{3\nu}$ [Eq. (8.25)] and the final relation used Eq. (8.20). The final relation is identical to that expected by Eq. (7.120), the product of $G(\tau_Z)$ [Eq. (8.32)] and τ_Z [Eq. (8.25)]. The Zimm model applies to the relaxation of the entire chain in dilute solution (where hydrodynamic interactions dominate). The intrinsic viscosity is calculated from the polymer contribution to the solution viscosity using Eq. (8.31) and the relation between mass concentration and volume fraction $c = \phi M_0/(b^3\mathcal{N}_{Av})$ [(see Eq. (1.18)]:

$$[\eta] = \lim_{c\to 0}\frac{\eta - \eta_s}{\eta_s c} \approx \frac{b^3\mathcal{N}_{Av}}{M_0}N^{3\nu-1} \approx \frac{R^3\mathcal{N}_{Av}}{M}. \tag{8.66}$$

This result is identical to Eqs (8.36) and (8.37), derived previously.

Using Eqs (7.149) and (7.150) with the approximate Zimm model prediction for the stress relaxation modulus [Eq. (8.64)] provides predictions of the storage and loss moduli that are valid for dilute solutions of linear chains (see Problem 8.16):

$$G'(\omega) \approx \frac{\phi kT\omega\tau_Z \sin\left[(1-1/(3\nu))\arctan(\omega\tau_Z)\right]}{b^3N\left[1+(\omega\tau_Z)^2\right]^{(1-1/(3\nu))/2}}, \tag{8.67}$$

$$G''(\omega) \approx \frac{\phi kT\omega\tau_Z \cos\left[(1-1/(3\nu))\arctan(\omega\tau_Z)\right]}{b^3N\left[1+(\omega\tau_Z)^2\right]^{(1-1/(3\nu))/2}}. \tag{8.68}$$

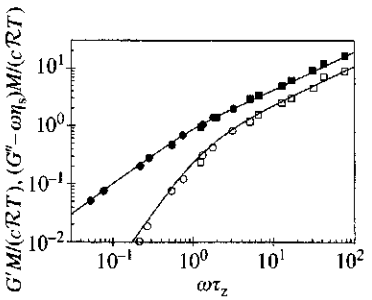

Fig. 8.7
Oscillatory shear data on dilute solutions of polystyrene with $M = 860\,000\ \mathrm{g\,mol^{-1}}$ in two θ-solvents (circles are in decalin at 16 °C and squares are in di-2-ethylhexyl phthalate at 22 °C). Open symbols are the dimensionless storage modulus and filled symbols are the dimensionless loss modulus, both extrapolated to zero concentration. The curves are the predictions of the Zimm model [Eqs (8.67) and (8.68)]. Data from R. M. Johnson *et al.*, *Polym. J.* **1**, 742 (1970).

These predictions of the Zimm model are compared with experimental data on dilute polystyrene solutions in two θ-solvents in Fig. 8.7. The Zimm model gives an excellent description of the viscoelasticity of dilute solutions of linear polymers.

As in the Rouse model, the mean-square displacement of monomer j during time τ_p is of the order of the mean-square size of the section containing N/p monomers involved in a coherent motion at this time:

$$\langle[\vec{r}_j(\tau_p) - \vec{r}_j(0)]^2\rangle \approx b^2\left(\frac{N}{p}\right)^{2\nu} \approx b^2\left(\frac{\tau_p}{\tau_0}\right)^{2/3}. \tag{8.69}$$

The time dependence of mode index p [Eq. (8.62)] was used to get the final result. Notice that this final result has an exponent that does not depend on

solvent quality. The mean-square displacement of a monomer in the Zimm model is subdiffusive on intermediate time scales:

$$\langle [\vec{r}_j(t) - \vec{r}_j(0)]^2 \rangle \approx b^2 \left(\frac{t}{\tau_0} \right)^{2/3} \quad \text{for } \tau_0 < t < \tau_Z. \tag{8.70}$$

Consistent with the fact that the longest relaxation time of the Zimm model is shorter than the Rouse model, the subdiffusive monomer motion of the Zimm model [(Eq. (8.70)] is always faster than in the Rouse model [Eq. (8.58)] with the same monomer relaxation time τ_0. This is demonstrated in Fig. 8.8, where the mean-square monomer displacements predicted by the Rouse and Zimm models are compared. Each model exhibits subdiffusive motion on length scales smaller than the size of the chain, but motion becomes diffusive on larger scales, corresponding to times longer than the longest relaxation time.

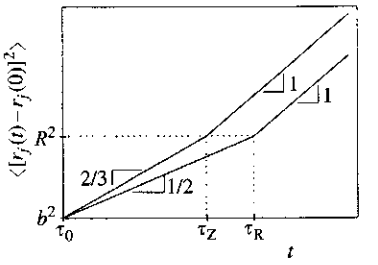

Fig. 8.8
Time dependence of the mean-square monomer displacements predicted by the Rouse and Zimm models on logarithmic scales.

8.5 Semidilute unentangled solutions

There are two limits for unentangled polymer dynamics:

(1) The Zimm limit applies to dilute solutions, where the solvent within the pervaded volume of the polymer is hydrodynamically coupled to the polymer. Polymer dynamics are described by the Zimm model in dilute solutions.

(2) The Rouse limit applies to unentangled polymer melts because hydrodynamic interactions are screened in melts (just as excluded volume interactions are screened in melts). Polymer dynamics in the melt state (with no solvent) are described by the Rouse model, for short chains that are not entangled.

In semidilute solutions there is a length scale, called the **hydrodynamic screening length** ξ_h, separating these two types of dynamics. On length scales shorter than the hydrodynamic screening length (for $r < \xi_h$), the hydrodynamic interactions dominate and dynamics are described by the Zimm model. On length scales larger than the screening length (for $r > \xi_h$) the hydrodynamic interactions are screened by surrounding chains and the dynamics are described by the Rouse model.

In Section 5.3, the static correlation length ξ was defined for semidilute solutions. This correlation length separates single-chain (dilute-like) conformations at shorter length scales ($r < \xi$) from many-chain (melt-like) statistics at longer length scales (for $r > \xi$). The concentration correlation blob of size ξ contains g monomers of a chain, with conformation similar to dilute solutions:

$$\xi \approx b g^{\nu}. \tag{8.71}$$

The exponent $\nu = 1/2$ in θ-solvents and $\nu \approx 0.588$ in good solvents. The correlation volumes are densely packed, so the volume fraction within

each correlation volume (gb^3/ξ^3) must be the same as the overall volume fraction of the solution ϕ:

$$\phi \approx \frac{gb^3}{\xi^3}. \tag{8.72}$$

The correlation length decreases with increasing concentration [Eq. (5.23)]:

$$\xi \approx b\phi^{-\nu/(3\nu-1)}. \tag{8.73}$$

The scaling exponent $\nu/(3\nu-1)=1$ in θ-solvents ($\nu=1/2$) and $\nu/(3\nu-1)\cong 0.76$ in good solvents ($\nu\cong 0.588$).

The hydrodynamic screening length ξ_h in semidilute solutions is expected to be proportional to the static correlation length[7] ξ:

$$\xi_h \approx \xi. \tag{8.74}$$

This proportionality makes sense in both limits. In the melt ($\phi=1$), both excluded volume and hydrodynamic interactions are fully screened to the level of individual monomers, so $\xi_h \approx \xi \approx b$. At the overlap concentration ($\phi=\phi^*$), both excluded volume and hydrodynamic interactions apply over length scales comparable to the size of the entire chain, with $\xi_h \approx \xi \approx R$.

The hydrodynamic screening length can neither be much larger nor much smaller that the static correlation length. Each of the N modes of a chain can, in principle, relax by either Rouse or Zimm motion. On small length scales, Zimm modes are faster than Rouse modes (see Fig. 8.8) because only solvent and other monomers on the same chain are hydrodynamically coupled. However, this situation changes beyond the correlation length, because Zimm motion would couple the motion of monomers from different chains. This extra coupling makes Rouse motion faster than Zimm motion for sections of chain that are larger than the static correlation length, so Rouse dynamics apply on larger length scales.

In semidilute solutions, both statics and dynamics are similar to dilute solutions on length scales shorter than the screening length. For short distances from a given monomer ($r<\xi$), essentially all other monomers are from the same chain (see Fig. 5.4). The chain conformation is similar to dilute solution and the dynamics are controlled by strong hydrodynamic interactions. Therefore, the relaxation time τ_ξ of a chain section of size ξ is described by the Zimm model and proportional to the correlation volume ξ^3:

$$\tau_\xi \approx \frac{\eta_s}{kT}\xi^3 \approx \frac{\eta_s b^3}{kT}\phi^{-3\nu/(3\nu-1)}. \tag{8.75}$$

On length scales larger than the screening length ξ the dynamics are many-chain-like, with both excluded volume and hydrodynamic interactions

[7] Experimental results appear to be consistent with the expectation that hydrodynamic interactions and excluded volume interactions are screened on similar length scales.

screened. The Rouse model applies to the random walk chain of N/g correlation blobs. The relaxation time of the whole chain τ_{chain} is given by Eq. (8.17), with τ_ξ the effective 'monomer' relaxation time, N/g the effective number of 'monomers':

$$\tau_{\text{chain}} \approx \tau_\xi \left(\frac{N}{g}\right)^2 \approx \frac{\eta_s}{kT}\xi^3 \left(\frac{N}{g}\right)^2. \tag{8.76}$$

The number of monomers in a correlation blob is determined by combining Eqs (8.72) and (8.73) [as was done previously in deriving Eq. (5.24)]:

$$g \approx \phi \left(\frac{\xi}{b}\right)^3 \approx \phi^{-1/(3\nu-1)}. \tag{8.77}$$

From Eqs (8.76) and (8.77), the concentration dependence of the relaxation time of the chain in semidilute solution is obtained:

$$\tau_{\text{chain}} \approx \frac{\eta_s b^3}{kT} N^2 \phi^{(2-3\nu)/(3\nu-1)}. \tag{8.78}$$

The concentration dependence of the polymer's relaxation time is a power law with exponent

$$\frac{2-3\nu}{3\nu-1} = 1 \quad \text{in } \theta - \text{solvents } (\nu = 1/2), \tag{8.79}$$

and

$$\frac{2-3\nu}{3\nu-1} \cong 0.31 \quad \text{in good solvents } (\nu \cong 0.588). \tag{8.80}$$

Note that if the polymer in dilute solution were highly extended with exponent $\nu > 2/3$, the relaxation time in unentangled semidilute solutions would be predicted to *decrease* with increasing concentration. This is actually observed for semidilute unentangled solutions of charged polymers, called polyelectrolytes, which have $\nu = 1$ in dilute solutions because of charge repulsion. However, for the neutral flexible polymers discussed here, the relaxation time of the chain always increases with concentration.

Polymers diffuse a distance of the order of their size R during their relaxation time τ_{chain}. Recall the size of a linear polymer chain in a semidilute solution [Eq. (5.26) with $v = b^3$]:

$$R \approx \xi \left(\frac{N}{g}\right)^{1/2} \approx bN^{1/2}\phi^{-(2\nu-1)/(6\nu-2)}. \tag{8.81}$$

The exponent

$$\frac{2\nu-1}{6\nu-2} = 0 \quad \text{in } \theta - \text{solvents } (\nu = 1/2), \tag{8.82}$$

because the chain maintains a nearly ideal conformation at all concentrations and

$$\frac{2\nu - 1}{6\nu - 2} \cong 0.12 \quad \text{in good solvents } (\nu \cong 0.588). \tag{8.83}$$

The diffusion coefficient D in semidilute solutions decreases as a power law in concentration:

$$D \approx \frac{R^2}{\tau_{\text{chain}}} \approx \frac{kT}{\eta_s b} \frac{\phi^{-(1-\nu)/(3\nu-1)}}{N}. \tag{8.84}$$

The semidilute diffusion coefficient can be written in terms of the Zimm diffusion coefficient of the chain D_Z [Eq. (8.23) valid for diffusion in dilute solutions] and the overlap concentration $\phi^* \approx N^{-(3\nu-1)}$ [Eq. (5.19)]:

$$D \approx D_Z \left(\frac{\phi}{\phi^*}\right)^{-(1-\nu)/(3\nu-1)}. \tag{8.85}$$

The scaling exponent

$$\frac{1 - \nu}{3\nu - 1} = 1 \quad \text{in } \theta - \text{solvents } (\nu = 1/2), \tag{8.86}$$

and

$$\frac{1 - \nu}{3\nu - 1} \cong 0.54 \quad \text{in good solvents } (\nu \cong 0.588).$$

The concentration dependence of the diffusion coefficient is plotted in Fig. 8.9 in the scaling form suggested by Eq. (8.85) for polymer solutions in good solvents. The expected exponent is observed over a limited range of approximately one decade above the overlap concentration ϕ^* and a stronger concentration dependence is seen at higher concentrations, where entanglements become important.

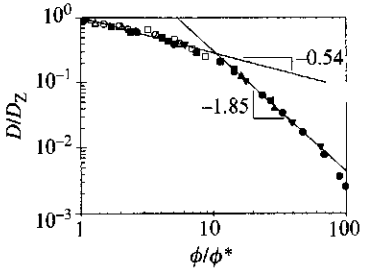

Fig. 8.9
Concentration dependence of diffusion coefficient in good solvent. Filled symbols are four molar masses of polystyrene in benzene spanning the range 78 000–750 000 g mol^{-1}, from L. Leger and J. L. Viovy, *Contemp. Phys.* **29**, 579 (1988). Open symbols are three molar masses of poly(ethylene oxide) in water spanning the range 73 000–660 000 g mol^{-1}, from W. Brown, *Polymer* **25**, 680 (1984). To facilitate comparison, ϕ^* was taken as the volume fraction at which $D = D_Z$ for each data set. The low concentration line is Eq. (8.85) and the high concentration line has the slope expected for entangled solutions in good solvent [Eq. (9.43)].

In semidilute solutions, hydrodynamic interactions are not screened on length scales smaller than the correlation length ξ. Each mode involves coherent motion of N/p monomers. If N/p is smaller than the g monomers in a correlation blob, motion associated with that mode is described by the Zimm model. On larger length scales, hydrodynamic interactions are screened and modes with index $p < N/g$ are described by the Rouse model. The number of monomers in a correlation blob is given by Eq. (8.77). The crossover mode index for hydrodynamic interaction is

$$p_\xi = \frac{N}{g} \approx N\phi^{1/(3\nu-1)}. \tag{8.87}$$

There are three time scales important for the stress relaxation modulus in semidilute unentangled solutions. The shortest time scale is the relaxation time of a monomer [Eq. (8.20)]. The intermediate time scale is the

Zimm relaxation time corresponding to the correlation blob [Eq. (8.75)]. The longest time scale is the Rouse relaxation time of the chain of correlation blobs [Eq. (8.78)].

The stress relaxation modulus follows the Zimm dependence on time scales shorter than τ_ξ, corresponding to motion of chain sections smaller than the correlation length:

$$G(t) \approx \frac{kT}{b^3}\phi\left(\frac{t}{\tau_0}\right)^{-1/(3\nu)} \quad \text{for } \tau_0 < t < \tau_\xi. \tag{8.88}$$

At the crossover time $t = \tau_\xi$ [Eq. (8.75)] the stress relaxation modulus is of the order of the osmotic pressure:

$$G(\tau_\xi) \approx \frac{kT}{b^3}\phi^{3\nu/(3\nu-1)} \approx \frac{kT}{\xi^3} \approx \Pi. \tag{8.89}$$

At longer times, the stress relaxation modulus follows the Rouse dependence:

$$G(t) \approx \frac{kT}{b^3}\phi^{3\nu/(3\nu-1)}\left(\frac{t}{\tau_\xi}\right)^{-1/2} \quad \text{for } \tau_\xi < t < \tau_{\text{chain}}. \tag{8.90}$$

The value of the stress relaxation modulus at the relaxation time of the chain can be determined from Eq. (8.90):

$$G(\tau_{\text{chain}}) \approx \frac{kT}{b^3}\phi^{3\nu/(3\nu-1)}\left(\frac{\tau_{\text{chain}}}{\tau_\xi}\right)^{-1/2} \approx \frac{kT}{b^3}\phi^{3\nu/(3\nu-1)}\frac{g}{N} \approx \frac{kT}{b^3 N}\phi. \tag{8.91}$$

Equations (8.76) and (8.77) were used to simplify this expression for $G(\tau_{\text{chain}})$. The terminal modulus is of order kT per chain, as it must be for any unentangled flexible chain [see Eq. (8.32)]. The stress relaxation modulus at long times is approximated well by the product of the power law and an exponential cutoff:

$$G(t) \approx \frac{kT}{b^3 N}\phi\left(\frac{t}{\tau_{\text{chain}}}\right)^{-1/2}\exp(-t/\tau_{\text{chain}}) \quad \text{for } t > \tau_\xi. \tag{8.92}$$

The time dependence of the stress relaxation modulus in semidilute unentangled solution is sketched in Fig. 8.10. Experimental verification of Rouse dynamics for frequencies smaller than $1/\tau_\xi$ was shown in Fig. 8.5, for a semidilute unentangled polyelectrolyte solution.

The polymer contribution to viscosity in semidilute unentangled solutions is obtained by integrating the stress relaxation modulus over time [Eq. (7.117)].

$$\eta - \eta_s = \int_0^\infty G(t)\,dt \approx \frac{kT}{b^3}\frac{\phi}{N}\tau_{\text{chain}} \approx \eta_s N\phi^{1/(3\nu-1)}. \tag{8.93}$$

In Problem 8.21, the integration is shown to be controlled by the longest relaxation time τ_{chain}.

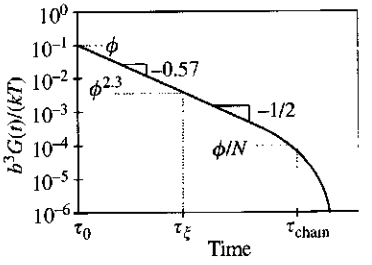

Fig. 8.10
Stress relaxation modulus of an unentangled semidilute solution of chains with $N = 10^3$ monomers at volume fraction $\phi = 0.1$ in an athermal solvent (logarithmic scales).

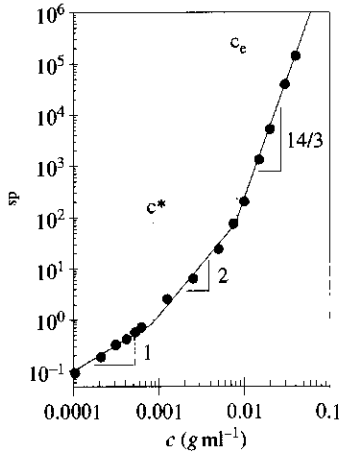

Fig. 8.11
Concentration dependence of specific viscosity for linear poly(ethylene oxide) with $M_w = 5 \times 10^6\,g\,mol^{-1}$ in water at 25.0 °C. Data courtesy of S. Singh.

This result can alternatively be obtained from a de Gennes scaling argument. At the overlap concentration $\phi^* \approx N^{1-3\nu}$, the polymer contribution to viscosity is of the order of the solvent viscosity, and grows as a power law in concentration in semidilute solution:

$$\eta - \eta_s \approx \eta_s \left(\frac{\phi}{\phi^*}\right)^x . \tag{8.94}$$

The exponent x can be determined from the condition that the long-time modes are Rouse-like, and therefore the polymer contribution to solution viscosity should be linearly proportional to polymer molar mass:

$$\eta - \eta_s \approx \eta_s N^{(3\nu-1)x} \phi^x , \tag{8.95}$$

$$(3\nu - 1)x = 1 \;\Rightarrow\; x = \frac{1}{3\nu - 1} . \tag{8.96}$$

In θ-solvents ($\nu = 1/2$), the exponent $1/(3\nu - 1) = 2$, and the viscosity is predicted to grow as the square of polymer concentration in unentangled semidilute θ-solutions:

$$\eta_{sp} \approx N\phi^2 \approx \left(\frac{\phi}{\phi^*}\right)^2 . \tag{8.97}$$

This concentration dependence is demonstrated in Fig. 8.11. In good solvents ($\nu \cong 0.588$), the exponent $1/(3\nu - 1) \cong 1.3$, and the viscosity is predicted to grow as a weaker power of concentration:

$$\eta_{sp} \approx N\phi^{1.3} \approx \left(\frac{\phi}{\phi^*}\right)^{1.3} . \tag{8.98}$$

8.6 Modes of a semiflexible chain

Polymer dynamics discussed in the previous sections of this chapter correspond to completely flexible chains and are related to modes on length scales larger than the Kuhn length. The relaxation mode structure on length scales shorter than the Kuhn length is significantly different. Many chains, in particular biopolymers, are locally quite stiff. A large part of the relaxation spectrum of such semiflexible chains corresponds to modes with wavelengths shorter than their Kuhn length. In this section, the mode spectrum of semiflexible chains without any intrinsic curvature or twist is described.

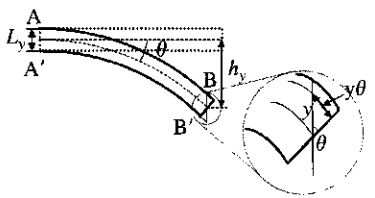

Fig. 8.12
Bending of a rod by angle θ. Insert: the elongation along a surface that is a distance y above the undeformed middle surface is $y\theta$ (and $y < 0$ below the middle surface, in compression).

8.6.1 Bending energy and dynamics

Consider an elastic beam of length L, thickness L_y and width L_z with Young's modulus E. It is instructive to calculate the elastic energy of bending this beam by a small angle θ (see Fig. 8.12):

$$\theta \approx \sin\left(\frac{h_y}{L}\right) \approx \frac{h_y}{L} . \tag{8.99}$$

The central part of the beam (dashed line in Fig. 8.12) is undeformed, the upper half of the beam (AB) is under tension, while the lower half (A′B′) is under compression. The deformation along the plane of the bent beam a distance y away from the undeformed central surface is $\Delta L = y\theta$ (see insert in Fig. 8.12). The corresponding extensional strain is $\varepsilon(y) \equiv \Delta L/L = y\theta/L$. The elastic energy density is the work done by deformation per unit volume. Stress is force per unit cross-sectional area and strain is the deformation per unit length, so elastic energy density is proportional to the product of stress and strain $\sigma\varepsilon = E\varepsilon^2$, where E is Young's modulus. The elastic energy of a thin slice of the beam of thickness dy and cross-sectional area LL_z is $E(y\theta/L)^2 LL_z dy$. The total elastic energy of a bent beam is obtained by integrating the contribution from each slice over the thickness of the beam:

$$U_L(\theta) \approx \int_{-L_y/2}^{L_y/2} E\left(\frac{y\theta}{L}\right)^2 LL_z \, dy \approx EL_z \frac{\theta^2}{L} \int_{-L_y/2}^{L_y/2} y^2 \, dy$$
$$\approx EL_z \frac{\theta^2}{L} L_y^3. \tag{8.100}$$

The Kuhn length b determines the crossover between stiff and flexible length scales. For rods or beams with length L of the order of the Kuhn length b, the angle of thermally induced fluctuations is of the order of unity $\theta \approx 1$:

$$U_b(1) \approx E\frac{L_y^3 L_z}{b} \approx kT. \tag{8.101}$$

This equation can be solved for the Kuhn length:

$$b \approx E\frac{L_y^3 L_z}{kT}. \tag{8.102}$$

The bending energy of a bent beam [Eq. (8.100)] then can be rewritten in terms of the Kuhn length:

$$U_L(\theta) \approx kT\frac{b}{L}\theta^2 \approx kT\frac{b}{L}\left(\frac{h_y}{L}\right)^2. \tag{8.103}$$

The last relation was obtained using Eq. (8.99) for the deformation angle θ. By writing Eq. (8.103) in terms of the Kuhn length, it becomes much more general and applies to beams with cross-sections that are not rectangular (such as the bending of a cylindrical rod).

Since the beam or rod is a solid, it has natural modes of bending with wavelengths that allow the ends of the beam to be stationary. The first (longest wavelength) mode has wavelength $\lambda = 2L$, the second mode has $\lambda = L$, the third mode has $\lambda = 2L/3$, etc. The fourth mode (with $\lambda = L/2$) is illustrated in Fig. 8.13. Spontaneous thermally induced vibration modes of the beam will form at these wavelengths, and the amplitude of each mode

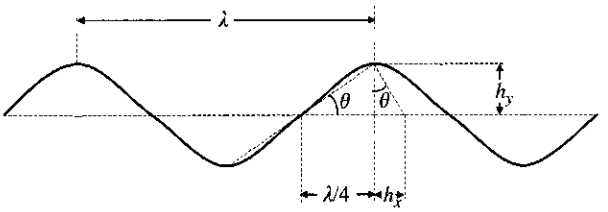

Fig. 8.13
Schematic of the fourth vibration mode (with wavelength $\lambda = L/2$) of a rigid rod of length L. The transverse oscillation with amplitude h_y reduces the projected rod length along the x-axis. The amount that the rod length is reduced, per wavelength λ, oscillates with longitudinal amplitude h_x.

is determined by setting the bending energy from Eq. (8.103) at length scale λ equal to the thermal energy kT:

$$U_\lambda \approx kTb\frac{h_y^2}{\lambda^3} \approx kT. \tag{8.104}$$

This equation can be solved for the mean-square amplitude of these modes in the transverse direction:

$$h_y^2 \approx \frac{\lambda^3}{b}. \tag{8.105}$$

To understand the dynamics of the bending fluctuations associated with these natural modes, a force balance per unit length is required. The force per unit length associated with the bending mode of wavelength λ is calculated by differentiating the energy U_λ and it is resisted by the frictional dissipation:

$$\frac{1}{\lambda}\frac{\mathrm{d}U_\lambda}{\mathrm{d}h_y} \approx kTb\frac{h_y}{\lambda^4} \approx -\frac{\zeta}{b}\frac{\mathrm{d}h_y}{\mathrm{d}t}. \tag{8.106}$$

To understand the frictional dissipation term, recall that the friction coefficient ζ of a Kuhn segment of length b is the ratio of force and velocity in a liquid. Hence, ζ/b is the ratio of force per unit length and the velocity $\mathrm{d}h_y/\mathrm{d}t$. This equation can be solved by separation of variables and integration:

$$\int \frac{\mathrm{d}h_y}{h_y} \approx -\frac{kTb^2}{\zeta\lambda^4}\int \mathrm{d}t. \tag{8.107}$$

The solution is exponentially decaying in time $h_y \sim \exp(-t/\tau)$ with relaxation time τ proportional to the fourth power of the wavelength λ of the mode:

$$\tau \approx \frac{\zeta}{kTb^2}\lambda^4. \tag{8.108}$$

Alternatively, the wavelength of a bending mode is proportional to the 1/4 power of its relaxation time:

$$\lambda \approx \left(\frac{kTb^2}{\zeta}t\right)^{1/4} \approx b\left(\frac{kT}{\zeta b^2}t\right)^{1/4} \approx b\left(\frac{t}{\tau_0}\right)^{1/4}. \tag{8.109}$$

The final relation uses the relaxation time of a Kuhn monomer of length b [Eq. (8.108) with $\lambda \approx b$]:

$$\tau_0 \approx \frac{\zeta b^2}{kT}. \tag{8.110}$$

This longest bending mode matches the shortest relaxation time in the Rouse and Zimm models [the relaxation time of a monomer τ_0, Eq. (8.15)].

8.6.2 Tensile modulus and stress relaxation

The two similar triangles in Fig. 8.13 can be used to relate the transverse amplitude h_y and the longitudinal amplitude h_x:

$$\frac{h_x}{h_y} = \frac{h_y}{\lambda/4}. \tag{8.111}$$

The longitudinal amplitude of each mode can then be written in terms of the mode wavelength and the Kuhn length:

$$h_x \approx \frac{h_y^2}{\lambda} \approx \frac{\lambda^2}{b}. \tag{8.112}$$

The final relation made use of Eq. (8.105). The **spring constant** κ_λ (units of force/length) arising from the mode with wavelength λ can be estimated from the fact that the energy of each mode $\kappa_\lambda h_x^2$ is of the order of kT:

$$\kappa_\lambda \approx \frac{kT}{h_x^2} \approx kT\frac{b^2}{\lambda^4}. \tag{8.113}$$

The tensile force f_λ from the mode with wavelength λ arising from application of a small stretch δL is the product of the spring constant and the stretch:

$$f_\lambda \approx \kappa_\lambda \delta L \approx kT\frac{b^2}{\lambda^4}\delta L \approx kT\frac{b^2}{\lambda^3}\frac{\delta L}{\lambda} \approx kT\frac{b^2}{\lambda^3}\varepsilon_\lambda. \tag{8.114}$$

The last relation introduces the extensional strain $\varepsilon_\lambda \equiv \delta L/\lambda$.

The stress borne by a liquid of semiflexible chains from the mode with wavelength λ is the product of the tensile force f_λ in a chain and the line density of the chains in the liquid. The line density can be estimated from the number density of chains c_n/N, where c_n is the monomer number density (the number density of Kuhn segments). The contour length of each chain is Nb and therefore the line density of chains in the liquid is $c_n b$:

$$\sigma_\lambda \approx f_\lambda c_n b \approx kTc_n\left(\frac{b}{\lambda}\right)^3 \varepsilon_\lambda. \tag{8.115}$$

Young's modulus due to the mode with wavelength λ is the ratio of stress and strain:

$$E_\lambda = \frac{\sigma_\lambda}{\varepsilon_\lambda} \approx kTc_n\left(\frac{b}{\lambda}\right)^3. \tag{8.116}$$

Substituting the relation between relaxation time and mode wavelength [Eq. (8.109)] into the expression for modulus [Eq. (8.116)] leads to the time-dependent stress relaxation modulus that decays as the $-3/4$ power of time:

$$E(t) \approx kTc_n\left(\frac{b}{\lambda}\right)^3 \approx kTc_n\left(\frac{t}{\tau_0}\right)^{-3/4} \quad \text{for } \tau_g < t < \tau_0. \tag{8.117}$$

The short time limit τ_g corresponds to the fastest stiff mode, with shortest wavelength determined by the smallest physical length scale using Eq. (8.108). For polymer chains this smallest length is of the order of the bond length l:

$$\tau_g \approx \frac{\zeta l^4}{kTb^2} \approx \tau_0\left(\frac{l}{b}\right)^4. \tag{8.118}$$

Note that the stress decay is faster than that of the Rouse and Zimm models. Figure 8.14 compares the prediction of Eq. (8.117) with oscillatory shear data on the stiff biopolymer myosin in dilute solution. Myosin clearly exhibits a stronger frequency dependence than the flexible chain models predict, and is reasonably consistent with the 3/4 slope expected from Eq. (8.117).

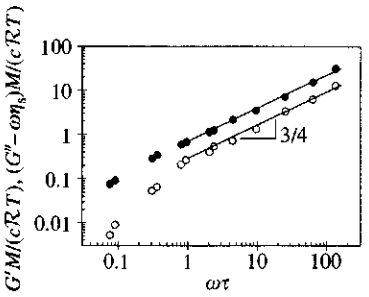

Fig. 8.14
Oscillatory shear data on dilute solutions of the stiff biopolymer myosin, from R. W. Rosser *et al.*, *Macromolecules* **11**, 1239 (1978). Open circles are the dimensionless storage modulus and filled circles are the dimensionless loss modulus, both extrapolated to zero concentration.

8.7 Temperature dependence of dynamics

8.7.1 Time–temperature superposition

Both the Rouse and Zimm models, as well as other molecular models to be discussed in Chapter 9, tacitly assume that the relaxation time associated with each mode has the same temperature dependence. Each mode's relaxation time is the product of temperature-independent factors[8] and the monomer relaxation time τ_0 [see Eqs (8.44) and (8.61)]. This has two important consequences for polymer melts and solutions.

First of all, the temperature dependence of all relaxation times is controlled by the ratio of friction coefficient and absolute temperature [see Eq. (8.15)]:

$$\tau \sim \frac{\zeta}{T}. \tag{8.119}$$

The temperature dependence of the modulus at any relaxation time τ is proportional to the product of the polymer mass density ρ and absolute

[8] These factors include the coil size, which can have a weak temperature dependence that is ignored in this discussion.

temperature T [see Eq. (8.45)]:

$$G(\tau) \sim \rho T. \tag{8.120}$$

Viscosity is the product of relaxation time and the modulus at the relaxation time [Eq. (7.120)]. The temperature dependence of viscosity is proportional to the product of liquid density and friction coefficient:

$$\eta \approx \tau G(\tau) \sim \rho\zeta. \tag{8.121}$$

The ratio of viscosity and density is the **kinematic viscosity**, which is directly measured in gravity-driven flows. The kinematic viscosity has the same temperature dependence as the friction coefficient. The density of polymer melts weakly decreases as temperature is raised,[9] imparting a weak temperature dependence to the modulus at any relaxation time τ. The temperature dependence of the viscosity of polymer melts is dominated by the strong temperature dependence of the friction coefficient. Near the glass transition temperature T_g, the friction coefficient changes by roughly a factor of 10 when temperature is changed by 1 K, while far above T_g (at $T > T_g + 100\,K$) approximately $25\,K$ temperature change is needed to change the friction coefficient by a factor of 10.

The second important consequence of the relaxation times of all modes having the same temperature dependence is the expectation that it should be possible to superimpose linear viscoelastic data taken at different temperatures. This is commonly known as the **time–temperature superposition** principle. Stress relaxation modulus data at any given temperature T can be superimposed on data at a reference temperature T_0 using a time scale multiplicative shift factor a_T and a much smaller modulus scale multiplicative shift factor b_T:

$$G(t, T) = b_T G\left(\frac{t}{a_T}, T_0\right). \tag{8.122}$$

The reference temperature T_0 can be chosen to be any convenient temperature, such as a temperature where the liquid is used or the glass transition temperature of the liquid. Equation (8.119) determines the time scale shift factor,

$$a_T = \frac{\zeta T_0}{\zeta_0 T}, \tag{8.123}$$

where ζ_0 is the friction coefficient at the reference temperature T_0. This time scale shift factor describes the (model independent) temperature dependence of diffusion coefficient:

$$\frac{D(T_0)}{D(T)} = \frac{\zeta T_0}{\zeta_0 T} = a_T. \tag{8.124}$$

[9] The density of a liquid changes by about 10% when temperature is changed by 100 K.

The modulus scale shift factor is determined from Eq. (8.120),

$$b_T = \frac{\rho T}{\rho_0 T_0}, \tag{8.125}$$

where ρ_0 is the density at the reference temperature. Often, Eqs (8.123) and (8.125) do not work perfectly, and the shift factors are treated as adjustable parameters. The temperature dependence of the various dynamic properties can be calculated in terms of the shift factors a_T and b_T. For example, the temperature dependence of viscosity is given by their product (η_0 is the viscosity at the reference temperature):

$$\frac{\eta}{\eta_0} = \frac{\rho\zeta}{\rho_0\zeta_0} = a_T b_T. \tag{8.126}$$

Time–temperature superposition also applies to other linear viscoelastic data, with the same shift factors. Two examples are the complex modulus in oscillatory shear,

$$G^*(\omega, T) = b_T G^*(\omega a_T, T_0), \tag{8.127}$$

and the creep compliance:

$$J(t, T) = \frac{J((t/a_T), T_0)}{b_T}. \tag{8.128}$$

Using data on logarithmic scales, Eqs (8.122), (8.127), and (8.128) allow simple shifting of data at different temperatures to obtain superposition. The strong temperature dependence of the time (or frequency) scale shift factor a_T makes time–temperature superposition a valuable tool for extending the time (or frequency) range of data at a given temperature. The resulting superimposed curve is a **master curve** for that particular polymer at the chosen reference temperature.

An example of time–temperature superposition is shown in Fig. 8.15 for a poly(vinyl methyl ether) (PVME) melt at a reference temperature of $T_0 = -24\,^\circ\mathrm{C}$. Data for G' and G'' were measured as a function of frequency roughly in the range $10^{-2}\,\mathrm{rad\,s^{-1}} < \omega < 10^{2}\,\mathrm{rad\,s^{-1}}$ at six temperatures (shown in the right-hand side of Fig. 8.14). $T_0 = T_g = -24\,^\circ\mathrm{C}$ was selected as the reference temperature and the data at the five other temperatures were superimposed to make the master curve on the left-hand side of Fig. 8.15. In practice, this shifting is first applied to the temperatures closest to T_0, and data sets at temperatures further from T_0 are subsequently added to build up the master curve. The master curve on the left-hand side of Fig. 8.15 has the rheological response at the reference temperature for over 11 decades in frequency! These data extend from the **glassy modulus** G_g at high frequencies all the way to the terminal response (with $G' \sim \omega^2$ and $G'' \sim \omega$) at low frequencies, thereby characterizing the full linear viscoelastic response of this polymer melt. The longest relaxation time is estimated as the reciprocal of the lowest frequency where $G' = G''$. Figure 8.15 shows that this relaxation time is $\tau \cong 2 \times 10^7\,\mathrm{s}$. To directly

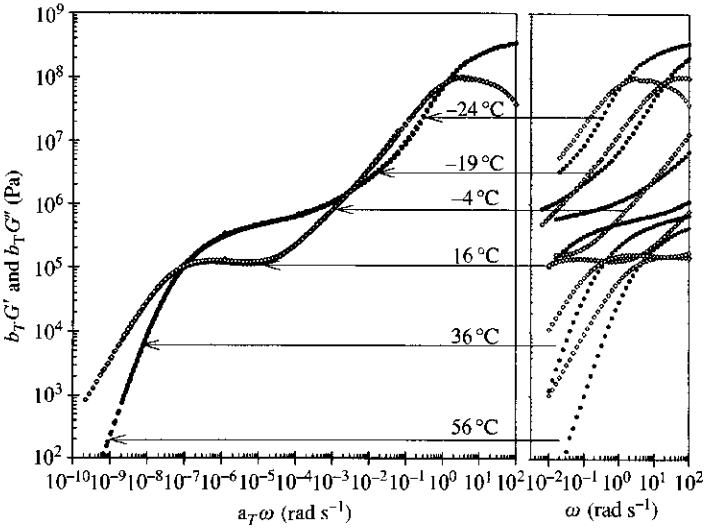

Fig. 8.15
Demonstration of the time–temperature superposition principle, using oscillatory shear data (G', filled circles and G'', open diamonds) on a PVME melt with $M_w = 124\,000$ g mol^{-1}. The right-hand plot shows the data that were acquired at the six temperatures indicated, with $T_g = -24\,°C$ chosen as the reference temperature. All data were shifted empirically on the modulus and frequency scales to superimpose, constructing master curves for G' and G'' in the left-hand plot. Data and plot courtesy of J. A. Pathak.

probe this frequency at the reference temperature of $T_0 = T_g = -24\,°C$, one complete oscillation period would take $2\pi\tau \cong 10^8\,s \cong 4$ years! Even graduate students are not so patient. Experiments in the frequency range $10^{-2}\,rad\,s^{-1} < \omega < 10^2\,rad\,s^{-1}$ can be done in 2 h (allowing time for thermal equilibration) so the six temperatures studied in Fig. 8.15 can easily be measured in one day by a properly motivated graduate student.

The temperature dependence of the friction coefficient is not very well understood. The simplest model is a thermally activated **Arrhenius equation**:

$$\eta \sim \exp\left(\frac{E_a}{kT}\right). \tag{8.129}$$

The activation energy for flow E_a is a constant at sufficiently high temperatures (typically more than 100 K above the glass transition). At these high temperatures where Eq. (8.129) applies, the activation energy is usually in the range $2kT < E_a < 20kT$. At lower temperatures, the density of the liquid becomes high enough that monomers get in each others way when they try to move.

One simple way to account for this crowding is based on the concept of **free volume**. The molecules in the liquid 'occupy' the vast majority of the liquid's volume V, partly as the atoms that make up the molecules and partly as inaccessible volume that is blocked from access by steric factors. The remaining small fraction of the volume fV is 'free' to be used for molecular motion. As the liquid is cooled, the density increases and the free volume decreases. This slows molecular motion and increases the effective activation energy for flow. The **Doolittle equation** relates the viscosity to the fraction f of the liquid's volume that is free,

$$\eta \sim \exp\left(\frac{B}{f}\right), \tag{8.130}$$

where B is an empirical constant of order unity. The Doolittle equation effectively assumes that the activation energy for flow is reciprocally related to the fractional free volume f. The simplest assumption is that the free volume should have a linear temperature dependence,

$$f = \alpha_f (T - T_\infty). \tag{8.131}$$

where α_f is the thermal expansion coefficient of the free volume (a constant with dimensions of reciprocal temperature) and T_∞ is the **Vogel temperature** where the free volume is zero. The Vogel temperature is typically about 50 K below the glass transition (see Table 8.3). At the glass transition, most polymers have roughly the same free volume:

$$f_g \cong 0.025 \quad \text{at } T_g. \tag{8.132}$$

The Doolittle equation [Eq. (8.130)] can be combined with the assumed linear temperature dependence of free volume [Eq. (8.131)] to get the **WLF equation**, so-named for Williams, Landel, and Ferry, who first applied it to polymer melts in 1955:

$$\frac{\eta}{\eta_0} = \exp\left(B\left[\frac{1}{f} - \frac{1}{f_0}\right]\right) \tag{8.133}$$

$$= \exp\left(\frac{B}{\alpha_f}\left[\frac{1}{T - T_\infty} - \frac{1}{T_0 - T_\infty}\right]\right)$$

$$= \exp\left(\frac{B}{\alpha_f}\left[\frac{T_0 - T}{(T - T_\infty)(T_0 - T_\infty)}\right]\right)$$

$$= \exp\left(\frac{B}{f_0}\frac{(T_0 - T)}{(T - T_\infty)}\right). \tag{8.134}$$

The final result used Eq. (8.131) for the free volume f_0 at the reference temperature T_0. This 'derivation' relies on several unsubstantiated assumptions [most notably Eqs (8.130) and (8.131)] and hence the WLF equation is a phenomenological description of the temperature dependence of viscosity.

In practice, the small modulus scale shift is often ignored and the time (or frequency) scale shift factor a_T is directly fit to Eq. (8.134) instead of the viscosity ratio [effectively assuming $b_T = 1$ in Eq. (8.126)]. A plot of $\log a_T$ (or $\log[\eta/\eta_0]$) against $(T - T_0)/(T - T_\infty)$ is prepared using the Vogel temperature T_∞ to linearize the plot and the constant B/f_0 is determined from the slope. An example of a linearized Vogel plot is shown in Fig. 8.16 for high molar mass linear chain melts of poly(vinyl methyl ether). The WLF equation provides a good description of the temperature dependence of dynamics for non-crystalline polymers in the temperature range $T_g < T < T_g + 100$ K. The choice of reference temperature is completely arbitrary, but often it is chosen to be T_g and then the free volume in Eq. (8.134) is f_g.

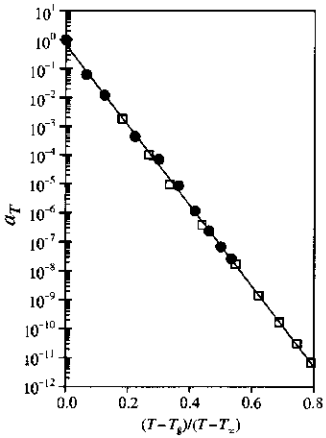

Fig. 8.16
Vogel plot used to determine the coefficients of the WLF equation, using data for high molar mass linear PVME melts. Open squares are data of R. M. Kannan and T. P. Lodge, *Macromolecules* **30**, 3694 (1997) and filled circles are data of J. A. Pathak *et al.*, *Macromolecules* **32**, 2553 (1999). The Vogel temperature T_∞ is adjusted to make this plot linear and B/f_g is determined from the slope.

8.7.2 Transition zone of polymer melts

The transition zone is the range of frequency (or time) over which the storage modulus (or stress relaxation modulus) changes from the glassy modulus to the modulus at the terminal relaxation time for unentangled polymer liquids. For entangled polymer liquids, such as the PVME melt in Fig. 8.15, the transition zone is the range over which the modulus changes from the rubbery plateau modulus to the glassy modulus ($0.003\,\mathrm{rad\,s^{-1}} < a_T\omega < 100\,\mathrm{rad\,s^{-1}}$ in Fig. 8.15).

The low-frequency end of the transition zone is qualitatively described by the Rouse model of Section 8.4.1 with $G(t) \sim t^{-1/2}$ and $G'(\omega) \sim \omega^{1/2}$, and relaxation modes corresponding to coherent motion of many Kuhn monomers. The higher frequency part of the transition zone has a stronger frequency dependence of the storage modulus $G'(\omega) \sim \omega^{\alpha}$ with $\alpha > 1/2$. It is tempting to associate the part of the transition zone chracterized by the 3/4 power law frequency dependence of the storage modulus $G'(\omega) \sim \omega^{3/4}$ with the modes described by the semiflexible chain model of Section 8.6. Indeed, the $G'(\omega)$ data in the frequency range $0.003\,\mathrm{rad\,s^{-1}} < a_T\omega < 0.03\,\mathrm{rad\,s^{-1}}$ approximately obey the Rouse scaling and the $G'(\omega)$ data in the frequency range $0.03\,\mathrm{rad\,s^{-1}} < a_T\omega < 1\,\mathrm{rad\,s^{-1}}$ roughly show the semiflexible chain scaling.

However, the crossover between these two limiting regimes is not well understood, so there is no quantitative description of viscoelasticity for the entire transition zone. Quite generally, the crossover between various scaling regimes is fairly broad and caution must be used when trying to apply power laws in a crossover between regimes. The transition zone is even worse than most crossovers because dynamics of flexible polymers at small length scales (shorter than Kuhn monomer size b) start to be influenced by polymer-specific chemical details. Hence, the crossover from flexible to stiff modes in the transition zone is not universal—each monomer type has a distinct viscoelastic response. For a given monomer, the transition zone does not depend on either chain length or large-scale molecular architecture. The observed viscoelastic response typically has a frequency dependence that is intermediate between the Rouse and semiflexible chain limits $G(t) \sim t^{-\alpha}$ with $0.5 \leq \alpha \leq 0.75$.

Our discussion above focuses on intramolecular effects, but leaves out any intermolecular effects. Current ideas about relaxation in glass-forming liquids speculate that monomer motion is cooperative, involving multiple monomers collectively rearranging in a cooperative fashion. While there is some evidence for this cooperative motion, it is an area of active research that has not yet yielded a generally accepted model. Intermolecular constraints such as the requirement of cooperative relaxations may change the dynamic modulus at very high frequencies.

At still higher frequencies than the highest frequency in Fig. 8.14, polymer liquids exhibit a solid response, with storage modulus G' independent of frequency and equal to the glassy modulus G_g. A typical value of the glassy modulus is of order 10^9Pa (see Table 8.2). The glassy modulus

Table 8.2 Glassy modulus of amorphous polymers

Polymer	G_g (GPa)	T_g (K)
Polyisobutylene	2.4	203
1,4-Polyisoprene	1.5	210
Polypropylene	0.86	259
Polystyrene	1.1	373

is considerably larger than the starting value of the Rouse model $G(\tau_0) \approx kT/b^3$ of kT/v_0 which is of order 10^7 Pa.

This same glassy modulus describes the linear elastic response of the polymer at temperatures below its glass transition temperature T_g, [see Hooke's law, Eq. (7.98)]. The physical reason that the liquid's response becomes similar to that of the glass is that at such high frequencies (or short time scales) monomers (and even small parts of monomers) do not have time to move and relax stress.

8.7.3 Short linear polymer melts

The Rouse model describes the terminal viscoelastic response of polymer melts consisting of linear chains that are too short to form entanglements. For example, Eq. (8.53) describes the viscosity of such short linear polymer melts. However, the viscosity is proportional to the product of friction coefficient of a monomer and the number of monomers per chain. Isothermal viscosity data are *not* proportional to the number of monomers in the chain because the friction coefficient depends on chain length for short chains. Indeed, the glass transition temperature depends on chain length for melts of short chains. The physical reason is that the monomers near the chain ends have more free volume than monomers in the middle of the chain. Assuming Eq. (8.132) applies, there should be a lowering of the glass transition temperature that is proportional to the number density of chain ends ($2\rho \mathcal{N}_{Av}/M_n$), see Problem 8.31:

$$T_g = T_{g\infty} - \frac{C}{M_n}. \tag{8.135}$$

The constant C is typically in the range 10^4–10^5 K g mol^{-1}, which means that for long chains with $M_n > 10^4$–10^5 g mol^{-1}, the glass transition is practically independent of chain length, adopting its long chain limiting value $T_{g\infty}$. The physical significance of the constant C is that it is the molar mass at which the glass transition temperature is 1 K lower than the high molar mass limit $T_{g\infty}$. Representative values of C and $T_{g\infty}$ are listed in Table 8.3.

To test the Rouse prediction that viscosity is proportional to chain length, viscosity data at constant friction coefficient must be used instead of viscosity data at constant temperature. If the coefficient of thermal expansion of the free volume α_f in Eq. (8.131) were independent of chain

Table 8.3 Molar mass dependence of the glass transition temperature [see Eq. (8.136)] and WLF coefficients of high molar mass polymers [see Eq. (8.134) with $T_0 = T_g$]

Polymer	C (K g mol^{-1})	$T_{g\infty}$ (K)	B/f_g	T_∞ (K)
Polybutadiene	1.2×10^4	174	25.6	112
Poly(methyl methacrylate)	6.9×10^4	388	76.9	308
Polystyrene	1.7×10^5	373	30.3	325

length, the simplest procedure to compare viscosities at the same free volume and hence constant friction coefficient would be to measure viscosity at a certain temperature increment above the glass transition (constant $T - T_g$). However, α_f increases as the chains get shorter, precluding the use of a constant $T - T_g$ to attain a constant friction coefficient.[10]

The simplest way to correct viscosity data to constant friction coefficient is to first fit the temperature dependence of viscosity of each individual sample to the WLF equation [Eq. (8.134)], which determines B/f_0. At a given reference temperature, sufficiently long chains have the same B/f_0 and progressively lower values of B/f_0 are obtained for shorter chains, since they have more free volume at a given temperature. The viscosity data at the reference temperature can then be corrected to the friction coefficient of the long chains at the reference temperature using Eq. (8.133). Viscosity data subjected to such a correction are shown in Fig. 8.17 for polybutadiene, polyisobutylene and polystyrene, roughly 120 K above their glass transitions. All linear polymer melts have viscosity proportional to molar mass ($\eta \sim M$) for sufficiently short chains, when the data are determined at a constant friction coefficient as opposed to isothermal data. Longer chains have entanglement effects (discussed in Chapter 9) and have $\eta \sim M^{3.4}$. The full chain length dependence of the viscosity (at constant friction coefficient) of all three polymers are quantitatively described by a simple crossover function:

$$\eta \sim \zeta M \left[1 + \left(\frac{M}{M_c}\right)^{2.4}\right]. \tag{8.136}$$

Equation (8.136) is tested in Fig. 8.17 (solid curves) and found to describe the molar mass dependence of constant friction coefficient viscosity data for all three of these linear polymers. The **critical molar mass** M_c for entanglement effects in viscosity is always a factor of 2–4 larger than the entanglement molar mass M_e that was defined in Eq. (7.47).

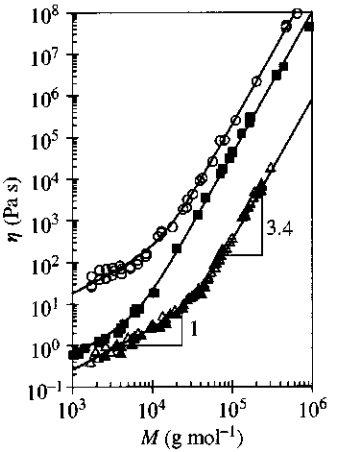

Fig. 8.17
Viscosity data for three linear polymers corrected to the friction coefficient of high molar mass polymer at roughly $T_g + 120$ K, fit to Eq. (8.137) (curves). Open circles are polyisobutylene ($T = 50\,^\circ$C) with $M_c = 14\,000$ g mol^{-1}. filled squares are polybutadiene ($T = 25\,^\circ$C) with $M_c = 6700$ g mol^{-1}. open triangles are free radically prepared polystyrene ($T = 217\,^\circ$C), and filled triangles are anionically prepared polystyrene ($T = 217\,^\circ$C) with $M_c = 35\,000$ g mol^{-1}. Polybutadiene data are from R. H. Colby *et al.*, *Macromolecules* **20**, 2226 (1987). Polyisobutylene and polystyrene data are from T. G. Fox *et al.*, *J. Am. Chem. Soc.* **70**, 2384 (1948), *J. Phys. Chem.* **55**. 221 (1951), and *J. Chem. Phys.* **41**. 344 (1964).

8.8 Randomly branched polymers

As an illustration of the Rouse model, consider the polydisperse mixture of polymers produced by random branching with short chains between branch points. The molar mass distribution and size of the branched polymers in this critical percolation limit were discussed in Section 6.5. Close to the gel point, some very large branched polymers (with $M > 10^6$) are formed and the intuitive expectation is that such large branched polymers would be entangled. However, recall that hyperscaling requires polymers of a given size in the critical percolation class only overlap with shorter molecules. Since these shorter polymers relax much more rapidly, each polymer relaxes with no effective topological constraints.

[10] The thermal expansion coefficient of the free volume α_f for the shortest polybutadiene chains in Fig. 8.17 is larger than the long chain value by a factor of 1.4.

Unfortunately, there is no accurate theoretical estimate of the strength of hydrodynamic interaction or the extent of hydrodynamic screening of polydisperse branched polymers. Hydrodynamic screening usually correlates well with excluded volume screening. As was demonstrated in Chapter 6, excluded volume interactions are partially screened in the critical percolation limit. Therefore, at least partial screening of hydrodynamic interactions might be expected in these systems. Experiments indicate that hydrodynamic interactions are completely screened in melts of polydisperse branched polymers near the gel point and they can be described by the Rouse model.

Regardless of its complex architecture, any polymer relaxing with no topological constraints and no hydrodynamic interactions is well-represented by the Rouse model, with friction proportional to molar mass. To estimate the terminal response of randomly branched polymers, we apply this reasoning to the characteristic polymers, with size ξ consisting of N^* monomers. The diffusion coefficient of these chains is given by the Einstein relation [Eq. (8.4)]:

$$D_R \approx \frac{kT}{N^*\zeta}. \tag{8.137}$$

Equation (8.137) is perfectly analogous to Eq. (8.12) for a linear polymer (in both cases ζ is the friction coefficient of a single monomer). The Rouse relaxation time of this characteristic polymer, τ^* will be the longest relaxation time in the ensemble of branched polymers. It is determined as the time required for the characteristic polymer to move a distance of order of its own size ξ:

$$\tau^* \approx \frac{\xi^2}{D_R} \approx \frac{\zeta}{kT} N^* \xi^2. \tag{8.138}$$

Equation (8.138) is perfectly analogous to Eq. (8.13) for a linear polymer. This simple argument for the relaxation time will require the relaxation time to be proportional to the product of degree of polymerization and the square of size for the Rouse model of *any* polymer. The scaling of the characteristic polymer's degree of polymerization is $N^* \sim |\varepsilon|^{-1/\sigma}$ with $\sigma \cong 0.45$ [Eq. (6.95)] and the scaling of its size is $\xi \sim |\varepsilon|^{-\nu}$, where $\nu \cong 0.88$ is the critical exponent for the correlation length ξ near the gel point [Eq. (6.125)]. These power laws determine the divergence of the longest relaxation time as the gel point is approached (as the relative extent of reaction $\varepsilon \to 0$):

$$\tau^* \sim |\varepsilon|^{-(2\nu+1/\sigma)} \sim |\varepsilon|^{-4.0}. \tag{8.139}$$

The value of the relaxation modulus at this terminal relaxation time is of order kT per characteristic polymer. The hyperscaling ideas discussed in Section 6.5.3 require that the characteristic polymers are just at their

overlap concentration (they are space-filling but not overlapping). Hence, the Rouse terminal modulus [Eq. (7.93) with $P = 1$] is

$$G(\tau^*) \approx \frac{kT}{\xi^3} \sim |\varepsilon|^{3\nu} \sim |\varepsilon|^{2.6}, \tag{8.140}$$

and the viscosity is the product of this modulus and the relaxation time [Eq. (7.120)].

$$\eta \approx G(\tau^*)\tau^* \sim |\varepsilon|^{\nu-1/\sigma} \sim |\varepsilon|^{-1.3}. \tag{8.141}$$

In practice, the gel point is often difficult to determine with sufficient precision to test these scaling laws. Instead, viscosity and relaxation time can be correlated with weight-average molar mass ($M_w \sim |\varepsilon|^{-\gamma}$ with $\gamma \cong 1.82$) [Eq. (6.103)]:

$$\eta \sim M_w^{(1/\sigma-\nu)/\gamma} \sim M_w^{0.75}, \tag{8.142}$$

$$\tau^* \sim M_w^{(2\nu+1/\sigma)/\gamma} \sim M_w^{2.2}. \tag{8.143}$$

Comparison of these prediction with experimental data on randomly branched polyesters is shown in Fig. 8.18. The line in part (a) has the slope of 0.75 expected by Eq. (8.142) and the line in part (b) has a slope of 2.28 which is slightly larger than the value expected by Eq. (8.143). The agreement is quite good, and indicates that the Rouse model applies to these polymers up to weight-average molar masses exceeding 10^6 g mol^{-1}.

The Rouse relaxation time τ_R of a branched polymer of N monomers with size R is a generalization of Eq. (8.138):

$$\tau_R \approx \frac{\zeta}{kT} N R^2 \approx \frac{\zeta b^2}{kT} N^{1+2/\mathcal{D}} \approx \tau_0 N^{1+2/\mathcal{D}}. \tag{8.144}$$

The final relation uses the fractal dimension of the randomly branched polymer, which is $\mathcal{D} \cong 2.53$ for critical percolation in three dimensions. The fact that randomly branched polymers are fractal means that the size r of a polymer section has the same dependence on the number g of

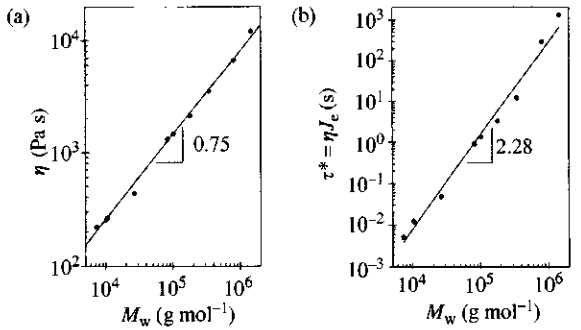

Fig. 8.18
Viscosity (a) and longest relaxation time (b) of randomly branched polyesters with average degree of polymerization between branch points of $N_0 = 2$, at $T = T_g + 64$ K. Data are from C. P. Lusignan *et al.*, *Phys. Rev. E* **52**, 6271 (1995).

monomers in the section $r \approx bg^{1/\mathcal{D}}$ as the size R and degree of polymerization N of the whole polymer $R \approx bN^{1/\mathcal{D}}$ (see Section 1.4). The Rouse model of randomly branched polymers exhibits **fractal dynamics**: the relaxation time $\tau(g)$ of a polymer section of g monomers has the same dependence on the number of monomers g as the whole chain [Eq. (8.144)]:

$$\tau(g) \approx \tau_0 g^{1+2/\mathcal{D}}. \tag{8.145}$$

At time $t = \tau(g)$ smaller randomly branched polymers with degree of polymerization $N < g$ are almost completely relaxed, while larger branched polymers with degree of polymerization $N > g$ consist of N/g unrelaxed sections of size r, each storing elastic energy of order kT. The time dependence of the number of monomers g in these crossover sections is obtained from (Eq. 8.145):

$$g \approx \left(\frac{t}{\tau_0}\right)^{1/(1+2/\mathcal{D})}. \tag{8.146}$$

Equation (8.140) states that the terminal modulus $G(\tau^*)$ is kT per characteristic polymer. Hyperscaling also requires polymers of a given size r and sections of larger polymers of the same size to be just at their overlap concentration, so their pervaded volumes r^3 densely fill all space. This means that Eq. (8.140) can be generalized for the stress relaxation modulus at the time scale where each chain section of size r relaxes:

$$G(t) \approx \frac{kT}{r^3} \approx \frac{kT}{b^3} g^{-3/\mathcal{D}} \approx \frac{kT}{b^3}\left(\frac{t}{\tau_0}\right)^{-3/(\mathcal{D}+2)} \quad \text{for } \tau_0 < t < \tau^*. \tag{8.147}$$

The stress relaxation modulus decays as a power law in time with exponent $3/(\mathcal{D}+2) \cong 0.66$. This power law dependence continues up to the longest relaxation time τ^* of the characteristic branched polymer. At the gel point this power law extends forever because τ^* diverges [see Eq. (8.139)].

For oscillatory shear, Eqs (7.149) and (7.150) allow calculation of the intermediate frequency behaviour of storage and loss moduli of randomly branched polymers below the gel point:

$$G'(\omega) \sim G''(\omega) \sim \omega^{3/(\mathcal{D}+2)} \quad \text{for } 1/\tau^* < \omega < 1/\tau_0. \tag{8.148}$$

This power law character extends over the entire frequency range $\omega < 1/\tau_0$ at the gel point, where τ^* diverges. Critical percolation expects $\mathcal{D} \cong 2.53$, so the storage and loss moduli at the gel point are parallel power laws with exponent $3/(\mathcal{D}+2) \cong 0.66$. The loss tangent at the gel point is

$$\tan\delta \equiv \frac{G''}{G'} = \tan\left(\frac{3\pi}{2(\mathcal{D}+2)}\right) \cong 1.70, \tag{8.149}$$

for all sufficiently small frequencies ($\omega < 1/\tau_0$). The frequency dependence of storage and loss moduli for unentangled randomly branched polymers are compared with the predictions of the Rouse model in Fig. 8.19 (see Problem 8.35 for the full functional form).

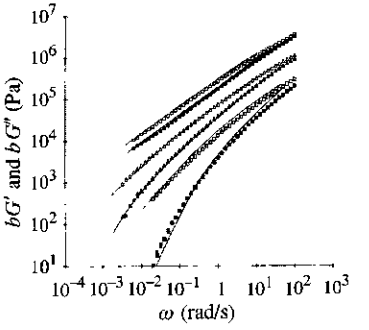

Fig. 8.19
Storage modulus (filled symbols) and loss modulus (open symbols) for three randomly branched polyesters 41 K above their glass transition temperature. Squares have $M_w = 57\,000\ \mathrm{g\,mol^{-1}}$ ($b = 1$), triangles have $M_w = 380\,000\ \mathrm{g\,mol^{-1}}$ ($b = 3$), and the circles correspond to a sample extremely close to the gel point ($b = 10$). The curves are predictions from fractal dynamics based on the Rouse model.

8.9 Dynamic scattering

Scattering techniques for measuring various static and thermodynamic properties of polymers, such as molar mass, size, conformations, interaction parameters, etc. were described in experimental sections of Chapters 1–5. In addition to static properties, scattering can provide important information about dynamic properties of polymeric systems. This section focuses on dynamic scattering from dilute solutions, but similar methods are used in semidilute and concentrated solutions.[11]

The instantaneous scattering intensity $I(q, t)$ at wavevectors of magnitude q [see Eq. (2.131)] depends on the spacial arrangement of scattering centres (positions and conformations of molecules) at time t. As molecules move, changing their conformations and locations in space, the scattering intensity $I(q, t)$ fluctuates in time [see Fig. 8.20(a)]. The value of scattering intensity, averaged over a long time interval t, is the static scattering intensity $I(q)$ discussed in Chapters 1–5:

$$I(q) = \langle I(q,0)\rangle \equiv \lim_{t\to\infty} \frac{1}{t}\int_0^t I(q,t')\,\mathrm{d}t'. \tag{8.150}$$

Fluctuations of the instantaneous scattering intensity $I(q,t)$ about its average value $I(q)$ contain information about polymer dynamics on the length scale $1/q$. In order to extract this information it is useful to consider a memory of the instantaneous intensity $I(q,t'')$ at time t'' that still remains after an elapsed time t (at time $t''+t$). This memory is defined mathematically through a **time autocorrelation function** [see Fig. 8.20(b)]:

$$\langle I(q,0)I(q,t)\rangle \equiv \lim_{t'\to\infty} \frac{1}{t'}\int_0^{t'} I(q,t'')I(q,t''+t)\,\mathrm{d}t''. \tag{8.151}$$

At $t = 0$, the autocorrelation function $\langle [I(q,0)]^2\rangle$ is the mean-square value of the intensity. The limiting value of the autocorrelation function at times much longer than the correlation time τ is the square of the average intensity because the values of $I(q,0)$ and $I(q,t)$ are independent of each other for $t \gg \tau$:

$$\lim_{t\to\infty}\langle I(q,0)I(q,t)\rangle = \langle I(q,0)\rangle\langle I(q,t)\rangle = \langle I(q,0)\rangle^2. \tag{8.152}$$

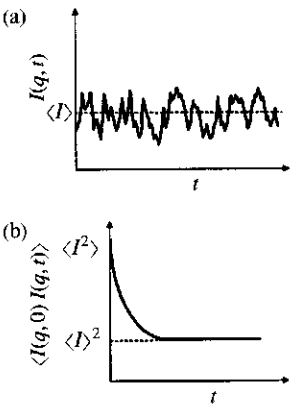

Fig. 8.20
(a) Intensity of scattered light as a function of time. (b) Time autocorrelation function of the scattered intensity as a function of time.

[11] Here we only consider dynamic scattering from isotropic solutions.

Hence, the autocorrelation function always decays from the mean of the squared static intensity to the square of the mean intensity [see Fig. 8.20(b)]. In the simplest case of a single relaxation mode, the time autocorrelation function decays like a single exponential with correlation time τ:

$$\langle I(q,0)I(q,t)\rangle = \langle I(q,0)\rangle^2 + [\langle [I(q,0)]^2\rangle - \langle I(q,0)\rangle^2]\exp\left(-\frac{t}{\tau}\right). \tag{8.153}$$

The memory of the initial intensity $I(q, 0)$ decays at the correlation time τ.

The autocorrelation function depends on how molecules move and rearrange on length scales $1/q$ during time t. Therefore, the correlation time τ is expected to depend on q.

Scattering from dilute solutions was discussed in Section 3.5. The intermolecular scattering regime was defined for reciprocal wavevectors $1/q$ larger than the distance between molecules. In this regime the scattering intensity is proportional to the square of the difference in the number of molecules in the neighbouring volumes q^{-3}. The average of the square of this difference determines the static scattering intensity [Eq. (3.126)]. The time variations in the scattering intensity are directly related to the time variations in the number of molecules in volumes q^{-3}. The memory of the number of molecules in a given volume q^{-3} persists as long as most of the molecules that were in this volume initially did not have time to leave it. The correlation time τ is therefore of the order of the time required for molecules to diffuse out of the volume. Since the diffusion distance is q^{-1}, the correlation time is $\tau \approx (q^{-1})^2/D$ [Eq. (8.1)]. A more careful analysis of the problem determines the numerical prefactor:

$$\tau = \frac{1}{2q^2D}. \tag{8.154}$$

Hence, the time autocorrelation function provides a direct means to determine the diffusion coefficient D in dilute monodisperse solutions:

$$\langle I(q,0)\ I(q,t)\rangle = \langle I(q,0)\rangle^2 + [\langle [I(q,0)]^2\rangle - \langle I(q,0)\rangle^2]\exp\ (-2q^2Dt). \tag{8.155}$$

In practice, the autocorrelation function is fit to a simple expression with three fitting parameters—the amplitude A, the base line B and the diffusion coefficient D:

$$\langle I(q,0)I(q,t)\rangle = [A\exp(-q^2Dt)]^2 + B. \tag{8.156}$$

It is crucial to realize that the baseline at long times has to equal the square of the mean static intensity ($B = \langle I(q,0)\rangle^2$). If this criterion is not realized, then artefacts such as dust are influencing the data! Another criterion

for proper measurement of the diffusion coefficient is to make sure that it is independent of q by following the intensity correlations at different scattering angles.

The diffusion coefficients of dilute solutions of polystyrene in toluene are plotted in Fig. 8.20. Data on dilute solutions of flexible polymers obey Eq. (8.23). The data in Fig. 8.21 exhibit the expected crossover from θ-solvent scaling ($\nu = 1/2$) at low molar masses where the coils are smaller than the thermal blob to athermal solvent scaling ($\nu = 0.588$) at high molar masses where there are many thermal blobs per chain.

The hydrodynamic radius of polymers can be obtained from the measured diffusion coefficients in dilute solution and the known solvent viscosity η_s using the Stokes–Einstein relation [Eq. (8.9)]:

$$R_h = \frac{kT}{6\pi\eta_s D} = \frac{kTq^2\tau}{3\pi\eta_s}. \tag{8.157}$$

Toluene at 25 °C has a viscosity $\eta_s \cong 5.6 \times 10^{-4}$ Pa s and Fig. 8.21 shows that polystyrene with $M_w = 10^6$ g mol^{-1} has diffusion coefficient $D \cong 1.3 \times 10^{-11}$ m^2 s^{-1}. Equation (8.157) determines the hydrodynamic radius of this polymer to be $R_h \cong 30$ nm. A typical wavevector in a light scattering experiment is $q \approx 10^7$ m^{-1} the correlation time is $\tau \approx 0.38$ ms.

Experimental results for the ratio R_g/R_h are compared with expectations based on the Zimm model for various polymer structures in Table 8.4. In general, increasing the density of monomers decreases the ratio R_g/R_h towards the value for hard spheres of $R_g/R_h = \sqrt{3/5} \cong 0.77$ (see Table 2.4), as seen by increasing the number f of arms in a star polymer, for instance. Experiment shows that the $f = 270$-arm star polymer is practically in the hard sphere limit (see Table 8.4), owing to crowding. Large generation number dendrimers also correspond to the hard sphere limit. Increasing the solvent quality generally increases R_g/R_h. Polydispersity also increases the ratio R_g/R_h, and randomly branched polymers near their

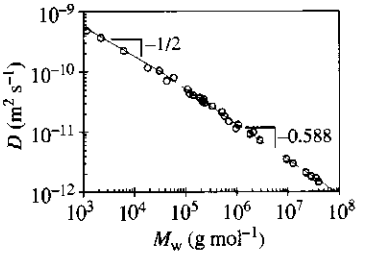

Fig. 8.21
Diffusion coefficient from dynamic light scattering for dilute polystyrene solutions in the good solvent toluene (open circles). The lines show the limiting power laws with slopes expected by Eq. (8.23) ($\nu = 1/2$ inside the thermal blob and $\nu = 0.588$ at higher molar masses). The lines cross at $M_w \approx 30\,000$ g mol^{-1}, consistent with the molar mass inside a thermal blob estimated from intrinsic viscosity of polystyrene in toluene in Fig. 8.3. Data from D. W. Schaefer and C. C. Han, in *Dynamic Light Scattering* (R. Pecora, editor) Plenum, New York (1985).

Table 8.4 Ratio of radius of gyration and hydrodynamic radius for different polymer architectures

Polymer structure	Solvent	R_g/R_h Zimm theory	R_g/R_h experiment
Randomly branched	Good	—	2.0
Linear monodisperse	Good	1.6	1.5
Randomly branched	θ	1.7	—
Linear $M_w/M_n = 2$	θ	1.7	—
Linear monodisperse	θ	1.5	1.3
3-Arm star	θ	1.4	1.2
4-Arm star	θ	1.3	1.05
12-Arm star	θ	1.17	0.93
18-Arm star	θ	1.14	0.82
270-Arm star	θ	1.08	0.77
Hard sphere	—	0.77	0.77

gel point (with very large polydispersity) in good solvent have the largest $R_g/R_h \cong 2.0$.

The experimental values of R_g/R_h are always smaller than the theoretical estimates, indicating that the Zimm model underestimates the hydrodynamic radius. More recent calculations predict R_g/R_h in far better agreement with experiment (for example, linear chains are predicted by Oono[12] to have $R_g/R_h \cong 1.56$ in good solvent have $R_g/R_h \cong 1.24$ in θ-solvent).

In polydisperse solutions, the decay of the autocorrelation function is not a single exponential and it is challenging to extract the distributions of diffusion coefficients and sizes from the non-exponential decay of the intensity correlations. In the case of a bidisperse distribution with diffusion coefficients that differ by at least a factor of 2, it is possible to fit the decay of the intensity correlations by a sum of two exponentials and obtain the corresponding sizes and relative concentrations of the two components:

$$\langle I(q,0)I(q,t)\rangle = [A_1 \exp(-q^2 D_1 t) + A_2 \exp(-q^2 D_2 t)]^2 + B. \quad (8.158)$$

The coefficients A_1 and A_2 are proportional to the relative concentrations of the two components present in the bidisperse solution.[13] The intensity autocorrelation function $\langle I(q,0)\ I(q,t)\rangle$ is fit to the *square* of the sum of modes because it can be related to the square of the electric field autocorrelation function $\langle E^*(q,0)\ E(q,t)\rangle$:

$$\begin{aligned}\langle I(q,0)\ I(q,t)\rangle &\sim \langle |E(q,0)|^2 |E(q,t)|^2\rangle \\ &\approx \langle |E(q,0)|^2\rangle^2 + \langle E^*(q,0)\, E(q,t)\rangle^2. \end{aligned} \quad (8.159)$$

Equation (8.159) is strictly valid for a Gaussian distribution of electric fields. The electric field autocorrelation function is related to the **dynamic structure factor** $S(q,t)$ [compare it with the static scattering function $S(q)$ in Eq. (3.121)]:

$$\begin{aligned}\langle E^*(q,0)\ E(q,t)\rangle &\sim S(q,t) \\ &\equiv \frac{1}{n}\sum_{j=1}^{n}\sum_{k=1}^{n}\langle \exp[-i\vec{q}\cdot(\vec{r}_j(t) - \vec{r}_k(0))]\rangle. \end{aligned} \quad (8.160)$$

The number of monomers in the scattering volume (see Section 1.7.2) is n and $\vec{r}_j(t)$ is the position of monomer j at time t. The dynamic structure factor of a bidisperse solution can be represented as a sum of two modes [Eq. (8.158)].

In the case of a more general polydispersity, the time autocorrelation function corresponds to the sum of many modes:

$$\langle I(q,0)\ I(q,t)\rangle = \left[\sum_i A_i \exp(-q^2 D_i t)\right]^2 + B. \quad (8.161)$$

[12] Y. Oono, *J. Chem. Phys.* **79**, 520 (1983) and *Adv. Chem. Phys.* **61**, 301 (1985).
[13] $c_1/c_2 = A_1/A_2$, where c_i is the concentration of species i.

In a continuous representation it can be written as a Laplace transform of the distribution $A(\Gamma)$ of decay rates $\Gamma = q^2 D$:

$$\langle I(q,0)\, I(q,t)\rangle = \left[\int_0^\infty A(\Gamma)\exp(-\Gamma t)\,\mathrm{d}\Gamma\right]^2 + B. \tag{8.162}$$

Determination of the distribution of modes $A(\Gamma)$ and the related distribution of sizes requires inversion of the Laplace transform, which is an ill-defined problem for a limited data set containing any noise. There are some numerical programs (such as CONTIN©) that attempt to perform this inverse transformation. The resulting distributions do sometimes (but not always) correlate (but not coincide) with the actual distribution of hydrodynamic radii in solution.

Dynamic modes of semidilute solutions can also be studied using dynamic scattering. The dynamic structure factors $S(q, t)$ of these more complicated systems still have a simple diffusive behaviour at low values of the wavevector q [Eqs (8.156), (8.159), and (8.160)]:

$$S(q,t) = S(q,0)\exp(-q^2 D t) \quad \text{for } qR < 1. \tag{8.163}$$

However, for non-dilute systems, the diffusion coefficient obtained from the low q time dependence of $S(q, t)$ may not be the diffusion coefficient of the polymers. For example, in semidilute solutions the dominant decay in $S(q, t)$ corresponds to correlations disappearing at the scale of the correlation length. In such cases, the diffusion coefficient is called the **cooperative diffusion coefficient.**

The logarithm of the ratio of the dynamic structure factor and the static structure factor is linear in time for diffusive motion described by a single diffusion coefficient:

$$\ln\left[\frac{S(q,t)}{S(q,0)}\right] = -q^2 D t \approx -q^2\langle[r(t) - r(0)]^2\rangle \quad \text{for } qR < 1. \tag{8.164}$$

The mean-square displacement of the monomers is diffusive [Eq. (8.1)] on large length scales ($qR < 1$) corresponding to times longer than the relaxation time:

$$\langle[r(t) - r(0)]^2\rangle \approx Dt. \tag{8.165}$$

Dynamic scattering can also provide information about relaxation modes of polymers at higher values of the wavevector q ($qR > 1$). Equation (8.164) can be generalized to higher wavevectors and to semidilute and concentrated solutions by noticing that the decay of the dynamic structure factor is determined by the ratio of mean-square monomer displacement and the square of the reciprocal wavevector $(1/q)^2$:

$$\ln\left[\frac{S(q,t)}{S(q,0)}\right] \approx -q^2\langle[r(t) - r(0)]^2\rangle. \tag{8.166}$$

For the Rouse model the mean-square displacement is proportional to the square root of time [Eq. (8.58)]. The logarithm of the dynamic structure factor of the Rouse model then also scales as the square root of time for $\tau_0 < t < \tau_R$:

$$\ln\left[\frac{S(q,t)}{S(q,0)}\right] \approx -q^2 b^2 \left(\frac{t}{\tau_0}\right)^{1/2} \quad \text{for Rouse model } 1/R < q < 1/b. \tag{8.167}$$

For the Zimm model the mean-square displacement of monomers is faster [Eq. (8.70)] leading to the logarithm of the Zimm dynamic structure factor scaling as the 2/3 power of time for $\tau_0 < t < \tau_Z$:

$$\ln\left[\frac{S(q,t)}{S(q,0)}\right] \approx -q^2 b^2 \left(\frac{t}{\tau_0}\right)^{2/3} \quad \text{for Zimm model } 1/R < q < 1/b. \tag{8.168}$$

More generally, dynamic scattering methods are used to study many aspects of polymer dynamics. Full discussion of those methods is beyond the scope of this book.

8.10 Summary of unentangled dynamics

The Rouse model is the simplest molecular model of polymer dynamics. The chain is mapped onto a system of beads connected by springs. There are no hydrodynamic interactions between beads. The surrounding medium only affects the motion of the chain through the friction coefficient of the beads. In polymer melts, hydrodynamic interactions are screened by the presence of other chains. Unentangled chains in a polymer melt relax by Rouse motion, with monomer friction coefficient ζ. The friction coefficient of the whole chain is $N\zeta$, making the diffusion coefficient inversely proportional to chain length:

$$D_R = \frac{kT}{N\zeta}. \tag{8.169}$$

In contrast, the Zimm model considers the motion of beads (or monomers) to be hydrodynamically coupled with other monomers. Both the polymer and the solvent molecules within the pervaded volume of the chain move together in dilute solutions. The diffusion coefficient of a chain in the Zimm model is of the same form as the Stokes–Einstein relation [Eq. (8.9)] for diffusion of a colloidal particle in a liquid:

$$D_Z \approx \frac{kT}{\eta_s R}. \tag{8.170}$$

The intrinsic viscosity of polymers in dilute solutions is an extremely important measure of the coil size, owing to its simplicity and precision. The Zimm model leads directly to the Fox–Flory equation for intrinsic

viscosity, which in turn leads to the Mark–Houwink equation:

$$[\eta] = \Phi \frac{R^3}{M} = KM^{3\nu-1}. \tag{8.171}$$

During their relaxation time τ, polymers diffuse a distance of order their own size ($\tau \approx R^2/D$). The relaxation times of the Rouse and Zimm models are then easily obtained from the diffusion coefficients:

$$\tau_R \approx \frac{\zeta N R^2}{kT} \approx \tau_0 N \left(\frac{R}{b}\right)^2 \quad \text{and} \quad \tau_Z \approx \frac{\eta_s R^3}{kT} \approx \tau_0 \left(\frac{R}{b}\right)^3. \tag{8.172}$$

The final relations are written in terms of the relaxation time of a monomer $\tau_0 \approx \eta_s b^3/kT \approx \zeta b^2/kT$. These relations are very general, and can be applied whenever the topological interactions, called entanglements (discussed in detail in Chapter 9), can be ignored.

In semidilute solutions, the hydrodynamic interactions affect dynamics only up to the scale of the hydrodynamic screening length, which is of the order of the correlation length. On length scales larger than the correlation length, both excluded volume and hydrodynamic interactions are screened by the presence of other chains. This screening becomes increasingly important as concentration is raised, and eventually the melt state is reached where hydrodynamic interactions are fully screened down to the scale of individual monomers. For unentangled chains in semidilute solution, the chain sections within a correlation volume relax by Zimm motion and the sections of chain larger than the correlation length relax by Rouse motion. The relaxation time of the chain in unentangled semidilute solution is our first (and the simplest) example of a hierarchy of relaxation processes. The correlation blob relaxes by Zimm motion on the time scale τ_ξ, while the whole chain relaxes as a Rouse chain of blobs at the time scale τ_{chain}:

$$\tau_\xi \approx \frac{\eta_s \xi^3}{kT} \approx \tau_0 \left(\frac{\xi}{b}\right)^3 \quad \text{and} \quad \tau_{chain} \approx \tau_\xi \left(\frac{N}{g}\right)^2 \approx \tau_0 \left(\frac{\xi}{b}\right)^3 \left(\frac{N}{g}\right)^2. \tag{8.173}$$

There are many examples of hierarchies of relaxation processes in Chapter 9.

The time-dependent viscoelastic response of polymers is broken down into individual modes that relax on the scale of subsections of the chain with N/p monomers. The Rouse and Zimm models have different structure of their mode spectra, which translates into different power law exponents for the stress relaxation modulus $G(t)$:

$$G(t) \approx \frac{kT}{b^3} \phi \left(\frac{t}{\tau_0}\right)^{-\kappa} \exp(-t/\tau). \tag{8.174}$$

The longest mode relaxes at time τ (τ_Z for the Zimm model, with exponent $\kappa = 1/(3\nu)$ and τ_R for the Rouse model, with exponent $\kappa = 1/2$). While the difference between these exponents is small, they can be measured quite precisely, allowing unambiguous identification of Rouse and Zimm motion.

Problems

Section 8.1

8.1 In unentangled polymer melts

(i) Are hydrodynamic interactions important or screened?
(ii) Which model describes dynamics?
(iii) Is the friction coefficient of the polymer proportional to the chain size R or the number of monomers in the chain N?

8.2 Consider a polymer chain represented by $N = 20$ beads connected by springs of root-mean-square size $b = 5\,\text{Å}$ diffusing in a melt of similar chains with bead friction coefficient $\zeta = 3 \times 10^{-10}\,\text{g s}^{-1}$ at 22 °C.

(i) What is the root-mean-square end-to-end distance R of this chain?
(ii) What is best model describing the dynamics of the chain in a melt? What is the friction coefficient of the chain?
(iii) What is the diffusion coefficient D of the chain?
(iv) Estimate the longest relaxation time τ of the chain.
(v) Estimate the viscosity of the melt.

Section 8.2

8.3 In dilute polymer solutions

(i) Are hydrodynamic interactions important or screened?
(ii) Which model describes dynamics?
(iii) Is the friction coefficient of the polymer proportional to the chain size R or the number of monomers in the chain N?

8.4 Consider a polymer chain represented by $N = 100$ beads connected by springs of root-mean-square size $b = 5\,\text{Å}$ in a dilute θ-solution at 22.5 °C with solvent viscosity $\eta_s = 0.6\,\text{cP} = 6 \times 10^{-3}\,\text{g (cm s)}^{-1}$.

(i) What is best model describing the dynamics of the chain in a dilute solution? What is the friction coefficient of the chain?
(ii) What is the diffusion coefficient D of the chain?
(iii) What is the longest relaxation time τ of the chain?
(iv) Estimate the specific viscosity $\eta_{sp} = (\eta - \eta_s)/\eta_s$ of a solution at volume fraction $\phi = 0.01$?

8.5 Comparison of polymer and solvent diffusion in dilute solution.

(i) Calculate the time scale for diffusion of a solvent molecule, initially located at the centre of a polymer's pervaded volume, to diffuse out of the pervaded volume. Assume the solvent is the same size b as a monomer.
(ii) Use the Zimm model to show that the time scale for the polymer to diffuse out of the same volume is a factor of N^{ν} longer than the solvent diffusion time.
(iii) Show that the ratio of diffusion coefficients of the polymer and the solvent is $N^{-\nu}$.
(iv) Why is the ratio of time scales (part ii) reciprocally related to the ratio of diffusion coefficients (part iii)?

Section 8.3

8.6 (i) Calculate the scaling predictions of the Rouse and Zimm models for the intrinsic viscosity $[\eta]$ and relaxation time τ of dilute solutions of a rigid rod polymer of length L.

(ii) Compare the calculated relaxation times in part (i) with the result for the rotational relaxation time of a rod in dilute solution that includes hydrodynamic interactions of monomers along the rod,

$$\tau = \frac{\pi \eta_s L^3}{3kT \ln (L/2b)}, \tag{8.175}$$

where b is the diameter of the rod.

(iii) Calculate Rouse and Zimm model predictions for $[\eta]$ and τ for a general fractal with fractal dimension $\mathcal{D}$ and show that the rigid rod limit and the ideal chain have the expected results when $\mathcal{D} = 1$ and $\mathcal{D} = 2$.

8.7 Intrinsic viscosity of a dendrimer

(i) Use the Fox–Flory equation to determine the intrinsic viscosity of a dendrimer of generation g, functionality f, and core functionality n, assuming that the degree of polymerization is given by Eq. (6.35) and the size increases linearly with generation number ($R = bg$).

(ii) Using monomer size $b = 7$ Å, a monomer mass of 100 g mol^{-1}, functionality $f = 3$, and core functionality $n = 6$, plot the intrinsic viscosity as a function of generation g from $g = 1$ to $g = 10$.

(iii) Qualitatively explain the shape of the plot in part (ii).

8.8 Derive the following general relation between intrinsic viscosity and overlap concentration:

$$c^* \approx \frac{1}{[\eta]}. \tag{8.176}$$

8.9 Estimate the specific viscosity at the overlap concentration using the following equations:

(i) Huggins equation [Eq. (1.97)] for good solvent with $k_H = 0.3$;
(ii) Huggins equation for θ-solvent with $k_H = 0.8$;
(iii) The Zimm model [Eq. (8.33)] for good solvent;
(iv) The Zimm model for θ-solvent;
(v) The Rouse model for semidilute unentangled solutions in good solvent [Eq. (8.98)];
(vi) The Rouse model for semidilute unentangled solutions in θ-solvent [Eq. (8.97)].

Hint: Remember $[\eta] \approx 1/c^*$.

Section 8.4

8.10 Calculate the stress relaxation modulus $G(t)$, valid for all times longer than the relaxation time of a monomer, for a monodisperse three-dimensional melt of unentangled flexible fractal polymers that have fractal dimension $\mathcal{D} < 3$. Assume complete hydrodynamic screening. *Hint*: Keep the fractal dimension general and make sure your result coincides with the Rouse model for $\mathcal{D} = 2$.

8.11 The Fox-Flory prefactor

The Zimm stress relaxation modulus has the same form as Eq. (8.55) with the Zimm relaxation times [Eqs. (8.26) and (8.61)] replacing the Rouse times.

(i) Show that the intrinsic viscosity can be expressed as a sum over the stress relaxation times

$$[\eta] = \frac{\mathcal{R}T}{\eta_s M} \sum_{p=1}^{\infty} \tau_p$$

(ii) Derive the Fox-Flory prefactor Φ of Eq. (8.37) in a θ-solvent from the Zimm stress relaxation times. *Hint*: Use the approximation of a sum $\sum_{p=1}^{\infty} p^{-3/2} \cong 2.6124$.

8.12 Diffusion of a long chain in a melt of shorter chains

Consider dilute long probe chains with N_A Kuhn monomers of length b in a melt of chemically identical unentangled shorter chains with N_B Kuhn monomers.

(i) What is the root-mean-square end-to-end distance R_A of probe chains? *Hint*: Consider two separate cases $N_A < N_B^2$ and $N_A > N_B^2$ and review section 4.5.2.

(ii) What would be the diffusion coefficient of the probe chain D_R, if its dynamics were Rouse-like with monomeric friction coefficient ζ?

(iii) Show that if the dynamics were Zimm-like, the diffusion coefficient of the probe chain for the case $N_A < N_B^2$ would be

$$D_Z \approx \frac{kT}{\zeta N_A}\left(\frac{N_A}{N_B^2}\right)^{1/2} \quad \text{for } N_A < N_B^2. \tag{8.177}$$

Compare this Zimm diffusion coefficient D_Z with the Rouse diffusion coefficient D_R of part (ii). *Hint*: The viscosity of an unentangled melt of shorter N_B-chains is predicted by the Rouse model [Eq. (8.53)].

(iv) Show that in the case $N_A > N_B^2$ the Zimm-like diffusion coefficient of the probe chain would be

$$D_Z \approx \frac{kT}{\zeta N_A}\left(\frac{N_A}{N_B^2}\right)^{2/5} \quad \text{for } N_A > N_B^2. \tag{8.178}$$

Compare this Zimm diffusion coefficient D_Z with the Rouse diffusion coefficient D_R of part (ii).

(v) What is the relation between the degrees of polymerization of the probe chain N_A and melt chains N_B for which $D_Z \approx D_R$? Compare this hydrodynamic crossover to the excluded volume crossover.

(vi) If the faster modes dominate dynamics, what is the mode structure of a very long probe chain in unentangled melt of shorter chains at short and long time scales (and correspondingly short and long length scales)? Compare your answer with the mode structure in semidilute unentangled solutions.

8.13 Consider a steady shear flow (with shear rate $\dot{\gamma}$) of a monodisperse melt of unentangled N-mers with monomeric friction coefficient ζ:

(i) Show that a relative drift velocity of a chain with respect to a typical chain it overlaps with is

$$V \approx \dot{\gamma} R \approx \dot{\gamma} b \sqrt{N}.$$

(ii) Using the energy dissipation rate per monomer ζV^2, where V is the relative velocity of monomers, show that the rate of energy dissipation per chain is

$$\dot{w} = \zeta b^2 N^2 \dot{\gamma}^2$$

for a chain with friction coefficient $N\zeta$.

(iii) Estimate the rate of energy dissipation per unit volume $\dot{W}$ if the volume per monomer in the melt is v_0.

(iv) Using the relation between the rate of energy dissipation per unit volume $\dot{W}$ and viscosity η

$$\dot{W} = \eta \dot{\gamma}^2$$

obtain the expression for viscosity of unentangled melts.

8.14 (i) Derive the approximate Rouse model predictions for G' and G'' [Eqs (8.49) and (8.50)] from the approximate Rouse prediction for the stress relaxation modulus [Eq. (8.48)].
(ii) Show that at intermediate frequencies ($1/\tau_R \ll \omega \ll 1/\tau_0$) the Rouse model of an ideal linear chain predicts G' and G'' [Eqs (8.49) and (8.50)] scaling as $\sqrt{\omega}$ [Eq. (8.51)].
(iii) What is the value of the loss tangent $\tan\delta$ in this intermediate frequency range of the Rouse model?

8.15 (i) Starting from the exact Rouse stress relaxation modulus [Eq. (8.55)], derive the exact expressions for storage and loss moduli of the Rouse model

$$G'(\omega) = kT\frac{\phi}{Nb^3}\sum_{p=1}^{N}\frac{(\omega\tau_p)^2}{1+(\omega\tau_p)^2}, \tag{8.179}$$

$$G''(\omega) = kT\frac{\phi}{Nb^3}\sum_{p=1}^{N}\frac{\omega\tau_p}{1+(\omega\tau_p)^2}, \tag{8.180}$$

with stress relaxation time of the p-th mode $\tau_p = \tau_R/p^2$ related to the Rouse stress relaxation time τ_R of the chain [Eq. (8.18)].
(ii) Demonstrate that the exact solution follows the asymptotic behaviour of Eq. (8.51), $G'(\omega) \sim G''(\omega) \sim \omega^{1/2}$ at intermediate frequency scales $\tau_R^{-1} \ll \omega \ll \tau_0^{-1}$, where the monomer relaxation time is $\tau_0 = \tau_R/N^2$.
(iii) Compare the exact storage and loss moduli with the approximate ones [Eqs. (8.49) and (8.50)].

8.16 (i) Derive the approximate Zimm model predictions for G' and G'' [Eqs (8.67) and (8.68)] from the approximate Zimm stress relaxation modulus [Eq. (8.64)].
(ii) Show that at intermediate frequencies ($1/\tau_Z \ll \omega \ll 1/\tau_0$) the Zimm model for a linear polymer in a θ-solvent predicts G' and G'' [Eqs (8.67) and (8.68)] scale as $\omega^{2/3}$.
(iii) What is the value of the loss tangent $\tan\delta$ in this intermediate frequency range of the Zimm model?

8.17 What is the physical reason that the 2/3 exponent in Eq. (8.70) for subdiffusive Zimm motion is independent of solvent quality?

Section 8.5

8.18 In semidilute polymer solutions:
(i) Are hydrodynamic interactions important or screened?
(ii) On which scales do Rouse and Zimm models apply for semidilute unentangled solutions?

8.19 Derive a general expression for the viscosity of a blend of dilute long chains with N_A monomers (with volume fraction ϕ) in a matrix of shorter chains of the same species, but with N_B monomers. Be sure to include both the cases where the long chains swell ($N_A > N_B^2$) and where they do not ($N_A < N_B^2$).

8.20 What is the physical significance of the fact that the value of the stress relaxation modulus at the relaxation time of a correlation blob $G(\tau_\xi)$ is proportional to the osmotic pressure in semidilute solutions?

8.21 (i) What is the prediction of the Rouse–Zimm model of semidilute unentangled solutions for the stress relaxation modulus $G(t)$ at very short times $t < \tau_0$?

(ii) Show that the time integral of the stress relaxation modulus in unentangled semidilute solutions over all time regimes (and therefore the solution viscosity) is dominated by the longest relaxation time [Eq. (8.93)].

8.22 Estimate the time dependence of the mean-square displacement of a monomer in an unentangled semidilute solution.

(i) For time scales $t < \tau_\xi$, where τ_ξ is the relaxation time of a chain section inside a correlation volume.

(ii) For time scales $\tau_\xi < t < \tau_{\text{chain}}$, where τ_{chain} is the longest relaxation time of the polymer.

(iii) For time scales $t \geq \tau_{\text{chain}}$.

Section 8.6

8.23 Consider a semi-flexible rod with Young's modulus $E = 10^8$ Pa and cross-section $L_y = L_z = 1$ nm. Estimate the Kuhn length of this rod at room temperature. How does the Kuhn length change if the cross-section changes to $L_y = L_z = 5$ nm?

8.24 Estimate the frequency dependence of the storage and loss modulus of semiflexible chains at intermediate frequencies $\tau_g^{-1} \ll \omega \ll \tau_0^{-1}$ from Eq. (8.117), keeping in mind that Young's modulus is three times the shear modulus ($E(t) = 3G(t)$). What is the value of the loss tangent $\tan \delta$ in this intermediate frequency range?

Section 8.7

8.25 Derive the relation between WLF coefficients [B/f_0 and T_∞ in Eq. (8.134)] for two choices of the reference temperature T_0. *Hint*: The Vogel temperature T_∞ will not change when the reference temperature is changed, but f_0 will change.

8.26 (i) Estimate B/f_g for high molar mass linear PVME melts from Fig. 8.16, ignoring any modulus scale shift b_T.

(ii) Estimate the value of the empirical constant B in the Doolittle equation (8.130).

8.27 The relaxation time of a polybutadiene melt at room temperature (298 K) is 1 s. Estimate the relaxation time of this melt at the glass transition temperature using Table 8.3 and ignoring any modulus scale shift.

8.28 If the temperature dependence of the free volume is assumed to be

$$f = -\frac{\mathrm{B}}{9 \ln((T - T_c)/T_c)},$$

derive the following dynamic scaling expression for the temperature dependence of viscosity:

$$\frac{\eta}{\eta_0} = \left(\frac{T_0 - T_c}{T - T_c}\right)^9. \tag{8.181}$$

8.29 (i) Determine the temperature dependence of the apparent activation energy E_a in the WLF equation [Eq. (8.134)] using the definition

$$E_a = k\frac{\mathrm{d}\ \ln(\eta/\eta_0)}{\mathrm{d}(1/T)}. \tag{8.182}$$

(ii) Show that the high temperature limit of the WLF activation energy is

$$E_\infty = \frac{Bk}{\alpha_f} \tag{8.183}$$

where α_f is the thermal expansion coefficient of the free volume [Eq. (8.131)].

(iii) A typical value of this high-temperature limiting activation energy is $E_\infty \cong 50\ \mathrm{kJ\ mol^{-1}}$. By how much does the temperature need to increase in the high temperature limit to have the viscosity decrease by a factor of ten?

8.30 Polymer melts typically have their Vogel temperature 50 K below their glass transition temperature.

(i) Assuming that the fractional free volume $f_g \cong 0.025$ at $T_g = T_\infty + 50\ \mathrm{K}$ [Eq. (8.132)], what is the coefficient of thermal expansion for the free volume?

(ii) What is the fractional free volume at $T_g + 10\ \mathrm{K}$ and at $T_g + 100\ \mathrm{K}$?

(iii) How much do we need to raise the temperature to lower the viscosity by a factor of 10 from its value at T_g? Assume $B = 1$.

(iv) How much do we need to raise the temperature to lower the viscosity by a factor of 10 from its value at $T_g + 100\ \mathrm{K}$? Assume $B = 1$.

8.31 Assuming that the chain ends have more free volume than monomers in the middle of the chain, derive the molar mass dependence of the glass transition temperature of polymer melts [Eq. (8.135)].

8.32* Demonstrate that the glass transition temperature of ring polymers decreases with increasing molar mass.
Hint: Consider the molar mass dependence of the entropy of ring polymers.

Section 8.8

8.33* Rouse model for polydisperse fractals

The arguments of Section 8.8 can be generalized to describe the relaxation modulus of any polydisperse mixture of fractal polymers with distribution function $n(N)$, the number of N-mers per monomer. The relaxation modulus has contribution kT from each unrelaxed section of g monomers at time $t = \tau(g)$ [see Eq. (8.145)]. The number density of N-mers is $n(N)/b^3$. The number density of unrelaxed sections of g monomers consists of contributions of N/g from all chains with degree of polymerization $N > g$:

$$G(t) \approx kT \int_g^\infty \frac{N}{g}\frac{n(N)}{b^3}\,\mathrm{d}N.$$

Use this equation for a general polydisperse fractal polymer and the distribution function of Eq. (6.93) to rederive the Rouse stress relaxation modulus of the melt randomly branched polymers found in the three-dimensional percolation polymerization reactor [Eq. (8.147)]. *Hint*: Use hyperscaling.

8.34 Calculate the stress relaxation modulus $G(t)$ for a polydisperse unentangled melt of linear polymers with a power law distribution of chain lengths

$n(N) = AN^{-\tau}$, where $A = \tau - 1$ is a normalization constant and $\tau > 2$ is the polydispersity exponent. Assume that all excluded volume and hydrodynamic interactions are screened.

8.35* Rouse model of randomly branched polymers

The full-time dependence of the stress relaxation modulus of randomly branched unentangled polymers is best derived from the fractal dynamics of Section 8.8 using the relaxation rate spectrum $P(\varepsilon)$:

$$G(t) = \int_0^\infty P(\varepsilon)\, \exp(-\varepsilon t)\, \mathrm{d}\varepsilon. \tag{8.184}$$

(i) Show that the relaxation rate spectrum of a single branched polymer between the relaxation rate of the linear section between branch points ε_x and the relaxation rate of the entire chain ε_N is

$$P(\varepsilon)\, \mathrm{d}\varepsilon \approx \left(\frac{\varepsilon}{\varepsilon_x}\right)^{1/(1+2/\mathcal{D})} \frac{\mathrm{d}\varepsilon}{\varepsilon},$$

where $\mathcal{D}$ is the fractal dimension.

(ii) Show that the contribution to $G(t)$ from one branched polymer with N monomers is

$$G_N(t) = \int_{\varepsilon_N}^{\varepsilon_x} \left(\frac{\varepsilon}{\varepsilon_x}\right)^{1/(1+2/\mathcal{D})} \exp(-\varepsilon t) \frac{\mathrm{d}\varepsilon}{\varepsilon}.$$

(iii) Derive the stress relaxation modulus of the polydisperse ensemble of randomly branched polymers by summing the response from each molecule in the distribution using

$$G(t) = \int_{N_x}^{N^*} N n(N)\, G_N(t)\, \mathrm{d}N,$$

where N_x is the number of monomers between branch points, N^* is the characteristic degree of polymerization, and $n(N) \sim N^{-\tau}$ is the number density distribution function.

(iv) What is tacitly assumed in the calculation of part (iii)?

(v) Determine the contribution to the complex modulus of one branched polymer from the result of part (ii).

(vi) Using an integration similar to part (iii), show that the complex modulus of the polydisperse ensemble of randomly branched polymers is

$$G^*(\omega) \sim \frac{\mathrm{i}\omega}{1 - (N_x/N^*)^{\tau-2}} \times \left[\int_{\varepsilon_{x^*}}^{\varepsilon_x} \frac{(\varepsilon/\varepsilon_x)^{(\tau-1)/(1+2/\mathcal{D})}}{\mathrm{i}\omega + \varepsilon} \frac{\mathrm{d}\varepsilon}{\varepsilon} - \left(\frac{N_x}{N^*}\right)^{\tau-2} \int_{\varepsilon_{x^*}}^{\varepsilon_x} \frac{(\varepsilon/\varepsilon_x)^{1/(1+2/\mathcal{D})}}{\mathrm{i}\omega + \varepsilon} \frac{\mathrm{d}\varepsilon}{\varepsilon}\right].$$

This form was used for the curves in Fig. 8.19.

8.36* The Rouse model (see the book by Doi and Edwards)

A polymer in the Rouse model is represented by a chain of N beads, each with friction coefficient ζ, located at positions $\{\vec{R}_1, \vec{R}_2, \ldots, \vec{R}_N\}$ and connected by springs with spring constant $3kT/b^2$, where k is the Boltzmann constant, T is the absolute temperature and b^2 is the mean-square unperturbed distance between neighboring beads. The frictional force due to motion of the j-th bead through the solvent $-\zeta(d\vec{R}_j/dt)$ is balanced by the sum of the forces acting on it from the two neighboring beads $(3kT/b^2)(\vec{R}_{j+1} - \vec{R}_j)$ and $(3kT/b^2)(\vec{R}_{j-1} - \vec{R}_j)$ as well as the random Brownian force $\vec{f}_j$. This random force is assumed to be Gaussian with zero

average $\langle \vec{f}_j \rangle = 0$ and with no correlations between different moments of time nor between different components of the force. The mean-square value of each component of the random Brownian force is related to the friction coefficient ζ of the beads by the fluctuation-dissipation theorem and is equal to $2\zeta kT$.

(i) Show that the continuum version of the equation of motion for the j-th bead is

$$\zeta \frac{\partial \vec{R}_j}{\partial t} = \frac{3kT}{b^2} \frac{\partial^2 \vec{R}_j}{\partial j^2} + \vec{f}_j \tag{8.185}$$

with zero average and delta-function correlated random force $\langle f_{j\alpha}(t) f_{i\beta}(t') \rangle = 2\zeta kT \delta(j-i) \delta_{\alpha\beta} \delta(t-t')$, where $f_{j\alpha}$ is the α-component of the random force acting on bead j, $\delta_{\alpha\beta}$ is the Kronecker delta and $\delta(n-m)$ is the Dirac delta function.

(ii) The end beads are attached to the rest of the chain by only one spring and these free ends can be modeled by adding two hypothetical beads at both ends ($j=0$ and $j=N+1$) with their positions coinciding with those of real end beads ($\vec{R}_0 = \vec{R}_1$ and $\vec{R}_{N+1} = \vec{R}_N$). Show that the boundary conditions in the continuum limit become $\partial \vec{R}_j / \partial j = 0$ for $j=0$ and $j=N$.

(iii) The motion of beads is directly coupled to the neighboring beads through the springs, reflected by the presence of the second derivative of bead position vector in the equation of motion for the Rouse model (Eq. 8.185). It is easier to solve this equation in terms of uncoupled variables, called normal modes. Normal modes for the Rouse model are defined by the cosine transform of the real coordinates

$$\vec{X}_p = \frac{1}{N} \int_0^N \cos\left(\frac{\pi j p}{N}\right) \vec{R}_j dj \tag{8.186}$$

Demonstrate that the Rouse equations for different normal modes are decoupled from each other with the form

$$\zeta_p \frac{\partial \vec{X}_p}{\partial t} = -k_p \vec{X}_p + \vec{f}_p \tag{8.187}$$

where $k_p = 6\pi^2 kTp^2/(Nb^2)$ and the friction coefficient of zeroth mode (corresponding to the center of mass position) is the friction of the whole chain $\zeta_0 = N\zeta$, while the friction coefficient of all other normal modes is twice as large $\zeta_p = 2N\zeta$ for $p = 1,2,3,\ldots$. Show that the average cosine transform of the random force is zero $\langle \vec{f}_p \rangle = 0$, while its correlation function is $\langle f_{p\alpha}(t) f_{q\beta}(t') \rangle = 2\zeta_p kT \delta_{pq} \delta_{\alpha\beta} \delta(t-t')$, where $f_{p\alpha}$ is the α-component of the random force acting on mode p.

(iv) Prove that the time correlation function of each normal mode decays exponentially with time

$$\langle X_{p\alpha}(t) X_{q\beta}(0) \rangle = \delta_{pq} \delta_{\alpha\beta} \frac{kT}{k_p} \exp\left(-\frac{t}{2\tau_p}\right) \tag{8.188}$$

where the times $\tau_p = \tau_R/p^2$ and $\tau_1 = \tau_R$ is the Rouse stress relaxation time of the chain (Eq. 8.18).

(v) Show that the end-to-end vector of the chain can be expressed as the sum over odd normal modes $\vec{R} \equiv \vec{R}_N - \vec{R}_0 = -4 \sum_{odd\ p} \vec{X}_p$ and therefore its time correlation function is

$$\left\langle \vec{R}(t) \bullet \vec{R}(0) \right\rangle = \frac{8}{\pi^2} Nb^2 \sum_{odd\ p} \frac{1}{p^2} \exp\left(-\frac{p^2}{2\tau_R} t\right) \tag{8.189}$$

(vi) The polymeric contribution to stress can be expressed as the sum over all monomers in the polymer $\sigma_{\alpha\beta} = -\phi/(Nb^3)\sum_j \langle \vec{F}_{j\alpha} R_{j\beta}\rangle$, where $\phi/(Nb^3)$ is the number density of the chains and $\vec{F}_{j\alpha} = (3kT/b^2)(\vec{R}_{j+1} + \vec{R}_{j-1} - 2\vec{R}_j)$ is the force acting on the j-th monomer from other monomers. Demonstrate that the polymeric contribution to the stress can be written in the continuum limit and expressed in terms of normal modes as

$$\sigma_{\alpha\beta} = \frac{\phi}{Nb^3}\frac{3kT}{b^2}\int_0^N \left\langle \frac{\partial R_{j\alpha}}{\partial j}\frac{\partial R_{j\beta}}{\partial j}\right\rangle dj = \frac{\phi}{Nb^3}\sum_{j=1}^{N} k_p \langle X_{p\alpha} X_{q\beta}\rangle \qquad (8.190)$$

Calculate the stress relaxation modulus of the Rouse model (Eq. 8.55) by showing that after a small step shear strain γ at time $t=0$ the correlation function of normal modes decays as $\langle X_{px}(t) X_{qy}(t)\rangle = (\gamma kT/k_p)\exp(-t/\tau_p)$.

Section 8.9

8.37 Does the diffusion coefficient measured in dilute solution using Eq. (8.156) rely on proper instrumental calibration to get the absolute intensity?

8.38 The correlation length in semidilute solution can be experimentally determined by measuring the diffusion coefficient of very dilute colloidal spheres of various sizes, provided that the spheres do not interact with the polymers. Consider diffusion of a non-interacting sphere in a semidilute unentangled solution.

(i) What equation determines the diffusion coefficient D of the sphere, if the sphere radius R is much smaller than the correlation length?
(ii) What equation determines the diffusion coefficient of the sphere, if it is much larger than the chain size?
(iii) Sketch the dependence of the product of sphere diffusion coefficient and sphere radius (DR) on sphere radius and explain how such a plot can be used to estimate the correlation length.

8.39* Calculate the Rouse model prediction for the dynamic structure factor for gels in the gelation regime.

Bibliography

Berry, G. C. and Fox, T. G. The viscosity of polymers and their concentrated solutions, *Adv. Polym. Sci.* **5**, 261 (1968).

Chu, B. (ed.) *Selected Papers on Quasielastic Light Scattering by Macromolecular, Supramolecular and Fluid Systems* (SPIE Press, New York, 1990).

Chu, B. *Laser Light Scattering: Basic Principles and Practice*, 2nd edn (Academic Press, New York, 1991).

Doi, M. *Introduction to Polymer Physics* (Clarendon Press, Oxford, 1996).

Doi, M. and Edwards, S. F. *The Theory of Polymer Dynamics* (Clarendon Press, Oxford, 1986).

Ferry, J. D. *Viscoelastic Properties of Polymers*, 3rd edn (Wiley, New York, 1980).

Graessley, W. W. The entanglement concept in polymer rheology, *Adv. Polym. Sci.* **16**, 1 (1974).

Kurata, M. and Stockmayer, W. H. Intrinsic viscosities and unperturbed dimensions of long chain molecules, *Fortschr. Hochpolym.-Forsch* **3**, 196 (1963).

Pecora, R. (ed.) *Dynamic Light Scattering: Applications of Photon Correlation Spectroscopy* (Plenum, New York, 1985).

Schmitz, K. S. *An Introduction to Dynamic Light Scattering from Macromolecules* (Academic Press, New York, 1990).

Entangled polymer dynamics

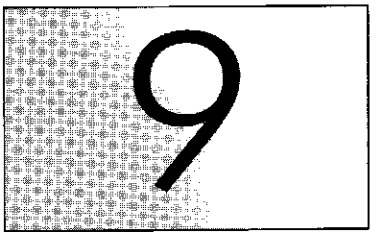

9.1 Entanglements in polymer melts

The Edwards tube model of polymer entanglements was already discussed in Section 7.3.1. The topological constraints imposed by neighbouring chains on a given chain restrict its motion to a tube-like region (see Fig. 7.10) called the confining tube. The motion of the chain along the contour of the tube (the primitive path) is unhindered by topological interactions. Displacement of monomers in the direction perpendicular to the primitive path is restricted by surrounding chains to an average distance a, called the tube diameter. The number of Kuhn monomers in a strand of size equal to the amplitude of transverse fluctuations (the tube diameter) is N_e, the number of monomers in an entanglement strand. For melts, excluded volume interactions are screened (see Section 4.5.2) and the tube diameter is determined by ideal chain statistics:

$$a \approx b\sqrt{N_e}. \tag{9.1}$$

The tube can be thought of as being composed of N/N_e sections of size a, with each section containing N_e monomers. The chain can be considered as either a random walk of entanglement strands (N/N_e strands of size a) or a random walk of monomers (N monomers of size b).

$$R \approx a\sqrt{\frac{N}{N_e}} \approx b\sqrt{N}. \tag{9.2}$$

The average contour length $\langle \mathbf{L} \rangle$ of the primitive path (the centre of the confining tube, see Fig. 7.10) is the product of the entanglement strand length a and the average number of entanglement strands per chain N/N_e.

$$\langle L \rangle \approx a\frac{N}{N_e} \approx \frac{b^2 N}{a} \approx \frac{bN}{\sqrt{N_e}}. \tag{9.3}$$

The average primitive path contour length $\langle \mathbf{L} \rangle$ is shorter than the contour length of the chain bN by the factor $a/b \approx \sqrt{N_e}$ because each entanglement strand in a melt is a random walk of N_e Kuhn monomers.

One manifestation of entanglement in long chains ($N \gg N_e$) is the appearance of a wide region in time (or frequency) where the modulus is

almost constant in a stress relaxation (or oscillatory shear) experiment. In analogy with crosslinked rubbers, this region is referred to as the **rubbery plateau**, and the nearly constant value of the modulus in this plateau regime is called the **plateau modulus** G_e. In analogy with an affine network, whose modulus is of order kT per network strand [Eq. (7.31)], the plateau modulus is of order kT per entanglement strand [Eq.(7.47)]. The number-average molar mass of an entanglement strand is called the entanglement molar mass M_e. The occupied volume of an entanglement strand with molar mass M_e in a melt with density ρ is the product of the number of Kuhn monomers per strand N_e and the Kuhn monomer volume v_0:

$$\frac{M_e}{\rho \mathcal{N}_{Av}} = v_0 N_e \approx v_0 \frac{a^2}{b^2} \approx \frac{v_0}{b^3} a^2 b. \tag{9.4}$$

Since monomers are space-filling in the melt, the number density of entanglement strands is just the reciprocal of the entanglement strand volume, leading to a simple expression for the plateau modulus of an entangled polymer melt [Eq. (7.47)].

$$G_e \approx \frac{\rho \mathcal{R} T}{M_e} \approx \frac{kT}{v_0 N_e} \approx \frac{b^3}{v_0} \frac{kT}{a^2 b}. \tag{9.5}$$

The number of chains P_e within the **confinement volume** a^3 is determined from the fact that monomers in the melt are space-filling:

$$P_e \approx \frac{a^3}{v_0 N_e} \approx \frac{b^3}{v_0} \sqrt{N_e}. \tag{9.6}$$

Table 9.1 shows N_e and P_e calculated from the measured plateau modulus. All flexible polymers have $P_e \cong 20$ overlapping entanglement strands defining the entanglement volume a^3, which is the **overlap criterion for entanglement** in polymer melts.

Table 9.1 Entanglement parameters for flexible linear polymer melts

Polymer	G_e (MPa)	M_e (g mol^{-1})	N_e	b (Å)	a (Å)	v_0 (Å^3)	P_e
Polyethylene at 140 °C	2.60	1000	7	14	36	320	21
Poly(ethylene oxide) at 140 °C	1.80	2000	15	11	40	210	21
1,4-Polybutadiene at 25 °C	1.15	1900	18	10	41	190	19
Polypropylene at 140 °C	0.47	5800	32	11	62	380	20
1,4-Polyisoprene at 25 °C	0.35	6400	56	8.2	62	210	20
Polyisobutylene at 25 °C	0.32	7100	26	13	64	500	20
Polydimethylsiloxane at 25 °C	0.20	12 000	32	13	74	650	20
Polystyrene at 140 °C	0.20	17 000	23	18	85	1200	22
Polyvinylcyclohexane at 160 °C	0.068	49 000	81	14	130	1100	22

9.2 Reptation in polymer melts

At first glance, understanding the motion of a polymer in the melt is daunting. Since roughly $\sqrt{N}$ other polymers share the pervaded volume of a given chain in the melt, chain motion appears to be a difficult many-body problem. However, by utilizing the Edwards tube concept, de Gennes cleverly reduced this many-body problem to the motion of a single chain confined to a tube of surrounding chains. Models that consider chain motion as being restricted to a tube-like region are referred to as **tube models**. The simplest tube model was proposed by de Gennes in 1971 for the motion of linear entangled polymers, and is called the **reptation model**.

9.2.1 Relaxation times and diffusion

In de Gennes' reptation model, an entangled chain diffuses along its confining tube in a way analogous to the motion of a snake or a worm (see Fig. 9.1). This motion of the chain consists of diffusion of small loops, along the contour of the primitive path. This curvilinear motion of a polymer along its tube satisfies the topological constraints imposed by surrounding chains and is characterized by the Rouse friction coefficient $N\zeta$. The **curvilinear diffusion coefficient** D_c that describes motion of the chain along its tube is simply the Rouse diffusion coefficient of the chain [Eq. (8.12)].

$$D_c = \frac{kT}{N\zeta}. \tag{9.7}$$

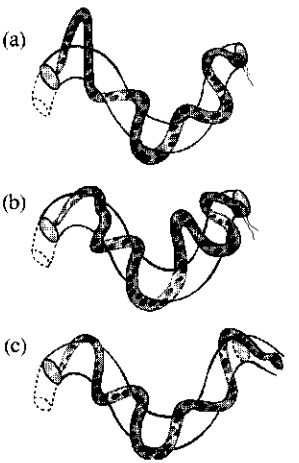

Fig. 9.1
Reptation steps: (a) formation of a loop at the tail of the snake and elimination of the tail segment of the confining tube: (b) propagation of the loop along the contour of the tube; (c) release of the loop at the head of the snake and formation of a new section of the confining tube.

The time it takes for the chain to diffuse out of the original tube of average length $\langle L \rangle$ is the **reptation time**:

$$\tau_{rep} \approx \frac{\langle L \rangle^2}{D_c} \approx \frac{\zeta b^2}{kT}\frac{N^3}{N_e} = \frac{\zeta b^2}{kT} N_e^2 \left(\frac{N}{N_e}\right)^3. \tag{9.8}$$

Here, Eq. (9.3) was used for the average contour length of the tube. The reptation time τ_{rep} is predicted to be proportional to the cube of the molar mass. The experimentally measured scaling exponent is higher than 3:

$$\tau \sim M^{3.4}. \tag{9.9}$$

We will discuss the possible reasons for the disagreement between the simple reptation model and experiments in Section 9.4.5.

The first part of the final relation of Eq. (9.8) is the Rouse time of an entanglement strand containing N_e monomers:

$$\tau_e \approx \frac{\zeta b^2}{kT} N_e^2. \tag{9.10}$$

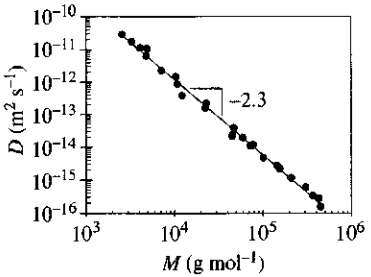

Fig. 9.2
Molar mass dependence of the diffusion coefficient for melts of hydrogenated polybutadiene at 175 °C. Data compiled in T. P. Lodge *Phys. Rev. Lett.* **83**, 3218 (1999).

The ratio of the reptation time τ_{rep} and τ_e is the cube of the number of entanglements along the chain:

$$\frac{\tau_{rep}}{\tau_e} \approx \left(\frac{N}{N_e}\right)^3. \tag{9.11}$$

The chain moves a distance of order of its own size R in its reptation time τ_{rep}, since this is the time scale at which the tube is abandoned:

$$D_{rep} \approx \frac{R^2}{\tau_{rep}} \approx \frac{kT}{\zeta}\frac{N_e}{N^2}. \tag{9.12}$$

The diffusion coefficient of entangled linear polymers is predicted to be reciprocally proportional to the square of the molar mass, which also disagrees with experiments, as shown in Fig. (9.2):

$$D \approx \frac{R^2}{\tau} \sim M^{-2.3}. \tag{9.13}$$

9.2.2 Stress relaxation and viscosity

The reptation ideas discussed above will now be combined with the relaxation ideas discussed in Chapter 8 to describe the stress relaxation modulus $G(t)$ for an entangled polymer melt. On length scales smaller than the tube diameter a, topological interactions are unimportant and the dynamics are similar to those in unentangled polymer melts and are described by the Rouse model. The entanglement strand of N_e monomers relaxes by Rouse motion with relaxation time τ_e [Eq. (9.10)]:

$$\tau_e = \tau_0 N_e^2. \tag{9.14}$$

The Rouse model predicts that the stress relaxation modulus on these short time scales decays inversely proportional to the square root of time [Eq. (8.47)]:

$$G(t) \approx G_0\left(\frac{t}{\tau_0}\right)^{-1/2} \quad \text{for } \tau_0 < t < \tau_e. \tag{9.15}$$

The relaxation time of the Kuhn monomer τ_0 is the shortest stress relaxation time in the Rouse model, given by Eq. (8.56) with $p = N$:

$$\tau_0 = \frac{\zeta b^2}{6\pi^2 kT} \approx \frac{\zeta b^2}{kT}. \tag{9.16}$$

The stress relaxation modulus at τ_0 is the Kuhn modulus (kT per Kuhn monomer):

$$G_0 \approx G(\tau_0) \approx \frac{kT}{v_0}. \tag{9.17}$$

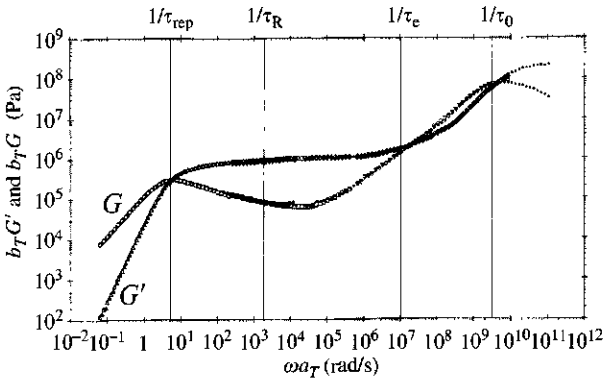

Fig. 9.3
Master curve at 25 °C from oscillatory shear data at six temperatures for a 1,4-polybutadiene sample with $M_w = 130\,000\,\mathrm{g\,mol^{-1}}$. Data from R. H. Colby, L. J. Fetters and W. W. Graessley, *Macromolecules* **20**. 2226 (1987).

Consider for example, a melt of 1,4-polybutadiene linear chains with $M = 130\,000\,\mathrm{g\,mol^{-1}}$. The molar mass of a polybutadiene Kuhn monomer is $M_0 = 105\,\mathrm{g\,mol^{-1}}$ (see Table 2.1) so this chain has $N = M/M_0 = 1240$ Kuhn monomers. At 25 °C, this polymer is 124 K above its glass transition and its oscillatory shear master curve is shown in Fig. 9.3. The time scale for monomer motion is $\tau_0 \cong 0.3$ ns, An entanglement strand of 1,4-polybutadiene has molar mass $M_e = 1900\,\mathrm{g\,mol^{-1}}$ (see Table 9.1) and therefore contains $N_e = M_e/M_o = 18$ Kuhn monomers. The whole chain has $N/N_e = M/M_e = 68$ entanglements. The Rouse time of the entanglement strand $\tau_e \cong 0.1\,\mu$s [Eq. (9.16)].

At the Rouse time of an entanglement strand τ_e, the chain 'finds out' that its motion is topologically hindered by surrounding chains. Free Rouse motion of the chain is no longer possible on time scales $t > \tau_e$. The value of the stress relaxation modulus at τ_e is the plateau modulus G_e, which is kT per entanglement strand [Eq. (9.5)]:

$$G_e = G(\tau_e) = \frac{G_0}{N_e} = \frac{kT}{\nu_0 N_e}. \tag{9.18}$$

The Rouse time of the chain is $\tau_R \cong 0.5$ ms:

$$\tau_R = \tau_0 N^2 = \tau_e \left(\frac{N}{N_e}\right)^2. \tag{9.19}$$

In the simple reptation model, there is a delay in relaxation (the rubbery plateau) between τ_e and the reptation time of the chain τ_{rep} [Eq. (9.11)]. By restricting the chain's Rouse motions to the tube, the time the chain takes to diffuse a distance of order of its size is longer than its Rouse time by a factor of $6\,N/N_e$. This slowing arises because the chain must move along the confining tube. The reptation time of the chain $\tau_{rep} = 0.2$ s is measured experimentally as the reciprocal of the frequency at which $G' = G''$ in Fig. 9.3 at low frequency (see Problem 9.8). In practice, this time is determined experimentally and τ_0, τ_e and τ_R are determined from τ_{rep}.

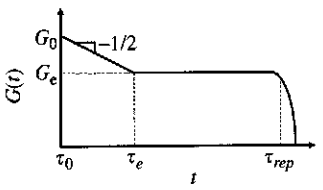

Fig. 9.4
Schematic representation of the stress relaxation modulus of entangled linear polymers on logarithmic scales.

The stress relaxation modulus is summarized schematically in Fig. 9.4. For long linear chains, the rubbery plateau can span many decades in time.

The diffusion coefficient of the chain is controlled by the reptation time [Eq. (9.12)]. The linear polybutadiene chain with $M = 130\,000\,\mathrm{g\,mol^{-1}}$ has $N = 1240$ Kuhn monomers, with Kuhn length $b = 10\,\text{Å}$ and coil size $R = b\sqrt{N} \cong 350\,\text{Å}$. Since linear polymers move a distance of order their own size in their reptation time, the reptation time of $\tau_{rep} \cong 0.2\,\mathrm{s}$ at 25 °C enables estimation of the diffusion coefficient $D \approx R^2/\tau_{rep} \cong 6 \times 10^{-15}\,\mathrm{m^2\,s^{-1}}$. Physically, this means that at 25 °C this polybutadiene chain moves about 350 Å in a random direction every 0.2 s.

The stress relaxation modulus in the reptation model is proportional to the fraction of original tube remaining at time t (see Fig. 9.1). As time goes on, sections of the original tube are abandoned when the chain end first visits them. Such a problem is called a first-passage time problem. The stress relaxation modulus $G(t)$ for the reptation model was calculated by Doi and Edwards in 1978 by solving the first-passage problem for the diffusion of a chain in a tube (see Problem 9.6):

$$G(t) = \frac{8}{\pi^2} G_e \sum_{\text{odd } p} \frac{1}{p^2} \exp\left(-\frac{p^2 t}{\tau_{rep}}\right). \tag{9.20}$$

The longest relaxation time in this model is the reptation time required for the chain to escape from its tube

$$\tau_{rep} = 6\tau_0 \frac{N^3}{N_e} = 6\tau_e \left(\frac{N}{N_e}\right)^3 = 6\tau_R \frac{N}{N_e} \tag{9.21}$$

where the Rouse time τ_R is the longest relaxation time of the Rouse model [Eq. (8.18)], which is half the end-to-end vector correlation time.

The main contribution[1] comes from the first mode $p = 1$ and the function is almost a single exponential [Eq. (7.111)]:

$$G(t) \approx G_e \exp(-t/\tau_{rep}). \tag{9.22}$$

The **Doi–Edwards equation** [Eq. (9.20)] is the first attempt at a molecular model for viscoelasticity of entangled polymers. It ignores tube length fluctuation modes that relax some stress on shorter time scales. These modes significantly modify dynamics of entangled polymers, as described in Section 9.4.5.

The reptation model prediction for the viscosity of an entangled polymer melt is determined by integrating Eq. (9.20):

$$\eta = \int_0^\infty G(t)\,\mathrm{d}t = \frac{8}{\pi^2} G_e \sum_{\text{odd } p} \frac{1}{p^2} \int_0^\infty \exp\left(-\frac{p^2 t}{\tau_{rep}}\right) \mathrm{d}t = \frac{\pi^2}{12} G_e \tau_{rep}. \tag{9.23}$$

[1] Fraction $8/\pi^2$ of the terminal relaxation is associated with the first mode with relaxation time τ_{rep} (see Problem 9.7).

The final result was obtained from the fact that $\sum_{\text{odd}\,p} 1/p^4 = \pi^4/96$. Since the stress relaxation is nearly a single exponential, the scaling prediction of the viscosity as the product of the plateau modulus [Eq. (9.5)] and the reptation time [Eq. (9.8)] is nearly quantitative:

$$\eta \approx G_e \tau_{rep} \approx G_e \tau_e \left(\frac{N}{N_e}\right)^3 \approx \frac{kT}{v_0 N_e} \frac{\zeta b^2 N_e^2}{kT} \left(\frac{N}{N_e}\right)^3 \approx \frac{\zeta b^2}{v_0} \frac{N^3}{N_e^2}. \tag{9.24}$$

The viscosity of a polymer melt is predicted to be proportional to molar mass for unentangled melts (the Rouse model) and proportional to the cube of molar mass for entangled melts (the reptation model).

$$\eta \sim \begin{cases} M & \text{for } M < M_c, \\ M^3 & \text{for } M > M_c. \end{cases} \tag{9.25}$$

As Fig. 8.17 shows, the critical molar mass M_c for entanglement effects in viscosity [defined in Eq. (8.136)] is typically a factor of 2–4 larger than the entanglement molar mass M_e [defined in Eq. (9.5)]. As shown in Fig. 9.5, the exponent in the entangled regime is $\cong 3.4$ for all linear entangled polymers. This exponent is significantly larger than the prediction of 3 by the simple reptation model [Eq. (9.24)]:

$$\eta \approx G_e \tau \sim M^{3.4}. \tag{9.26}$$

The deviations from the 3.4 power law at low molar masses ($M < M_c$) are because those chains are too short to be entangled (see Section 8.7.3). The deviations at very high molar mass are consistent with a crossover to pure reptation (see Section 9.4.5).

The simple reptation model does not properly account for all the relaxation modes of a chain confined in a tube. This manifests itself in all measures of terminal dynamics, as the longest relaxation time, diffusion coefficient and viscosity all have stronger molar mass dependences than the reptation model predicts. In Sections 9.4.5 and 9.6.2, more accurate analytical and numerical treatments of this problem are given with results that are in reasonable agreement with the experimental dependence of terminal dynamics on the molar mass of the chain [Eqs (9.9), (9.13), and (9.26)].

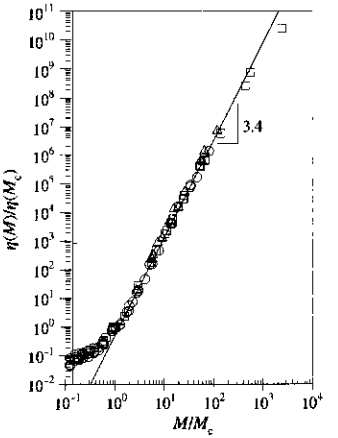

Fig. 9.5
Molar mass dependence of viscosity for polymer melts reduced by their critical molar mass. Open circles are polyisobutylene with $M_c = 14\,000\,\text{g mol}^{-1}$, from T. G. Fox and P. J. Flory, *J. Am. Chem. Soc.* **70**, 2384 (1948) and *J. Phys. Chem.* **55**, 221 (1951). Open squares are polybutadiene with $M_c = 6700\,\text{g mol}^{-1}$, from R. H. Colby *et al.*, *Macromolecules* **20**, 2226 (1987). Open triangles are hydrogenated polybutadiene with $M_c = 8100\,\text{g mol}^{-1}$, from D. S. Pearson *et al.*, *Macromolecules* **27**, 711 (1994).

9.3 Reptation in semidilute solutions

9.3.1 Length scales

Consider a semidilute solution with polymer volume fraction ϕ. The concentration dependence of the correlation length was discussed in Chapter 5:

$$\xi \approx b\phi^{-\nu/(3\nu-1)}. \tag{9.27}$$

In an athermal solvent the exponent $\nu \cong 0.588$ and the correlation length decreases with concentration as $\xi \approx b\phi^{-0.76}$, while in a θ-solvent the exponent $\nu = 1/2$ and the correlation length has a stronger concentration dependence $\xi \approx b\phi^{-1}$ [Eq. (5.52)]. The number of monomers g in a correlation volume ξ^3 was also determined in Chapter 5 [Eq. (5.24)]:

$$g \approx \frac{\phi \xi^3}{b^3} \approx \phi^{-1/(3\nu-1)}. \tag{9.28}$$

In an athermal solvent, the number of monomers in a correlation volume decreases with concentration as $g \approx \phi^{-1.3}$, while in a θ-solvent a stronger concentration dependence is expected with $g \approx \phi^{-2}$. The chain is always a random walk of correlation blobs, with end-to-end distance R [Eq. (5.26)]:

$$R \approx \xi \left(\frac{N}{g}\right)^{1/2} \approx bN^{1/2}\phi^{-(2\nu-1)/(6\nu-2)}. \tag{9.29}$$

In a good solvent, the chain size decreases with concentration as $R \approx bN^{1/2}\phi^{-0.12}$. In a θ-solvent ($\nu = 1/2$) there is no concentration dependence of chain size, as the chain is nearly ideal at all concentrations $R \approx bN^{1/2}$.

To understand the dynamics of entangled solutions, another length scale, the tube diameter a, must be specified. Just as in the melt, the confinement volume a^3 must contain multiple chains. Entanglements between chains are controlled by binary intermolecular contacts. In the athermal solvent limit, the number density of binary intermolecular contacts is proportional to the reciprocal of the correlation volume $\xi^{-3} \sim \phi^{3\nu/(3\nu-1)}$, and the distance between binary contacts is the reciprocal cube root of this number density $\xi \sim \phi^{-\nu/(3\nu-1)}$. Hence, the correlation length describes the distance between binary intermolecular contacts. *The tube diameter a in an athermal solvent is proportional to, but larger than, the correlation length ξ*:

$$a(\phi) \approx a(1)\phi^{-\nu/(3\nu-1)} \approx a(1)\phi^{-0.76} \quad \text{for an athermal solvent.} \tag{9.30}$$

The tube diameter in the melt, $a(1) \approx b\sqrt{N_e(1)}$, is given by Eq. (9.1) in terms of the number of Kuhn monomers in an entanglement strand in the melt $N_e(1)$. Notice that $a(1) > b$, which makes $a > \xi$ at all concentrations. Since the chain is a random walk of correlation blobs on scales larger than ξ, the entanglement strand is a random walk of correlation blobs, as depicted in Fig. 9.6.

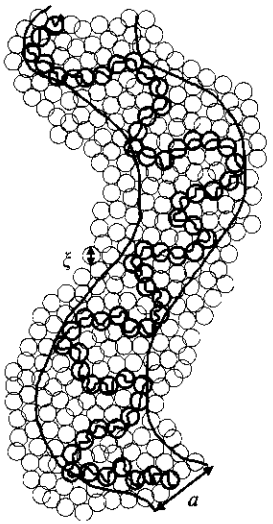

Fig. 9.6
The confining tube in a semidilute solution. Thick circles are the correlation blobs of the chain. Thin empty circles are the correlation blobs of surrounding chains.

In a θ-solvent, the correlation length is determined by ternary contacts between chains (see Section 5.4). This is because the effects of binary contacts on the free energy (or osmotic pressure) exactly cancel at the θ-temperature. The solvent-mediated energetic interaction between monomers exactly compensates for the hard core repulsion at the θ-temperature. Binary contacts between chains still occur, they simply have

no effect on the free energy, and this directly leads to nearly ideal chain statistics at all concentrations in a θ-solvent, and the applicability of mean-field theory. However, binary contacts still control entanglements between chains. The number density of space-filling correlation volumes in a θ-solvent is given by the mean-field result $\xi^{-3} \sim \phi^3$. The same mean-field ideas determine the number density of binary intermolecular contacts to be proportional to ϕ^2. Just as in the good solvent, the average distance between binary contacts is given by the reciprocal cube root of this number density, and in a θ-solvent the distance is proportional to $\phi^{-2/3}$. Once again, we expect the tube diameter to be proportional to, but larger than, the distance between binary contacts:

$$a(\phi) \approx a(1)\phi^{-2/3} \quad \text{for a } \theta\text{-solvent.} \tag{9.31}$$

The length scales ξ, a, and R are plotted as a function of concentration for a typical good solvent in Fig. 9.7. All three length scales change their concentration dependences from athermal to ideal at the concentration $\phi^{**} \approx v/b^3$ separating semidilute and concentrated solutions.

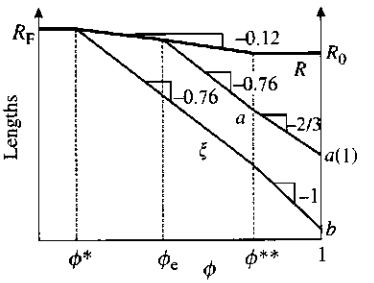

Fig. 9.7
Chain size R, tube diameter a, and correlation length ξ in a good solvent. The semidilute unentangled regime is $\phi^* < \phi < \phi_e$; the semidilute entangled regime is $\phi_e < \phi < \phi^{**}$ and; the concentrated regime is $\phi^{**} < \phi < 1$.

9.3.2 Entanglement concentration

The concentration at which the correlation length ξ is of the order of the coil size $R \approx bN^{\nu}$ is the overlap concentration ϕ^*, given by Eq. (5.19):

$$\phi^* \approx \frac{Nb^3}{R^3} \approx N^{1-3\nu}. \tag{9.32}$$

In an athermal solvent $\phi^* \approx N^{-0.76}$, while in a θ-solvent $\phi^* \approx N^{-1/2}$.

The concentration at which the tube diameter a [from Eqs (9.30) or (9.31)] equals the coil size R [Eq. (9.29)] is the **entanglement concentration** ϕ_e:

$$\phi_e \approx \begin{cases} [N_e(1)/N]^{(3\nu-1)} \approx [N_e(1)/N]^{0.76} & \text{for an athermal solvent,} \\ [a(1)/b]^{3/2}N^{-3/4} \approx [N_e(1)/N]^{3/4} & \text{for a } \theta\text{-solvent,} \end{cases} \tag{9.33}$$

where $N_e(1)$ is the number of Kuhn monomers in an entanglement strand in the melt. Note that the predictions for both solvents are very similar.

For $\phi > \phi_e$, entanglement effects control chain dynamics and the reptation model must be used as described below. Between the overlap concentration and the entanglement concentration ($\phi^* < \phi < \phi_e$), the solution is semidilute but not entangled, and the unentangled solution model of Section 8.5 describes dynamics. The width of this semidilute unentangled regime is given by the ratio of Eqs (9.33) and (9.32):

$$\frac{\phi_e}{\phi^*} \approx \begin{cases} [N_e(1)]^{3\nu-1} \approx [N_e(1)]^{0.76} & \text{for an athermal solvent,} \\ ([N_e(1)]^{3/4})/N^{1/4} & \text{for a } \theta\text{-solvent.} \end{cases} \tag{9.34}$$

Table 9.1 shows that the number of Kuhn monomers in an entanglement strand in the melt state varies over a wide range ($7 < N_e(1) < 80$) making $4 < \phi_e/\phi^* < 30$ for solutions in an athermal solvent. Since the entanglement concentration ϕ_e cannot be lower than the overlap concentration ϕ^*, the expressions for a θ-solvent [Eqs (9.31), (9.33), and (9.34)] are valid for $N < [N_e(1)]^3$. This condition is not very restrictive and it is satisfied for all experimental studies to date.

9.3.3 Plateau modulus

Owing to the fact that the tube diameter is always larger than the correlation length ($a > \xi$), the entanglement strand is a random walk of correlation volumes in any solvent:

$$a \approx \xi \sqrt{\frac{N_e}{g}}, \tag{9.35}$$

where N_e/g is the number of correlation volumes per entanglement strand. The above relation can be solved for the concentration dependence of the number of monomers in an entanglement strand:

$$N_e(\phi) \approx g\left(\frac{a}{\xi}\right)^2 \approx N_e(1)\begin{cases} \phi^{-1/(3\nu-1)} & \text{for an athermal solvent,} \\ \phi^{-4/3} & \text{for a } \theta\text{-solvent.} \end{cases} \tag{9.36}$$

The two predictions are nearly identical, since $1/(3\nu - 1) \cong 1.3$.

The occupied volume of an entanglement strand is $\xi^3 N_e/g \approx a^2\xi$. Since the correlation volumes are space-filling in solution, the number density of entanglement strands is simply the reciprocal of this volume. Analogous to Eq. (9.5), the plateau modulus of an entangled polymer solution is once again of the order of kT per entanglement strand,

$$G_e(\phi) \approx \frac{kT}{a^2\xi} \approx \frac{kT\phi}{b^3 N_e(\phi)} \approx G_e(1)\begin{cases} \phi^{3\nu/(3\nu-1)} & \text{for an athermal solvent,} \\ \phi^{7/3} & \text{for a } \theta\text{-solvent,} \end{cases} \tag{9.37}$$

where $G_e(1)$ is the plateau modulus of the melt, given by Eq. (9.5). The predictions for athermal and θ-solvents are essentially the same (the concentration dependence exponents are $\cong 2.3$ in both cases). This interesting result is experimentally confirmed, as shown in Fig. 9.8.

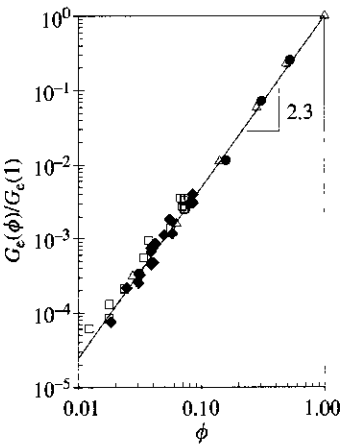

Fig. 9.8
Dilution effect on the plateau modulus of linear polymers. Filled diamonds are polystyrene in cyclohexane at 34.5 °C (θ-solvent), open squares are polystyrene in benzene at 25 °C (good solvent), filled circles are polybutadiene in dioctylphthalate at 25 °C (near θ-solvent) and open triangles are polybutadiene in phenyloctane (good solvent). PS data from M. Adam and M. Delsanti, *J. Phys. France* **44**, 1185 (1983); **45**, 1513 (1984). PB data from R. H. Colby *et al.*, *Macromolecules* **24**, 3873 (1991).

9.3.4 Relaxation times and diffusion

Topological constraints do not influence polymer motion on length scales smaller than the size of an entanglement strand. In entangled polymer solutions, chain sections with end-to-end distance shorter than the tube

diameter a move as they would in an unentangled solution. On length scales smaller than the correlation length ξ, hydrodynamic interactions are not screened. As with unentangled chains, the relaxation time τ_ξ of the strand within each correlation volume is determined by the Zimm result [Eq. (8.75)]:

$$\tau_\xi \approx \frac{\eta_s}{kT}\xi^3 \approx \frac{\eta_s b^3}{kT}\left(\frac{\xi}{b}\right)^3 \approx \tau_0\left(\frac{\xi}{b}\right)^3 \approx \tau_0\phi^{-3\nu/(3\nu-1)}. \tag{9.38}$$

On length scales larger than the correlation length ξ but smaller than the tube diameter a, hydrodynamic interactions are screened, and topological interactions are unimportant. Polymer motion on these length scales is described by the Rouse model. The relaxation time τ_e of an entanglement strand of N_e monomers is that of a Rouse chain of N_e/g correlation volumes [Eq. (8.76)]:

$$\tau_e \approx \tau_\xi\left(\frac{N_e}{g}\right)^2 \approx \tau_0[N_e(1)]^2\begin{cases}\phi^{-3\nu/(3\nu-1)} & \text{for an athermal solvent,}\\ \phi^{-5/3} & \text{for a } \theta\text{-solvent.}\end{cases} \tag{9.39}$$

On length scales larger than the tube diameter, topological interactions are important and the motion is described by the reptation model with the chain relaxation time given by the reptation time:

$$\tau_{rep} \approx \tau_e\left(\frac{N}{N_e}\right)^3 \approx \tau_0\left(\frac{\xi}{b}\right)^3\left(\frac{N_e}{g}\right)^2\left(\frac{N}{N_e}\right)^3. \tag{9.40}$$

Using Eqs (9.27), (9.28), and (9.36) transforms this into a simple relation for the concentration dependence of the reptation time:

$$\tau_{rep} \approx \tau_0\frac{N^3}{N_e(1)}\begin{cases}\phi^{3(1-\nu)/(3\nu-1)} & \text{for an athermal solvent,}\\ \phi^{7/3} & \text{for a } \theta\text{-solvent.}\end{cases} \tag{9.41}$$

The reptation time has a considerably weaker concentration dependence in athermal solvent than in θ-solvent, since $3(1-\nu)/(3\nu-1) \cong 1.6$. Note that Eq. (9.41) reduces to Eq. (9.20) when $\phi = 1$.

The diffusion coefficient in semidilute polymer solutions is determined from the fact that the chain diffuses a distance of order of its own size in its reptation time:

$$D \approx \frac{R^2}{\tau_{rep}} \approx \frac{b^2}{\tau_0}\frac{N_e(1)}{N^2}\begin{cases}\phi^{-(2-\nu)/(3\nu-1)} & \text{for an athermal solvent,}\\ \phi^{-7/3} & \text{for a } \theta\text{-solvent.}\end{cases} \tag{9.42}$$

The reptation prediction of the concentration dependence of diffusion coefficient in athermal solvent is slightly weaker than in θ-solvent, since

$(2-\nu)/(3\nu-1) \cong 1.85$. Figure 8.9 already showed that there is a low concentration regime that is semidilute but unentangled that is described by Eq. (8.85). That regime persists for roughly one decade in good solvent, as expected by Eq. (9.34). Above the entanglement concentration ϕ_e, the athermal solvent prediction of Eq. (9.42) applies for a range of concentration (see Fig. 8.9). At still higher concentrations, an even stronger concentration dependence is noted for the two highest concentrations in Fig. 8.9, consistent with the θ-solvent scaling prediction of Eq. (9.42) in concentrated solution (for $\phi > \phi^{**}$):

$$D \sim \begin{cases} \phi^{-0.54} & \text{for } \phi^* < \phi < \phi_e, \\ \phi^{-1.85} & \text{for } \phi_e < \phi < \phi^{**}, \\ \phi^{-7/3} & \text{for } \phi^{**} < \phi < 1. \end{cases} \tag{9.43}$$

9.3.5 Stress relaxation and viscosity

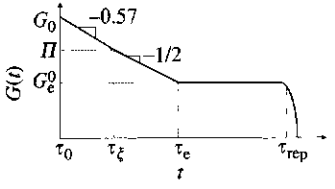

Fig. 9.9
Schematic representation of the stress relaxation modulus of an entangled polymer solution in an athermal solvent on logarithmic scales.

There are three different regimes of polymer dynamics on three different length and time scales for an entangled polymer solution in an athermal solvent. The stress relaxation modulus of such a solution is shown in Fig. 9.9. Two of the regimes are identical to those discussed in Section 9.2.2 and the other regime was discussed in Section 8.5.

Between τ_0 and the relaxation time of a correlation blob τ_ξ, both static and dynamic properties are similar to those in a dilute solution. Hydrodynamic interactions are important and dynamics of these small sections of chains are described by the Zimm model. The stress relaxation modulus on time scales between τ_0 and τ_ξ is similar to the Zimm result for unentangled solutions discussed in Section 8.5 [Eq. (8.88)]. The stress relaxation modulus decays with time as a power law with exponent $-1/(3\nu)$. This time dependence is $G(t) \sim t^{-0.57}$ in a good solvent with Flory exponent $\nu \cong 0.588$ and is $G(t) \sim t^{-2/3}$ in a θ-solvent. The stress relaxation modulus in this regime decays from the Kuhn modulus G_0 (kT per Kuhn monomer) to the osmotic pressure Π [kT per correlation blob, see Eq. (8.89)].

On intermediate length scales between the correlation length ξ and the tube diameter a, hydrodynamic interactions are screened and topological interactions are not important. The dynamics on these intermediate scales (for $\tau_\xi < t < \tau_e$) are described by the Rouse model with stress relaxation modulus similar to the Rouse result for unentangled solutions [Eq. (8.90) with the long time limit the Rouse time of an entanglement strand τ_e]. At τ_e, the stress relaxation modulus has decayed to the plateau modulus G_e[kT per entanglement strand, Eq. [(9.37), see Fig. 9.9)]. The ratio of osmotic pressure and plateau modulus at any concentration in semidilute solution in athermal solvents is proportional to the number of Kuhn monomers in an entanglement strand in the melt. In θ-solvents this ratio is considerably smaller and concentration dependent:

$$\frac{\Pi}{G_e} \approx \left(\frac{a}{\xi}\right)^2 \approx \begin{cases} N_e(1) & \text{for an athermal solvent,} \\ N_e(1)\phi^{2/3} & \text{for a } \theta\text{-solvent.} \end{cases} \tag{9.44}$$

At the Rouse time of an entanglement strand τ_e, the chain in semidilute solution 'finds out' that it is trapped in the confining tube. The stress relaxation modulus between τ_e and the reptation time τ_{rep} is almost constant and equal to the plateau modulus (see Fig. 9.9). At the reptation time [Eq. (9.41)], the stress relaxation modulus decays to zero exponentially [Eq. (9.22)].

The polymer contribution to the viscosity of an entangled polymer solution is estimated as the product of the plateau modulus [Eq. (9.37)] and the reptation time [Eq. (9.41)]:

$$\eta - \eta_s \approx G_e \tau_{rep} \approx \eta_s \frac{N^3}{[N_e(1)]^2} \begin{cases} \phi^{3/(3\nu-1)} & \text{for an athermal solvent,} \\ \phi^{14/3} & \text{for a } \theta\text{-solvent.} \end{cases} \tag{9.45}$$

The concentration dependence of viscosity is $\eta \sim \phi^{3.9}$ in an athermal solvent with Flory exponent $\nu \cong 0.588$ and $\eta \sim \phi^{4.7}$ in a θ-solvent. The $14/3 \cong 4.7$ exponent is demonstrated for poly(ethylene oxide) in water at 25.0 °C in Fig. 8.11. There are two different scaling regimes for the specific viscosity in an athermal solvent, corresponding to unentangled and entangled semidilute solutions:

$$\eta_{sp} \approx \begin{cases} (\phi/\phi^*)^{1/(3\nu-1)} & \text{for } \phi^* < \phi < \phi_e, \\ (\phi/\phi^*)^{3/(3\nu-1)}/[N_e(1)]^2 & \text{for } \phi_e < \phi < 1. \end{cases} \tag{9.46}$$

Data for different molar masses of the same polymer species combine into a single plot in good solvent [Fig. 9.10(a)] if specific viscosity $\eta_{sp} = (\eta - \eta_s)/\eta_s$ is plotted as a function of reduced concentration ϕ/ϕ^*. This simple data collapse works in a good solvent because the correlation length and the tube diameter are proportional to each other, with the same concentration exponents. The line in Fig. 9.10(a) has the slope of 3.9 expected by Eq. (9.46) for semidilute entangled solutions.

In a θ-solvent, the correlation length ξ and the tube diameter a have different concentration dependences [$\xi \approx b\phi^{-1}$, Eq. (9.27), with $\nu = 1/2$ and $a \approx a$ (1) $\phi^{-2/3}$, Eq. (9.31)]. The simple plot of relative viscosity η/η_s vs. ϕ/ϕ^* will only collapse data for different molar masses in unentangled solutions, but *not* in entangled solutions in a θ-solvent.

$$\eta_{sp} \approx \begin{cases} (\phi/\phi^*)^2 & \text{for } \phi^* < \phi < \phi_e, \\ (\phi/\phi^*)^{14/3} N^{2/3}/[N_e(1)]^2 & \text{for } \phi_e < \phi < 1. \end{cases} \tag{9.47}$$

Construction of a reduced data plot for the viscosity of entangled solutions of a given type of polymer in θ-solvents requires plotting $\eta_{sp}/N^{2/3}$ as a function of reduced concentration, as demonstrated in Fig. 9.10(b). This complicated form of data reduction is a direct consequence of the two length scales a and ξ having different concentration dependences in θ-solvent. The line in Fig. 9.10(b) has the slope predicted by Eq. (9.47).

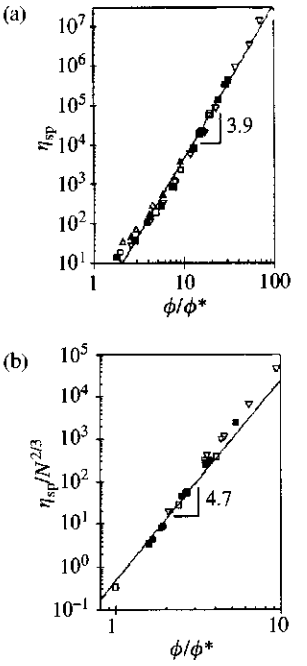

Fig. 9.10
Concentration dependence of viscosity in semidilute solutions of polystyrene at 35 °C. (a) Solutions in the good solvent toluene have ϕ/ϕ^* reduce data for different molar masses to a universal curve, using data from M. Adam and M. Delsanti, *J. Phys. France* **44**, 1185 (1983). (b) Solutions in the θ-solvent cyclohexane must have specific viscosity divided by $N^{2/3}$ for ϕ/ϕ^* to reduce data to a universal curve, using data from M. Adam and M. Delsanti, *J. Phys. France* **45**, 1513 (1984).
Open triangles are $M = 171\,000\ \mathrm{g\,mol^{-1}}$, filled triangles are $M = 422\,000\ \mathrm{g\,mol^{-1}}$, open circles are $M = 1\,260\,000\ \mathrm{g\,mol^{-1}}$, filled circles are $M = 2\,890\,000\ \mathrm{g\,mol^{-1}}$, open squares are $M = 3\,840\,000\ \mathrm{g\,mol^{-1}}$, filled squares are $M = 6\,770\,000\ \mathrm{g\,mol^{-1}}$, and open inverted triangles are $M = 20\,600\,000\ \mathrm{g\,mol^{-1}}$.

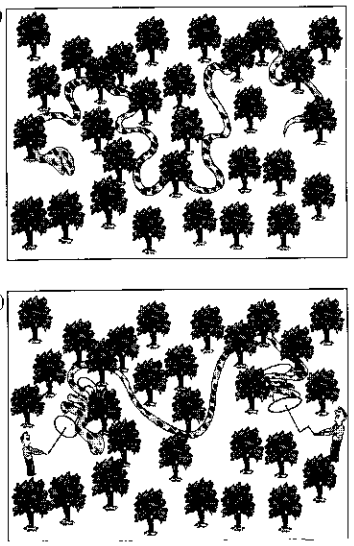

Fig 9.11
Frame (a) shows a two-dimensional model of a chain in a permanent entanglement network: a giant snake in a forest. Frame (b) shows two students reeling-in the ends of the snake to construct the primitive path.

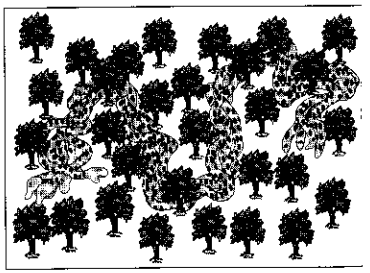

Fig. 9.12
A long-exposure photograph of the giant snake in the forest clearly defines its confining tube.

The entangled viscosity data in both good solvent and θ-solvent show stronger concentration dependences than predicted by the simple reptation model. The steeper experimental slopes are consistent with the additional relaxation modes discussed in Section 9.4.5 (see Problem 9.14).

In order to construct a universal plot for the viscosity of all entangled polymer solutions in a given class of solvent, it is necessary to also multiply the ordinates of Fig. 9.10 by $[N_e(1)]^2$ because different polymers have different numbers of Kuhn monomers in their entanglement strands in the melt (see Table 9.1). Such universal plots have indeed been constructed successfully in the literature.

9.4 Dynamics of a single entangled chain

9.4.1 Chain in an array of fixed obstacles

Chains in polymer melts and entangled polymer solutions form an effective entanglement network. Since chains in melts and solutions are free to diffuse, the entanglements they form with their neighbours are temporary and have finite lifetime. Any given chain can disentangle from its neighbours by its own motion (reptate away) or by the motion of its neighbours. Effects of the motion of surrounding chains on the dynamics of a given chain will be discussed in Section 9.5.

A simple case to consider first is a single chain diffusing through a network, where the network only imposes permanent topological obstacles[2] that retard the motion of the chain. Consider an ideal chain in an array of fixed topological obstacles. A two-dimensional schematic representation of this problem, a giant snake in a forest, is presented in Fig. 9.11a. The snake randomly meanders through the forest and each of its conformations are assumed to be as likely as any other (an ideal snake). If the snake gets tired of being in a certain conformation, it is difficult for it to get into a completely different one because of the trees in the forest. These trees constrain this poor reptile to move primarily along its contour. Sideways excursions, although possible, put the snake into uncomfortable conformations with loops. The topological constraints imposed by the trees determine that the preferred path for the motion of the snake is along the confining tube.

The primitive path is the centre line of the confining tube. It can be visualized by hiring one smart student and one brave student to reel in the snake at its ends (Fig. 9.11b). The final contour of the snake, when pulled taut, is the primitive path—the shortest path with the same 'topology' as the original conformation of the snake. A long-exposure photograph of the wiggling snake, taken by a curious student, depicts the whole confining tube in Fig. 9.12.

The reptation model assumes the contour length of the primitive path is fixed at its average value $\langle L \rangle$. In reality, the primitive path length

[2] Real networks can lead to correlation and excluded volume effects on chain conformation that we ignore here.

L fluctuates in time as the chain (or snake) moves. A full description of chain dynamics requires knowledge of the probability distribution of the primitive path lengths. This problem has been solved exactly by Helfand and Pearson in 1983 for a lattice model of a chain in a regular array of topological obstacles, but here we present a simple estimate of the probability distribution of primitive path lengths.

If an ideal linear chain is confined to a cylindrical pore of diameter a, it occupies a section of the pore of length $R_{\|} \approx b\sqrt{N}$ [Eq. (3.47)]. Entangled chains occupy a much longer length of confining tube $\langle L \rangle \approx bN/\sqrt{N_e} \gg b\sqrt{N}$, making them strongly stretched. The source of this stretching is the entropy gain at each tube end because each end segment of the primitive path is free to choose from multiple possible directions. This entropy gain leads to an approximately linear contribution to the free energy of a chain in a confining tube[3] of order kT per primitive path step,

$$F_{\text{ent}}(L) \approx -\Upsilon kT\frac{L}{a}, \tag{9.48}$$

where Υ is a numerical constant of order unity. This approximately linear potential can be thought of as arising from nearly constant entropic forces of order kT/a acting on the chain at the tube ends. The chain in its confining tube is effectively under a tension kT/a and can be represented as an array of Pincus blobs of size a (see Section 3.2.1). Stretching an ideal chain along the contour of its tube to length L raises its free energy by $\gamma kTL^2/(2Nb^2)$, where γ is an effective dimensionless spring constant of order unity. The total free energy of a chain in a tube is the sum of these two effects:

$$\begin{aligned} F(L) &\approx \frac{\gamma kTL^2}{2Nb^2} - \Upsilon kT\frac{L}{a} \\ &\approx \frac{\gamma kT}{2Nb^2}\left[L^2 - \frac{2\Upsilon Nb^2}{\gamma a}L + \left(\frac{\Upsilon Nb^2}{\gamma a}\right)^2\right] - \frac{kT\Upsilon^2 Nb^2}{2\gamma a^2} \\ &\approx \frac{\gamma kT}{2Nb^2}(L - \langle L \rangle)^2 - \frac{kT\Upsilon^2}{2\gamma}\frac{N}{N_e}. \end{aligned} \tag{9.49}$$

In the second line of Eq. (9.49), the term $kT\Upsilon^2 Nb^2/(2\gamma a^2)$ was added and subtracted so as to complete the square inside the square brackets, in order to recover the expression for the equilibrium tube length $\langle L \rangle \approx \Upsilon Nb^2/(\gamma a)$ [Eq. (9.3)]. This quadratic approximation for the free energy of **tube length fluctuations** around the average value $\langle L \rangle$ was first proposed by Doi and Kuzuu in 1980:

$$F(L) = \frac{\gamma kT}{2Nb^2}(L - \langle L \rangle)^2. \tag{9.50}$$

The constant term $kT\Upsilon^2 N/(2\gamma N_e)$ in Eq. (9.49) does not affect the dependence of the free energy $F(L)$ on the contour length L of the primitive

[3] The contribution to the free energy is not strictly linear because for each primitive path length L, the entropy of not only the ends, but of the rest of the chain in an entanglement network needs to be considered.

path. The quadratic approximation of the free energy leads to a Gaussian probability distribution of the tube length L for a chain with N monomers:

$$p(N,L) \sim \exp\left[-\frac{F(L)}{kT}\right] \sim \exp\left[-\frac{\gamma}{2Nb^2}(L-\langle L\rangle)^2\right]. \tag{9.51}$$

The average length of a tube with diameter a is $\langle L\rangle \approx aN/N_e$ [Eq. (9.3)]. A typical fluctuation in the tube length corresponds to a free-energy change of order $F(L) - F(\langle L\rangle) \approx kT$:

$$\sqrt{\langle (L-\langle L\rangle)^2\rangle} \approx b\sqrt{N} = R \approx a\sqrt{N/N_e}. \tag{9.52}$$

Thus, a typical tube length fluctuation is of the order of the root-mean-square end-to-end distance R of the chain and the confining tube has a wide range of typical lengths:

$$L \approx \langle L\rangle \pm R \approx a\left(\frac{N}{N_e} \pm \sqrt{\frac{N}{N_e}}\right). \tag{9.53}$$

These thermal fluctuations of the tube length are the basis of the **Doi fluctuation model**, leading to significant modifications of reptation dynamics for entangled linear chains. Linear chains in a permanent network relax stress by abandoning tube sections via tube length fluctuations and reptation. Since the branch point of a branched polymer prohibits its reptation, branches relax only by fluctuations in tube length. For this reason, we next consider relaxation of simple branched polymers: star polymers (next section), H-polymers and comb polymers (Section 9.4.3). Star polymers in particular relax primarily by fluctuations in tube length. The ideas of tube length fluctuations and reptation will be combined in Sections 9.4.4 and 9.4.5 to treat linear polymers relaxing in a permanent network.

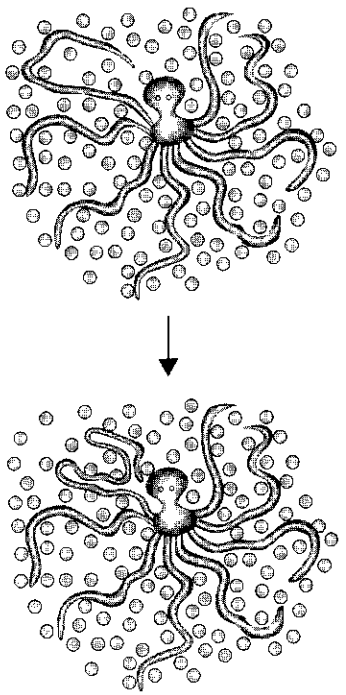

Fig. 9.13
Arm retraction of entangled star polymers demonstrated by an octopus in a fishing net. The circles are permanent topological constraints.

9.4.2 Entangled star polymers

All the discussions of entangled polymer dynamics above were limited to linear chains. The molecular architecture of the chain (star vs. linear vs. ring) significantly modifies polymer dynamics. Snake-like reptation is impossible for f-arm star polymers because they would have to drag $f-1$ arms along the tube of a single arm, significantly reducing the entropy of the star polymer. Therefore, the branch point of a star is usually localized in one cell of an entanglement net. Stars relax stress and diffuse by arm retractions, which are large (exponentially unlikely) fluctuations of the tube lengths of their arms. This is analogous to an octopus entangled in an array of topological constraints (a fishing net), sketched in Fig. 9.13.

The easiest way for the octopus to change the conformation of any of its arms without crossing the obstacles, represented by gray circles in Fig. 9.13, is by retracting that arm. Such arm retraction reduces the length L_a of its primitive path by forming loops. In Section 9.4.1, we demonstrated that such conformations with primitive path reduced by

more than the root-mean-square fluctuation R from its equilibrium length $\langle L_a \rangle$ are exponentially unlikely [Eq. (9.51)]. Arm retraction by distance $s = \langle L_a \rangle - L_a$ along the contour of the tube can be analysed as a thermally activated process in an effective potential $U(s) \equiv F(L_a)$ (see Fig. 9.14). This potential is typically approximated by a parabola [Eq. (9.50)]:

$$U(s) \approx \frac{\gamma kT}{2} \frac{(L_a - \langle L_a \rangle)^2}{N_a b^2} \approx \frac{\gamma kT}{2} \frac{s^2}{N_a b^2}. \tag{9.54}$$

The number of Kuhn monomers in each arm of the star is N_a and the effective spring constant of this harmonic potential is γ. Most of the time, the length L_a of the confining tube of an arm is close to its equilibrium value $\langle L_a \rangle$ with deviations from it $|s| \lesssim R = b\sqrt{N_a}$ [Eq. (9.53)] corresponding to an effective potential change of order kT.

Occasionally, there are large atypical fluctuations of the tube length (with $|s| = |L - \langle L \rangle| \gg R$) that are exponentially unlikely [Eq. (9.51)] because of the restricted number of conformations that allow such a state. The probability of the tube length to be reduced by s can be estimated by the Boltzmann weight in the effective potential $U(s)$ [Eq. (9.51)]:

$$p(s) \sim \exp\left(-\frac{U(s)}{kT}\right) \sim \exp\left(-\frac{\gamma}{2} \frac{s^2}{N_a b^2}\right). \tag{9.55}$$

The average time between these large fluctuations $\tau(s)$ is inversely proportional to their probability $p(s)$:

$$\tau(s) \sim \exp\left(\frac{\gamma}{2} \frac{s^2}{N_a b^2}\right). \tag{9.56}$$

The coefficient in front of the exponential depends on the degree of polymerization N of the arm as well as on the magnitude of arm retraction s, but the average retraction time is dominated by the exponential [Eq. (9.56)]. For these large tube length fluctuations, it is important to remember that the quadratic potential [Eq. (9.50)] and the related Gaussian distribution [Eq. (9.51)] are approximations valid for small tube length fluctuations $|L - \langle L \rangle| \ll L$. The probability of large tube length fluctuations deviates from the simple Gaussian form [Eq. (9.51)]. For example, Eq. (9.51) predicts that the probability for the primitive path to be reduced to $L = 0$ and for the chain to form a single loop is exponentially low in the number of entanglements per chain ($\exp[-\gamma N/(2N_e)]$). The actual probability indeed has an exponential dependence on the average number of entanglements per chain,

$$p(N, 0) \sim \exp\left(-\frac{\gamma'}{2} \frac{N_a}{N_e}\right), \tag{9.57}$$

but with a different coefficient in the exponential $\gamma' \neq \gamma$.

The relaxation time of a star in an array of fixed topological obstacles is equal to the time it takes to completely retract its arms, written here

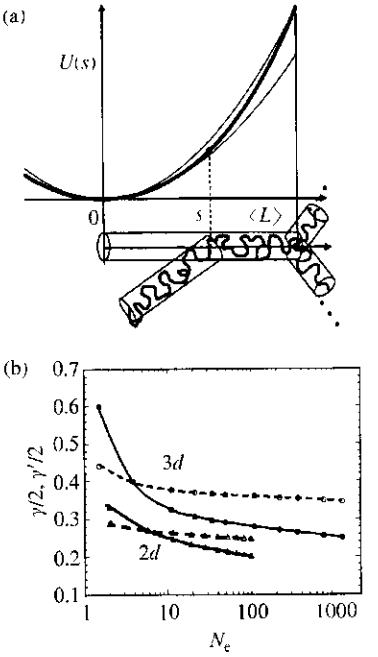

Fig. 9.14
(a) Effective potential for arm retraction for an entangled star polymer. The thin curves are harmonic approximations for small and large arm retractions. (b) Numerical results for the dependence of the effective spring constants γ (solid curves) and γ' (dashed curves) on the number of Kuhn monomers per entanglement strand on square (two-dimensional) and cubic (three-dimensional) lattices.

by including the power law 'prefactor' in the number of entanglements per arm:[4]

$$\tau_{\text{arm}} = \tau(\langle L\rangle) \sim \left(\frac{N_a}{N_e}\right)^{5/2} \exp\left(\frac{\gamma'}{2}\frac{\langle L\rangle^2}{N_a b^2}\right) \sim \left(\frac{N_a}{N_e}\right)^{5/2} \exp\left(\frac{\gamma'}{2}\frac{N_a}{N_e}\right). \quad (9.58)$$

The relaxation time of a star grows exponentially with the number of entanglements N_a/N_e per arm and is independent of the number of arms f in the star. The coefficient in the exponential is weakly dependent on the relative amount of arm retraction $s/\langle L\rangle$, changing from γ at small retractions to γ' at full retraction, because the harmonic potential is only an approximation of the actual potential. For polystyrene (with $N_e = 23$), the cubic lattice model predicts the spring constant of the harmonic potential to increase from $\gamma = 0.63$ for abandoning the first few tube sections to $\gamma' = 0.75$ for complete retraction of the arm $s = \langle L_a\rangle$ [see Fig. 9.14(b)]. However, this small change of γ to γ' changes the relaxation time of strongly entangled star polymers enormously. For example, a star with $N_a/N_e = 100$ entanglements per arm changes its relaxation time by a factor of $\exp(6) = 400$.

The stress relaxation modulus is proportional to the average fraction of entanglements per arm that have not yet relaxed by having the free end of the arm visiting that tube section. If s is the length of the tube that has been retracted and relaxed during time $t = \tau(s)$ then the stress relaxation modulus at time t is

$$G(t) \approx G_e \frac{\langle L_a\rangle - s}{\langle L_a\rangle} \quad \text{for } \tau_e < t < \tau_{\text{arm}}, \quad (9.59)$$

where G_e is the plateau modulus [Eq. (9.18)]. The stress relaxation modulus of a star polymer has a time dependence similar to that of a linear polymer with molar mass $2M_a$ (the span molar mass of the star polymer) for times shorter than the Rouse time of the span, as shown in the frequency dependence of the complex modulus in Fig. 9.15. At the terminal time τ_{arm},

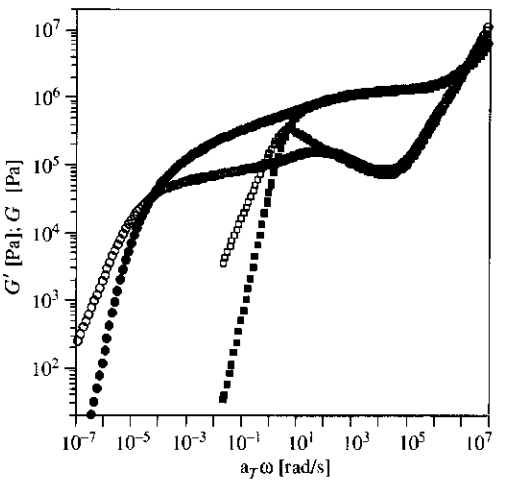

Fig. 9.15
Storage modulus (filled symbols) and loss modulus (open symbols) for linear 1,4-polybutadiene with $M_w = 160\,000\ \text{g mol}^{-1}$ (squares) and a 6-arm star 1,4-polybutadiene with $M_a = 77\,000\ \text{g mol}^{-1}$ (circles), both at a reference temperature of 28 °C. The linear polymer was chosen because it's molar mass is approximately the span molar mass of the star polymer. Data courtesy of L. Archer.

[4] See the Appendix of L. J. Fetters, *et al.*, *Macromolecules* **26**, 647 (1993).

there is of order one unrelaxed entanglement left per arm and the stress relaxation modulus is lower than the plateau modulus by the number of entanglements per arm:

$$G(\tau_{\text{arm}}) \approx \frac{N_e}{N_a} G_e. \tag{9.60}$$

The viscosity of entangled stars can be estimated as the product of the relaxation time and the terminal modulus:

$$\eta \approx G(\tau_{\text{arm}})\tau_{\text{arm}} \sim \left(\frac{N_a}{N_e}\right)^{3/2} \exp\left(\frac{\gamma'}{2}\frac{N_a}{N_e}\right). \tag{9.61}$$

The main feature is the exponential growth of the viscosity with the number of entanglements per arm N_a/N_e. Another interesting feature of the viscosity of entangled stars is that it is independent of the number of arms f. An experimental verification of this prediction is presented in Fig. 9.16. Viscosity of three-arm stars is $\sim 30\%$ lower than for stars with the same arm molar mass, but larger number of arms $f \geq 4$. This effect might be due to additional diving modes of a branch point down the tube of a three-arm star (see Problem 9.28).

Naively, one may think that for a branch point to hop between neighbouring entanglement cells, $f-2$ of the arms must simultaneously retract, forming essentially linear tube and $f-2$ large loops. This simultaneous retraction is an extremely unlikely event and its probability is the product of the already very low retraction probabilities for each of the $f-2$ arms. The problem with this naive approach is that it is indeed hard for an octopus to put on a sweater by pulling in all arms and then pushing them all out at the same time. It would be much easier for the octopus to retract one arm at a time. This way, in several steps of arm retraction it could form a favourable arrangement of tubes near the branch point for a successful hop of this branch point between neighbouring cells of an entanglement net.

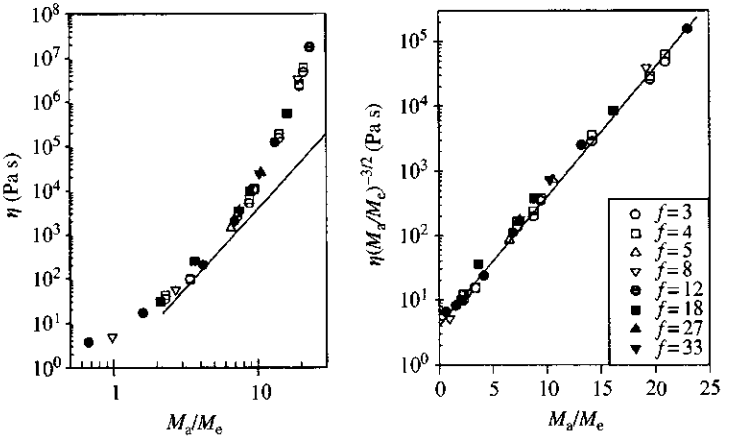

Fig. 9.16
Viscosity of polyisoprene star polymers with various numbers of arms at 60 °C. The left plot shows that viscosity is only a function of the number of entanglements per arm and that the viscosity of entangled linear polyisoprene (line with $M_a \equiv M/2$) is always lower. The right plot shows that Eq. (9.61) describes all star polymer viscosity data with the effective spring constant of the quadratic potential $\gamma' = 0.96$. Data from L. J. Fetters *et al.*, *Macromolecules* **26**, 647 (1993).

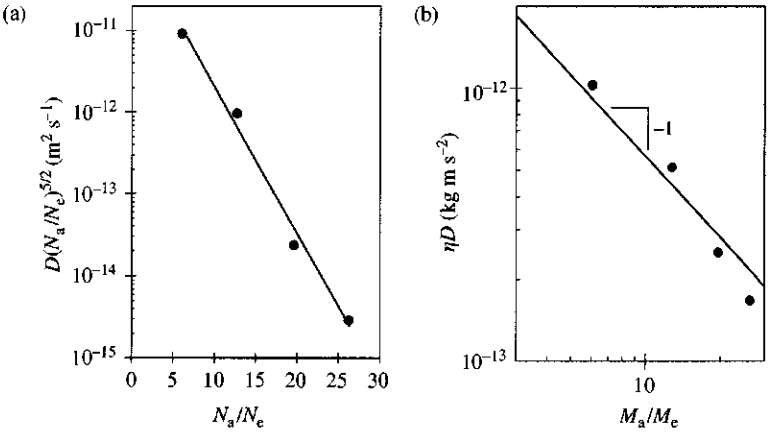

Fig. 9.17
(a) Diffusion coefficients of three-arm star hydrogenated polybutadienes at 165 °C. The slope determines $\gamma' = 0.82$. (b) The product of viscosity and diffusion coefficient is inversely proportional to the number of entanglements on each arm. Data are from C. R. Bartels *et al.*, *Macromolecules* **19**, 785 (1986).

Linear polymers move a distance of order of their own size during their relaxation time, leading to a diffusion coefficient $D \approx R^2/\tau$ [Eq. (9.12)]. However, the diffusion of entangled stars is different because at the time scale of successful arm retraction, the branch point can only randomly hop between neighbouring entanglement cells by a distance of order one tube diameter a. For this reason, diffusion of an entangled star is *much slower* than diffusion of a linear polymer with the same number of monomers:

$$D \approx \frac{a^2}{\tau_{\text{arm}}} \sim \left(\frac{N_a}{N_e}\right)^{-5/2} \exp\left(-\frac{\gamma'}{2}\frac{N_a}{N_e}\right). \tag{9.62}$$

The main feature of the diffusion coefficient of stars [Eq. (9.62)] is its exponential dependence on the number of entanglements per arm N_a/N_e related to the arm retraction time τ_{arm}. This prediction is in good agreement with experiments, as illustrated in Fig. 9.17(a) for diffusion of three-arm star hydrogenated polybutadienes. The product of viscosity [Eq. (9.61)] and diffusion coefficient [Eq. (9.62)] decreases with the number of entanglements per arm:

$$\eta D \approx G(\tau_{\text{arm}})a^2 \sim \frac{N_e}{N_a} \tag{9.63}$$

as shown in Fig. 9.17(b).

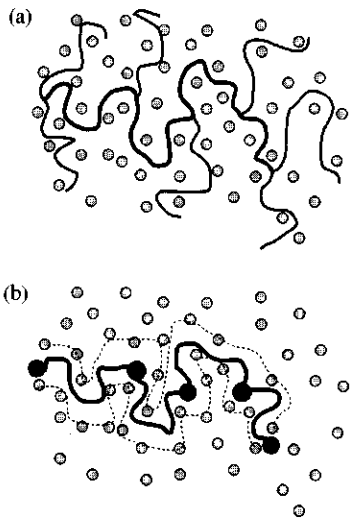

Fig. 9.18
(a) Entangled comb polymer with $q = 7$ branches and N_a monomers per branch and a backbone (thick line) with N_{bb} monomers. (b) Reptating backbone of a comb with N_{bb} monomers (thick line) and $q - 2 = 5$ high friction points (black circles) in its confining tube (dashed lines).

9.4.3 H-polymers and combs

The arm retraction mechanism of star dynamics can be applied to other entangled branched polymers, such as H-polymers and comb polymers (see Fig. 1.5) in an array of fixed topological obstacles. In the simplest case, all side branches of an H-polymer or a comb polymer are the same and contain N_a monomers (Fig. 9.18). The delineation of the comb into the backbone (thick line) and branches is done so that the ends of the backbone coincide with the branch points at the two ends of the polymer.

The retraction time of an arm τ_{arm} in an array of fixed obstacles is the same as the relaxation time of a star polymer with N_a monomers per arm [Eq. (9.58)]. On time scales shorter than τ_{arm}, the branch points are localized and cannot move between neighbour cells of the entanglement net. The branch points begin to hop between neighbouring cells of the entanglement net on the time scale of arm retraction τ_{arm}. Similar to star polymers, the length scale of these hops is of the order of the tube diameter a, allowing the effective friction coefficient for motion of the branch points to be determined by the retraction time of an arm:

$$\zeta_{br} \approx kT\frac{\tau_{arm}}{a^2}. \tag{9.64}$$

The backbone of the polymer moves by reptation along the contour of its tube, with curvilinear diffusion dominated by the branch point friction ζ_{br}. An H-polymer is the simplest comb polymer with $q=4$ branches per molecule. For any trifunctional comb polymer ($q \geq 4$) the number of branch points is $q-2$ since each end of the backbone has two branches. The total number of monomers in the reptating backbone is N_{bb}. We assume that branches are well-entangled, so that the branch points dominate the friction:

$$(q-2)\zeta_{br} \gg \zeta(N_{bb} + qN_a), \tag{9.65}$$

where ζ is the monomeric friction coefficient and $N_{bb}+qN_a$ is the total number of monomers in the whole chain. The curvilinear diffusion coefficient of the backbone along its confining tube is given by the Rouse model [Eq. (9.7)] with friction from the $q-2$ branch points:

$$D_c \approx \frac{kT}{(q-2)\zeta_{br}} \approx \frac{a^2}{(q-2)\tau_{arm}}. \tag{9.66}$$

The length of the confining tube of the backbone is $L_{bb} \approx aN_{bb}/N_e$ leading to the reptation time of the backbone:

$$\tau_{rep} \approx \frac{L_{bb}^2}{D_c} \approx \tau_{arm}(q-2)\left(\frac{N_{bb}}{N_e}\right)^2. \tag{9.67}$$

The diffusion coefficient of entangled H-polymers and combs is the mean-square size of the backbone divided by its reptation time:

$$D \approx \frac{N_{bb}b^2}{\tau_{rep}} \approx \frac{a^2}{\tau_{arm}(q-2)}\left(\frac{N_e}{N_{bb}}\right). \tag{9.68}$$

The stress relaxation modulus of combs and H-polymers consists of an arm-retraction part at shorter times ($t < \tau_{arm}$) and a reptation part at longer times ($\tau_{arm} < t < \tau_{rep}$).

9.4.4 Monomer displacement in entangled linear melts

On time scales shorter than the relaxation time of an entanglement strand τ_e, the sections of a linear chain involved in coherent motion are

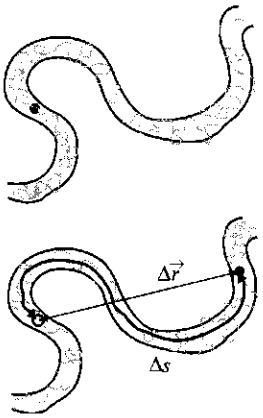

Fig. 9.19
Curvilinear displacement of a monomer (labelled by a dark circle) along the contour of the tube between two conformations is Δs. Only a short section of the tube is shown.

shorter than the entanglement strand and are not aware of the topological constraints. Since hydrodynamic interactions are screened in polymer melts, the motion on very short time scales $t < \tau_e$ is Rouse-like with mean-square monomer displacement given by the subdiffusive motion of the Rouse model [Eq. (8.58)].

$$\langle[\vec{r}(t) - \vec{r}(0)]^2\rangle \approx b^2\left(\frac{t}{\tau_0}\right)^{1/2} \quad \text{for } t < \tau_e. \tag{9.69}$$

On longer time scales $t > \tau_e$, topological constraints restrict polymer motion to the confining tube. Displacements of monomers tangential to the axis of the tube (primitive path) on length scales larger than the tube diameter a are suppressed by surrounding chains. Monomer displacement along the contour of the tube is unconstrained and follows the subdiffusive motion of the Rouse model [Eq. (8.58)] *along the primitive path.*

For times shorter than the Rouse time of the chain ($t < \tau_R$), each monomer participates in coherent motion of a chain segment consisting of $\sqrt{t/\tau_0}$ neighbouring monomers. The time-dependent curvilinear coordinate of a monomer along the contour of the tube is $s(t)$ (Fig. 9.19). The mean-square monomer displacement *along the tube* is of the order of the mean-square size of this section in three-dimensional space [Eq. (8.58)]:

$$\langle[s(t) - s(0)]^2\rangle \approx b^2\left(\frac{t}{\tau_0}\right)^{1/2} \approx a^2\left(\frac{t}{\tau_e}\right)^{1/2} \quad \text{for } \tau_e < t < \tau_R. \tag{9.70}$$

Since the tube itself is a random walk with step length a, the mean-square displacement of a monomer in three-dimensional space $\langle\Delta r^2\rangle$ is the product of the step length a and the contour length displacement $\sqrt{\langle\Delta s^2\rangle}$:

$$\langle\Delta r^2\rangle \approx a\sqrt{\langle\Delta s^2\rangle}. \tag{9.71}$$

Thus, the mean-square monomer displacement in space exhibits a weak one-fourth power law in time when the chain is confined to a tube:

$$\langle[\vec{r}(t) - \vec{r}(0)]^2\rangle \approx a\sqrt{\langle[s(t) - s(0)]^2\rangle} \approx a^2\left(\frac{t}{\tau_e}\right)^{1/4} \quad \text{for } \tau_e < t < \tau_R. \tag{9.72}$$

This time dependence is slower than for unrestricted Rouse motion [Eq. (8.58)] because displacement along the contour of the tube leads to a smaller displacement in space [Eq. (9.71)]. At the Rouse time of the chain,

$$\tau_R \approx \tau_0 N^2 \approx \tau_e\left(\frac{N}{N_e}\right)^2, \tag{9.73}$$

each monomer participates in coherent Rouse motion of the whole chain along the tube. The mean-square displacement of a monomer along the

tube at the Rouse time of the chain is of the order of the mean-square size of the *whole chain*:

$$\langle [s(\tau_R) - s(0)]^2 \rangle \approx b^2 N \approx R^2. \tag{9.74}$$

Note that the root-mean-square magnitude of these fluctuations is in perfect agreement with the value of tube length fluctuations derived above [Eq. (9.52)]. Even though this magnitude seems large, it is a small fraction of the contour length of the tube [Eq. (9.3)]:

$$\frac{R}{L} \approx \frac{bN^{1/2}}{bNN_e^{-1/2}} \approx \left(\frac{N_e}{N}\right)^{1/2}. \tag{9.75}$$

At times longer than the Rouse time τ_R, all monomers move coherently with the chain. The chain diffuses along the tube, with a curvilinear diffusion coefficient given by the Rouse model $D_c \approx R^2/\tau_R$:

$$\langle [s(t) - s(0)]^2 \rangle \approx D_c t \approx b^2 N \frac{t}{\tau_R} \approx a^2 \frac{N}{N_e} \frac{t}{\tau_R} \quad \text{for } t > \tau_R. \tag{9.76}$$

In entangled polymer melts this diffusion occurs along the contour of the tube, with the mean-square monomer displacement in space determined using Eq. (9.71):

$$\left\langle [\vec{r}(t) - \vec{r}(0)]^2 \right\rangle \approx a\sqrt{\langle [s(t) - s(0)]^2 \rangle}$$
$$\approx a^2 \left(\frac{N}{N_e}\right)^{1/2} \left(\frac{t}{\tau_R}\right)^{1/2} \quad \text{for } \tau_R < t < \tau_{rep}. \tag{9.77}$$

This curvilinear motion continues up to the reptation time τ_{rep} where the chain has curvilinearly diffused the complete length of the tube, of order aN/N_e. At times longer than the reptation time ($t > \tau_{rep}$) the mean-square displacement of a monomer is approximately the same as the centre of mass of the chain and is a simple diffusion with diffusion coefficient D [Eq. (9.12)].

There are four different regimes of monomer displacement in entangled linear polymer melts, shown in Fig. 9.20. The $t^{1/4}$ subdiffusive regime for the mean-square monomer displacement is a unique characteristic of Rouse motion of a chain confined to a tube, which has been found in both NMR experiments and computer simulations.

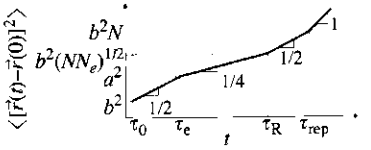

Fig. 9.20
Time dependence of the mean-square monomer displacement predicted by the reptation model for a melt of long entangled linear chains, on logarithmic scales.

9.4.5 Tube length fluctuations

Displacements of monomers at the two ends of the tube are unrelated to each other on time scales shorter than the Rouse time of the chain ($t < \tau_R$). These incoherent curvilinear displacements lead to tube length fluctuations [Eq. (9.70)]:

$$\langle [L(t) - L(0)]^2 \rangle \approx b^2 \left(\frac{t}{\tau_0}\right)^{1/2} \approx a^2 \left(\frac{t}{\tau_e}\right)^{1/2} \quad \text{for } \tau_e < t < \tau_R. \tag{9.78}$$

Doi was the first to point out that the decrease of tube length due to these fluctuations leads to partial relaxation of stress. The stress relaxation modulus $G(t)$ is not quite constant in the rubbery plateau, but decreases slightly with time. The weak time dependence of the stress relaxation modulus corresponds to the rate at which sections of the tube are vacated by the fluctuating chain. Subdiffusive Rouse dynamics along the contour of the tube [Eq. (8.58)] implies a $t^{1/4}$ time dependence of vacated sections of the tube [see Eq. (9.70)]:

$$\begin{aligned} G(t) &\approx G_e \frac{L(t)}{\langle L \rangle} \approx G_e \frac{\langle L \rangle - \sqrt{\langle [L(t) - L(0)]^2 \rangle}}{\langle L \rangle} \\ &\approx G_e \left[1 - \frac{b}{\langle L \rangle} \left(\frac{t}{\tau_0} \right)^{1/4} \right] \\ &\approx G_e \left[1 - \frac{N_e}{N} \left(\frac{t}{\tau_e} \right)^{1/4} \right] \quad \text{for } \tau_e < t < \tau_R. \end{aligned} \tag{9.79}$$

The last relation made use of the fact that $\langle L \rangle \approx aN/N_e \approx bN/\sqrt{N_e}$ and $\tau_e \approx \tau_0 N_e^2$. The tube length fluctuations grow and the stress relaxation modulus decreases up to the Rouse time of the whole chain [Eq. (8.17)]. Consequently, the stress relaxation modulus at the Rouse time of the chain is lower than G_e:

$$G(\tau_R) \approx G_e \left[1 - \frac{N_e}{N} \left(\frac{\tau_R}{\tau_e} \right)^{1/4} \right] \approx G_e \left[1 - \mu \sqrt{\frac{N_e}{N}} \right]. \tag{9.80}$$

The final result was obtained using Eq. (9.19) ($\tau_R/\tau_e \approx (N/N_e)^2$) and μ is a coefficient of order unity. The fraction $\sqrt{N_e/N}$ of the tube is vacated, and therefore relaxed, at the Rouse time of the chain by tube length fluctuations. The modulus at the relaxation time of the chain is also lower by the same factor:

$$G(\tau_{rep}) \approx G_e \left[1 - \mu \sqrt{\frac{N_e}{N}} \right]. \tag{9.81}$$

Since the distance that the chain must diffuse along the tube has been shortened by tube length fluctuations, the relaxation time is shorter than in the Doi–Edwards reptation model [Eq. (9.8)]:

$$\tau_{rep} \approx \frac{\langle L \rangle^2 [1 - \mu \sqrt{N_e/N}]^2}{D_c} \approx \tau_0 \frac{N^3}{N_e} \left[1 - \mu \sqrt{\frac{N_e}{N}} \right]^2. \tag{9.82}$$

The stress relaxation modulus then decays exponentially at the reptation time [Eq. (9.22)]. The terminal relaxation time can be measured quite precisely in linear viscoelastic experiments.[5] Hence, Eq. (9.82) provides the simplest direct means of testing the Doi fluctuation model and evaluating

[5] The modulus scale typically has a ±5% uncertainty owing to imperfect sample geometry which also affects viscosity but not relaxation times.

the parameter μ, as shown in Fig. 9.21. Requiring each data set to have an intercept of unity in Fig. 9.21 provides a correction to Eq. (9.21) for estimating τ_0. We conclude from Fig. 9.21 that $\mu \cong 1.0$, based primarily on computer simulations of the repton model (Section 9.6.2.6) because the experimental data are noisy owing to the usual $\pm 5\%$ uncertainties in determination of molar mass.

Recall that Fig. 9.3 showed the linear viscoelastic response of a polybutadiene melt with $M/M_e \cong 68$. The squared term in brackets in Eq. (9.82) is the tube length fluctuation correction to the reptation time. With $\mu = 1.0$ and $N/N_e = 68$, this correction is is 0.77. Hence, the Doi fluctuation model makes a very subtle correction to the terminal relaxation time of a typical linear polymer melt. However, this subtle correction imparts stronger molar mass dependences for relaxation time, diffusion coefficient, and viscosity.

Tube length fluctuation modes significantly modify the rheological response of entangled polymers. The effect of these modes is most clearly observed in the shape of the loss modulus $G''(\omega)$. The Doi–Edwards equation ignores tube length fluctuations and predicts an almost single exponential stress relaxation modulus with small contribution from higher order modes [Eq. (9.21)]. The corresponding loss modulus is obtained from the Doi–Edwards equation by integration using Eq. (7.150) (see Problem 9.8):

$$G''(\omega) = \frac{8G_e}{\pi^2} \sum_{p:\text{odd}} \frac{\omega\tau_{rep}}{(\omega\tau_{rep})^2 + p^4}. \tag{9.83}$$

In the rubbery plateau (for $3 \lesssim \omega\tau_{rep} \lesssim 300$ in Fig. 9.22), this Doi–Edwards reptation prediction gives $G'' \sim \omega^{-1/2}$. In contrast, a single exponential $G(t)$ leads to $G'' \sim \omega^{-1}$ at high frequencies. The shorter time modes, corresponding to $p = 3, 5, 7, \ldots$, make the reptation prediction of the loss modulus larger than that of a single exponential relaxation at high frequencies. The Doi fluctuation model has even more relaxation in the rubbery plateau, with $G'' \sim \omega^{-1/4}$ for frequencies larger than the reciprocal of the Rouse time of the chain (see Problem 9.36). Experimental data appear to obey a power law that is independent of polymer species (see Fig. 9.22) but with an intermediate exponent[6] ($G'' \sim \omega^{-0.3}$). At higher frequencies, differences between the two polymers are noted (particularly in G'') that are consistent with their 20% difference in M/M_e that creates a factor of 1.8 difference in τ_{rep}/τ_e. These differences show up at high frequency because the normalization of the axes in Fig. 9.22 requires overlap at low frequencies.

In Fig. 9.23(a), the loss moduli of two nearly monodisperse polybutadiene samples are simultaneously fitted by the predictions of the Doi–Edwards reptation model [Eq. (9.83)]. Experimental peaks are much

[6] Longitudinal Rouse modes of the chain along the tube may affect the value of this exponent.

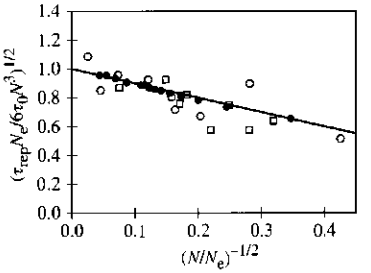

Fig. 9.21
Experimental verification of the Doi fluctuation model using data for polystyrene as open squares, from S. Onogi *et al.*, *Macromolecules* **3**, 109 (1970) and A. Schausberger *et al.*, *Rheol. Acta* **24**, 220 (1985), polybutadiene as open circles from R. H. Colby *et al.*, *Macromolecules* **20**, 2226 (1987) and filled circles from the repton model described in Section 9.6.2.6, courtesy of D. Shirvanyants. The line is Eq. (9.82) with $\mu = 1.0$.

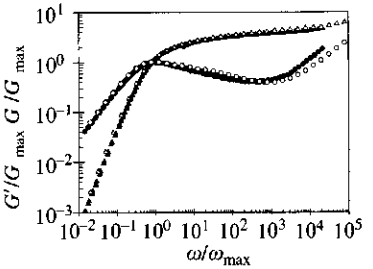

Fig. 9.22
Oscillatory shear data for two nearly monodisperse linear polymers with $M/M_e = 40$, reduced by their terminal loss modulus maximum. Triangles are the storage modulus G' and circles are the loss modulus G''. Filled symbols are for polybutadiene with $M_w = 70\,900\ \text{g mol}^{-1}$ ($M/M_e = 37$) from M. Rubinstein and R. H. Colby, *J. Chem. Phys.* **89**, 5291 (1988). Open symbols are for polystyrene with $M_w = 750\,000\ \text{g mol}^{-1}$ ($M/M_e = 44$) from A. Schausberger *et al.*, *Rheol. Acta* **24**, 220 (1985).

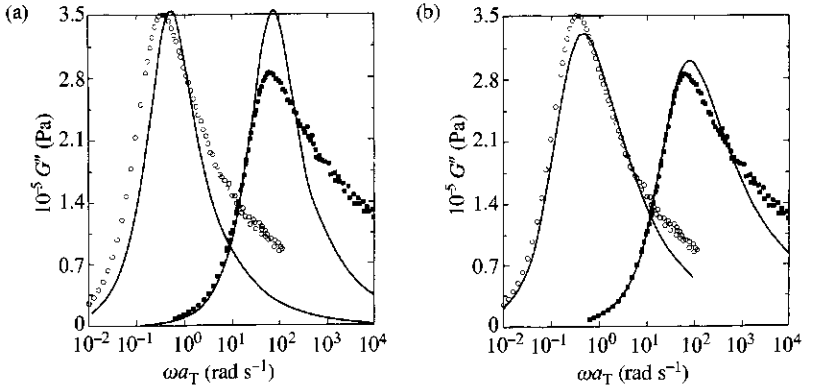

Fig. 9.23
Simultaneous fit of loss modulus data for the two monodisperse polybutadiene samples at 30 °C by (a) the Doi–Edwards equation and (b) the Doi tube length fluctuation model. Lines are the fitting results. Open circles are data for $M = 355\,000\ \mathrm{g\,mol^{-1}}$. Filled squares are data for $M = 70\,900\ \mathrm{g\,mol^{-1}}$. Data from M. Rubinstein and R. H. Colby, *J. Chem. Phys.* **89**, 5291 (1988).

broader, especially at high frequencies (short times). The breadth of the experimental peaks of the loss modulus increases with decreasing molar mass. This comparison suggests that the Doi–Edwards equation underestimates stress relaxation by ignoring tube length fluctuation modes [Eq. (9.79)]. The complete stress relaxation modulus due to motion of a chain in its tube consists of two parts:

(1) Rouse modes of the chain, including tube length fluctuations and longitudinal Rouse modes, are active at times shorter than the Rouse time of the chain.
(2) Reptation modes are active at times longer than the Rouse time of the chain.

The results of models that include tube length fluctuation modes [Fig. 9.23(b)] are in much better agreement with the experimentally measured loss modulus $G''(\omega)$ of monodisperse melts than the prediction of the Doi–Edwards reptation model [Eq. (9.83)]. Tube length fluctuation corrections predict that the loss peak broadens with decreasing molar mass because the fraction of the stress released by fluctuations is larger for shorter chains.

The viscosity can again be estimated as the product of the terminal modulus and the reptation time:

$$\eta \approx \tau_{\mathrm{rep}} G(\tau_{\mathrm{rep}}) \approx \frac{\tau_0 kT}{b^3}\frac{N^3}{N_{\mathrm{e}}^2}\left[1 - \mu\sqrt{\frac{N_{\mathrm{e}}}{N}}\right]^3. \qquad (9.84)$$

Doi's estimate of the effect of tube length fluctuations [Eq. (9.84)] predicts a molar mass dependence that approximates $\eta \sim N^{3.4}$ over a reasonable range of molar masses. Viscosity data from experiments and Repton model simulations are compared with the predictions of the Doi fluctuation model in Fig. 9.24. The Doi fluctuation model with $\mu = 1.0$ (solid curve) is in good agreement with both experimental and simulation data for $M > 10M_{\mathrm{e}}$. The data exhibit departures from the 3.4 power law (dashed line in Fig. 9.24) for long chains ($M > 300M_{\mathrm{e}}$) that are well described by the Doi fluctuation model.

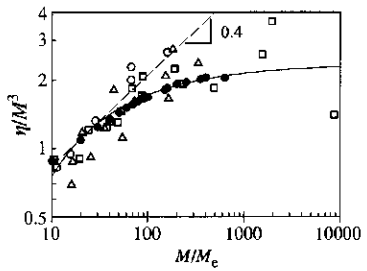

Fig. 9.24
Dependence of viscosity, reduced by the cube of molar mass, on the number of entanglements per chain. Filled circles are data from the 'Repton model' of Section 9.6.2, courtesy of D. Shirvanyants. Open symbols are experimental data for the three polymers in Fig. 9.5, shifted parallel to the η_0/M^3 axis to coincide with the 'Repton model' data. The curve is the Doi fluctuation model [Eq. (9.84)] with $\mu = 1.0$.

Other computer simulations, such as the Evans–Edwards model of a chain in an array of fixed obstacles (described in detail in Section 9.6.2) exhibit fluctuations of the tube length and also find stronger molar mass dependences of relaxation time $\tau \sim M^{3.3\pm0.2}$ and diffusion coefficient $D \sim M^{-2.4\pm0.1}$ than the simple reptation model without tube length fluctuations [Eqs (9.8) and (9.12)]. These results of computer simulations of a single chain in an array of fixed obstacles are in good agreement with experiments on entangled polymer solutions and melts over the entire range of molar masses covered by simulations ($M < 600 M_e$). *Tube length fluctuations are responsible for the stronger molar mass dependences of diffusion coefficient* (Fig. 9.2), *relaxation time* [Eq. (9.9)], *and viscosity* (Fig. 9.5) *than predicted by the simple reptation model.*

9.5 Many-chain effects: constraint release

In Section 9.4, the motion of a single chain in an array of fixed topological constraints was discussed. Such models apply to dynamics of a chain in a network or in a melt of extremely long chains. In a melt of shorter chains, the topological constraints that define the confining tube are formed by neighbouring chains, which also move along their respective tubes. As chain B moves away, the topological constraint it once imposed on chain A disappears (Fig. 9.25). A new set of conformations is now available for chain A. A third chain moves in and imposes a new topological constraint on chain A. The constraints hence fluctuate in time, keeping the time-average total number of topological constraints imposed on a given chain by its neighbours constant. As some neighbours move away and remove their constraints from a given chain, others move in and place new constraints on it.

The exchange of neighbours and their topological constraints imposed on a given chain leads to a modification of the tube that a given polymer is confined to and is called **constraint release**. When a neighbouring chain B moves away, chain A can explore an additional volume of the order of an entanglement mesh size a^3. If a new chain C moves in, it can locally confine chain A to this new volume, changing the conformation of the tube of A. This process can be modelled by a local jump of the tube, analogous to an elementary move of the Rouse model. The rate of these local jumps of the primitive path is reciprocally proportional to the lifetime τ of the topological constraints. Thus, *constraint release leads to Rouse-like motion of the confining tube and its primitive path.*

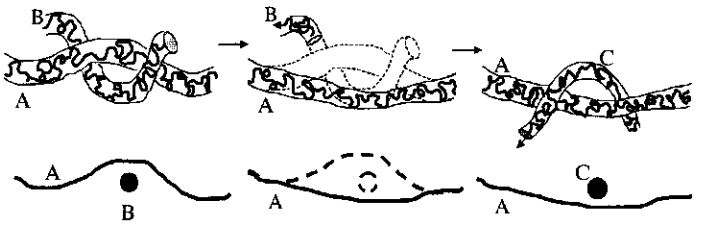

Fig. 9.25
Constraint release mechanism: when chain B reptates away, it releases the constraint on chain A. Later, this constraint is replaced by chain C, which confines chain A in a displaced tube.

9.5.1 Relaxation times and diffusion

Consider a single linear chain with P monomers in a melt of shorter N-mers. The P-mer has two relaxation mechanisms occurring simultaneously:

(1) Single-chain motion of the P-mer within its confining tube by reptation and tube length fluctuations.
(2) Constraint release as a Rouse motion of the tube confining the P-mer.

Whichever process relaxes the chain faster is the one that controls terminal dynamics.

The constraint release process for the P-mer can be modelled by Rouse motion of its tube, consisting of P/N_e segments, where N_e is the average number of monomers in an entanglement strand. The average lifetime of a topological constraint imposed on a probe P-mer by surrounding N-mers is the reptation time of the N-mers $\tau_{rep}(N)$. The relaxation time of the tube confining the probe chain by constraint release is the Rouse time of P/N_e tube segments [Eq. (8.17)] with segment relaxation time $\tau_{rep}(N)$ dictated by the reptation time of the surrounding N-mers:

$$\tau_{tube} \approx \tau_{rep}(N)\left(\frac{P}{N_e}\right)^2. \tag{9.85}$$

The diffusion coefficient of a P-mer in a melt of N-mers can be written as a sum of contributions from each of these two types of motion, assuming that each contributes independently to diffusion:

$$D \approx \frac{R^2}{\tau_{rep}(P)} + \frac{R^2}{\tau_{tube}}. \tag{9.86}$$

The reptation time of the P-mer is $\tau_{rep}(P)$ and the constraint release time τ_{tube} given in Eq. (9.85). The faster of the two types of motion controls the diffusion of the P-mer. For constraint release to significantly affect terminal dynamics, the Rouse relaxation time of the confining tube τ_{tube} must be shorter than the reptation time of the P-mer $\tau_{rep}(P)$:

$$\tau_{rep}(P) > \tau_{tube} \approx \tau_{rep}(N)\left(\frac{P}{N_e}\right)^2. \tag{9.87}$$

Very long P-mers have the constraint release time [Eq. (9.85)] shorter than their reptation time.[7] Such very long P-mers relax and diffuse by constraint release (Rouse motion of their tubes) before they get a chance to reptate out of their confining tubes. For shorter P-mers, the reptation time $\tau_{rep}(P)$ is shorter than the constraint release time τ_{tube} and reptation dominates the diffusion of these chains. Reptation certainly dominates diffusion in monodisperse solutions and melts (for $P = N$).

[7] Constraint release controls the terminal relaxation in the reptation model if $P/N_e > (N/N_e)^3$ and in the Doi fluctuation model if $P/N_e > (N/N_e)^{2.4}$.

Experiments on diffusion of deuterated polystyrene into a melt of hydrogenated polystyrene (Fig. 9.26) confirm the crossover assumed in Eq. (9.86). For very long matrix chains (large N), the terminal dynamics of the P-mer are controlled by reptation and consequently the diffusion coefficient of the P-mer only depends on the molar mass of the P-chains and is independent of N:

$$D \approx \frac{R^2}{\tau_{\text{rep}}(P)} \quad \text{for large } N. \tag{9.88}$$

On the other hand, if the matrix chains are short enough (small N) constraint release controls the terminal dynamics of the P-chains [Eq. (9.85)] and the diffusion coefficient of the P-mers depends strongly on N:

$$D \approx \frac{R^2}{\tau_{\text{tube}}} \quad \text{for small } N. \tag{9.89}$$

The solid line in Fig. 9.26 is the crossover between Eqs (9.88) and (9.89), and divides the data nicely into a regime of constraint release control, where D is strongly dependent on N/N_e for short-chain matrices [described by Eq. (9.89)] and a regime of reptation control, where D is independent of N for diffusion into long-chain matrices [described by Eq. (9.88)].

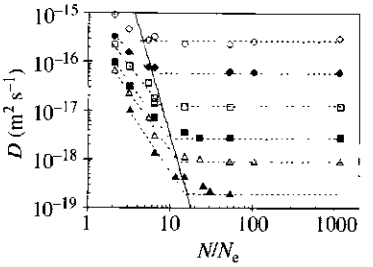

Fig. 9.26
Diffusion coefficient of trace amounts of deuterium-labelled polystyrene P-mers into polystyrene N-mer melts at 174 °C for six P-mers: open circles $M = 55\,000$ g mol^{-1}; filled circles $M = 110\,000$ g mol^{-1}; open squares $M = 255\,000$ g mol^{-1}; filled squares $M = 520\,000$ g mol^{-1}; open triangles $M = 915\,000$ g mol^{-1}; and filled triangles have $M = 2\,000\,000$ g mol^{-1}. Data from P. F. Green and E. J. Kramer, *Macromolecules* **19**, 1108 (1986).

9.5.2 Stress relaxation

Constraint release has a limited effect on the diffusion coefficient: it is important only for the diffusion of very long chains in a matrix of much shorter chains and can be neglected in monodisperse solutions and melts. The effect of constraint release on stress relaxation is much more important than on the diffusion and cannot be neglected even for monodisperse systems. Constraint release can be described by Rouse motion of the tube. The stress relaxation modulus for the Rouse model decays as the reciprocal square root of time [Eq. (8.47)]:

$$G(t) \sim (t/\tau)^{-1/2}. \tag{9.90}$$

Thus, a finite fraction of the stress relaxes by constraint release at time scales of the order of the constraint lifetime in the Rouse model of constraint release. This is also the time scale at which the stress relaxes by reptation in monodisperse entangled solutions and melts. Both processes simultaneously contribute to the relaxation of stress. Therefore, constraint release has to be taken into account for a quantitative description of stress relaxation even in monodisperse systems. The contribution of constraint release to stress relaxation in polydisperse solutions and melts is even more important as will be discussed below.

9.5.2.1 Stress relaxation in binary blends

Single-chain models, such as the Doi–Edwards reptation model [Eq. (9.21)] or the Doi tube length fluctuation model, assume a linear contribution to

the stress relaxation modulus from each component of a polydisperse system:

$$G(t) = \sum_N \phi_N G_N(t), \tag{9.91}$$

where ϕ_N is the volume fraction of N-mers and $G_N(t)$ is the single-chain stress relaxation modulus of N-mers. For a binary blend of long (L) and short (S) chains, these models predict a simple linear addition of the stress relaxation moduli of the two components weighted by their volume fractions:

$$G(t) = \phi_L G_L(t) + \phi_S G_S(t). \tag{9.92}$$

However, many experiments observe that the amount of stress relaxed at the time scale of the reptation time τ_S of shorter chains is much larger than the volume fraction of short chains. This is shown in Fig. 9.27(a), where the loss moduli of binary blends are compared with the predictions of Eq. (9.92) using the Doi–Edwards reptation model predictions for $G(t)$ [Eq. (9.21)] for the $G_L(t)$ and $G_S(t)$ relaxation functions. Recall from Section 7.6.5 that the magnitude of $G''(\omega)$ directly reflects the amount of relaxation occurring at each frequency ω. Hence, Eq. (9.92) strongly underestimates the amount of relaxation occurring when the short chains relax [the high-frequency peak in $G''(\omega)$].

Some of the stress relaxed at time scale τ_S occurs by release of constraints imposed on long chains by short ones, which makes a significant contribution to the stress relaxation at the reptation time of the short chains τ_S.

Topological constraints are often assumed to be *pairwise* entanglements between chains. There are three types of these pairwise entanglements in a binary blend: between two long chains (L–L); between two short chains (S–S), and between a short and a long chain (S–L). If the dynamics of each chain along its tube is approximated by the Doi–Edwards reptation model, there are two time scales in the problem—reptation times of long (τ_L) and short (τ_S) polymers. The constraint on a given chain, caused by a long neighbour, has lifetime τ_L, while the constraint imposed by a short neighbour has lifetime τ_S. The constraint release process in a binary blend can be represented by a Rouse model with two mobilities of the effective beads:

(1) slow, corresponding to entanglements with long chains;
(2) fast, corresponding to entanglements with short chains.

These two mobilities can be assumed to be randomly distributed along the tube with relative concentrations corresponding to the probabilities of entanglement with a chain of each type. The simplest assumption is that these relative concentrations are proportional to the volume fractions of each type of chain (for pairwise entanglements).

The combined stress relaxation modulus for both reptation and constraint release of a binary blend is

$$G(t) = \phi_L G_L(t) \Lambda_L(t) + \phi_S G_S(t) \Lambda_S(t), \tag{9.93}$$

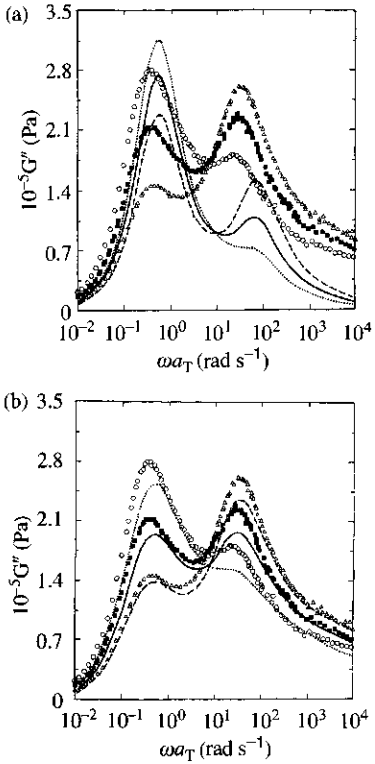

Fig. 9.27
Comparison of the loss modulus data for three blend compositions of the two polybutadiene samples in Fig. 9.23 at 30 °C with the predictions of (a) Doi–Edwards reptation model and (b) self-consistent constraint release model. Dotted lines are the predictions and open circles are the data for $\phi_L = 0.882$. Solid lines and filled squares are for $\phi_L = 0.768$. Dashed lines and open triangles are for $\phi_L = 0.638$. Data from M. Rubinstein and R. H. Colby, *J. Chem. Phys.* **89**, 5291 (1988).

where $\Lambda_L(t)$ and $\Lambda_S(t)$ are the stress relaxation functions due to constraint release (Rouse motion of tubes) of long and short chains (with two bead friction coefficients $\tau_L kT/a^2$ and $\tau_S kT/a^2$). This model is in reasonable agreement with experiments. Adding constraint release modes to the Doi–Edwards reptation model improves the dependence of the heights of the loss modulus peaks on the volume fractions ϕ_L and ϕ_S of components. But this model lacks the higher frequency modes because it does not include tube length fluctuations.

These tube length fluctuation modes (see Section 9.4.5) of the neighbouring chains affect the constraint release modes of a given chain. If entanglements between chains are assumed to be binary, there should be a **duality** between constraint release events and 'chain in a tube' relaxation events. A release of an entanglement by reptation or tube length fluctuation of one chain in its tube leads to a release of the constraint on the second chain. If this duality is accepted, the distribution of constraint release rates can be determined self-consistently from the stress relaxation modulus of the tube model.

The constraint release process in this self-consistent model is described by a Rouse model with random bead mobilities. The distribution of these mobilities is given by the constraint release rate distribution. The predictions of this self-consistent model are in good agreement with experiments on binary blends [see Fig. 9.27(b)].

The constraint release model represents the effects of surrounding polymers on the motion of a given chain by allowing transverse motion of the tube, controlled by the rate that entanglements are abandoned. The width of the confining tube stays, on average, constant in the constraint release process. While the more general problem of polydispersity effects on constraint release is well posed, it has not been solved thus far for anything beyond the simplest case of a binary blend. Consequently, other models that are easier to solve but are also less accurate have been proposed. For instance, Marrucci and Viovy have suggested that the tube diameter might be considered to increase as entanglements are abandoned. After a step strain the relaxed sections of the chains are assumed to be unable to confine the polymer any more, effectively becoming solvent-like at long time scales. The polymer is confined to a wider dilated tube and this process is called **tube dilation**. Problems 9.45–9.48 show that tube dilation has rather limited utility for linear polymers. Tube dilation has most effectively been applied to the dynamics of branched polymers with an exponentially broad distribution of relaxation rates (see Problem 9.49).

9.6 Computer simulations in polymer physics

Rapid advances in computer technology are making computer simulations powerful tools to study polymer properties. Computer simulations occupy an important intermediate position between theory and experiments. They can provide valuable tests of assumptions and predictions of theoretical models as well as attempt to mimic experimental systems, such as polymer solutions, melts, and networks.

There are two main approaches used to simulate polymer materials: molecular dynamics and Monte Carlo methods. The molecular dynamics approach is based on numerical integration of Newton's equations of motion for a system of particles (or monomers). Particles follow deterministic trajectories in space for a well-defined set of interaction potentials between them. In a qualitatively different simulation technique, called Monte Carlo, phase space is sampled randomly. Molecular dynamics and Monte Carlo simulation approaches are analogous to time and ensemble methods of averaging in statistical mechanics. Some modern computer simulation methods use a combination of the two approaches.

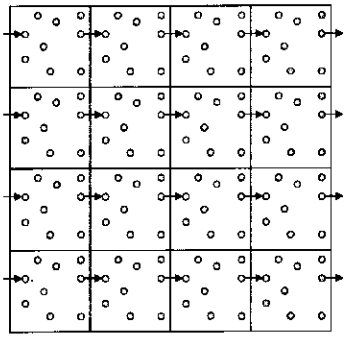

Fig. 9.28
Periodic boundary conditions for a two-dimensional cell.

9.6.1 Molecular dynamics

Consider a molecular dynamics simulation of a system consisting of K particles in a cubic box of volume $V = L^3$. Periodic boundary conditions are typically used to minimize surface effects. Periodic boundary conditions correspond to densely filling space with identical copies of the simulation box (see Fig. 9.28 for a two-dimensional sketch of periodic boundary conditions). As particles leave the simulation box from one side, they automatically reenter it from the opposite side.

In one of the simplest models, all particles are identical with mass m and size σ interacting with each other via a Lennard-Jones potential [Eq. (3.96)]. A cutoff in the potential is introduced at r_{cut} in order to speed-up the simulations:

$$U(r) = \begin{cases} 4\epsilon\left[(\sigma/r)^{12} - (\sigma/r)^{6}\right] - 4\epsilon\left[(\sigma/r_{\text{cut}})^{12} - (\sigma/r_{\text{cut}})^{6}\right] & \text{for } r < r_{\text{cut}}, \\ 0 & \text{for } r > r_{\text{cut}}. \end{cases} \tag{9.94}$$

A typical cutoff used for attractive interactions is $r_{\text{cut}} = 2.5\sigma$ and for purely repulsive interactions the cutoff is at the minimum of the potential $r_{\text{cut}} = 2^{1/6}\sigma$. The potential in Eq. (9.94) is shifted in order to make it continuous at the cutoff $U(r_{\text{cut}}) = 0$.

A simulation starts with an initial set of positions $\{\vec{r}_i\}$ and velocities $\{\mathrm{d}\vec{r}_i/\mathrm{d}t\}$ of all particles (with $i = 1, 2, \ldots, n$ for a system of n particles). Temperature T is determined from the average kinetic energy of the particles $\sum_i m_i (\mathrm{d}\vec{r}_i/\mathrm{d}t)^2/(2n)$. This average kinetic energy is conserved during the simulation and is equal to $3kT/2$ in three dimensions:

$$T = \frac{1}{3nk} \sum_{i=1}^{n} m_i \left(\frac{\mathrm{d}\vec{r}_i}{\mathrm{d}t}\right)^2. \tag{9.95}$$

The total force acting on particle i at position $\vec{r}_i$ is the sum of the forces from all other particles in the simulation box and is equal to its mass m_i times its acceleration:

$$m_i \frac{\mathrm{d}^2\vec{r}_i}{\mathrm{d}t^2} = -\sum_{j \neq i} \frac{\partial U(\vec{r}_i - \vec{r}_j)}{\partial(\vec{r}_i - \vec{r}_j)}. \tag{9.96}$$

Since this is basically a statement of Newton's second law applied to each particle, the n equations of the form of Eq. (9.96) are called **Newton's equations of motion**. These equations of motion are integrated over a small time step δt and new positions and velocities of all the particles are computed. The position of particle i at time $t+\delta t$ can be obtained by the Taylor series expansion in powers of the time step δt:

$$\vec{r}_i(t+\delta t) = \vec{r}_i(t) + \delta t \frac{\mathrm{d}\vec{r}_i}{\mathrm{d}t}\Big|_t + \frac{(\delta t)^2}{2}\frac{\mathrm{d}^2\vec{r}_i}{\mathrm{d}t^2}\Big|_t + \frac{(\delta t)^3}{6}\frac{\mathrm{d}^3\vec{r}_i}{\mathrm{d}t^3}\Big|_t + \cdots \tag{9.97}$$

Similarly, the position of particle i at earlier time $t-\delta t$ can also be written as a series expansion:

$$\vec{r}_i(t-\delta t) = \vec{r}_i(t) - \delta t \frac{\mathrm{d}\vec{r}_i}{\mathrm{d}t}\Big|_t + \frac{(\delta t)^2}{2}\frac{\mathrm{d}^2\vec{r}_i}{\mathrm{d}t^2}\Big|_t - \frac{(\delta t)^3}{6}\frac{\mathrm{d}^3\vec{r}_i}{\mathrm{d}t^3}\Big|_t + \cdots \tag{9.98}$$

Adding Eqs (9.97) and (9.98) provides the **Verlet algorithm** for calculation of the position of particle i at time $t+\delta t$:

$$\vec{r}_i(t+\delta t) = 2\vec{r}_i(t) - \vec{r}_i(t-\delta t) + (\delta t)^2 \frac{\mathrm{d}^2\vec{r}_i}{\mathrm{d}t^2}\Big|_t + O((\delta t)^4). \tag{9.99}$$

Acceleration $\mathrm{d}^2\vec{r}_i/\mathrm{d}t^2\big|_t$ of particle i is determined by Newton's equation of motion [Eq. (9.96)]. The position of the particle in the Verlet algorithm is calculated with the accuracy of $(\delta t)^4$, as denoted by $O((\delta t)^4)$. The Verlet algorithm for the velocity of particle i at time t is obtained from its positions at times $t+\delta t$ and $t-\delta t$ with accuracy of $(\delta t)^3$ [by subtracting Eq. (9.98) from Eq. (9.97)]:

$$\frac{\mathrm{d}\vec{r}_i}{\mathrm{d}t}\Big|_t = \frac{\vec{r}_i(t+\delta t) - \vec{r}_i(t-\delta t)}{2\delta t} + O((\delta t)^3). \tag{9.100}$$

Positions and velocities of all particles are calculated at every step of the molecular dynamics simulation, producing a complete time evolution of the system. In order for this time evolution to be accurate, the integration time step δt has to be much smaller than the shortest characteristic time of the system (the reciprocal Einstein frequency of the Lennard-Jones crystal). The simple Verlet algorithm is used for systems with constant number of particles, volume, and total energy. There are more sophisticated integration algorithms for simulations of systems at constant temperature that allow temperature rescaling to be done concurrently with the calculation of new positions and velocities of particles.

A physical quantity $\langle A \rangle$ is evaluated by the average of its instantaneous value $A(t)$ at time t over a long period of time (large number X of molecular dynamics steps) after initial equilibration during a sufficiently long run (with equilibration time t_0):

$$\langle A \rangle = \frac{1}{X}\sum_{j=1}^{X} A(t_0 + j\delta t). \tag{9.101}$$

If the simulation is long enough for the system to equilibrate (if it is much longer than all relaxation times), this time average is equivalent to the ensemble average.

In a more complicated simulation, particles are connected by bonds into small molecules or even into polymers. The atomic details included in a simulation depend on the specific problem being investigated. It is tempting to include the chemical details of monomers with accurate atomic potentials. Such simulations are carried out to answer detailed questions, such as the temperature dependence of density, or polarizability and solubility in a specific solvent. Including accurate potentials between atoms (e.g., bond-bending and bond-stretching C–C potentials) requires very small integration time steps (much shorter than vibration periods of these potentials) and makes complete relaxation of long chains with hundreds of monomers practically impossible. For example, a common time step of a molecular dynamics simulation is $\delta t = 10^{-15}$ s, while relaxation times of long polymers could be 10^{-3} s or even longer than 1 s. Computer technology is still a long way from simulations covering 12 or 15 orders of magnitude of time.[8] Therefore, multi-scale methods are being currently developed to bridge the gap between atomistic and course-grained models.

A simple generic bead–spring model of chains can be used to study universal polymer properties that do not depend on specific chemical details. Bonds between neighbouring Lennard-Jones particles in a chain can be represented by the finite extension non-linear elastic (FENE) potential,

$$U^{\mathrm{FENE}}(r) = \begin{cases} -\frac{\kappa}{2} r_{\mathrm{bond}}^2 \ln\left[1 - (r/r_{\mathrm{bond}})^2\right] & \text{for } r < r_{\mathrm{bond}}, \\ \infty & \text{for } r > r_{\mathrm{bond}}, \end{cases} \tag{9.102}$$

with typical values of bond length r_{bond} between 1.5σ and 2σ and typical values of bond strength κ between $5\epsilon/\sigma^2$ and $30\epsilon/\sigma^2$, where ϵ and σ are parameters of the Lennard-Jones potential [Eq. (9.94)]. Polymer solutions can be simulated by connecting some of the particles into polymers, while leaving the rest of the particles to represent solvent molecules. At low polymer concentrations, most of the particles in a simulation box are solvent molecules and most of the simulation time is occupied by calculation of their trajectories. It is necessary to keep explicit solvent molecules if the objective of the molecular dynamics is to simulate hydrodynamic flow or to investigate the details of the polymer–solvent interaction.

Explicit solvent is usually excluded from simulations directed at the study of solutions of longer chains for long times due to computational constraints (simulations with explicit solvent would be prohibitively long). Interactions between monomers are replaced by an effective potential mediated by implicit solvent of a given quality (see Chapter 3). The effects of collisions of explicit solvent molecules with monomers of the chains can be replaced by random forces acting on monomers in implicit solvent. These random forces are usually assumed to be non-correlated and therefore hydrodynamic interaction between monomers in explicit solvent

[8] Currently, 7–8 orders of magnitude in time are accessible on modern computers.

is lost as soon as explicit solvent molecules are replaced by random forces acting on monomers. Molecular dynamics simulation with random forces and corresponding viscous friction (called Brownian dynamics) is an example of a hybrid method.

A good example of results from a molecular dynamics simulation of entangled polymers is shown in Fig. 9.29. The 40 configurations of the chain shown are equally spaced in time up to the Rouse time of the chain. The chain is clearly confined to a tube-like region, with only the ends of the chain beginning to explore the rest of the volume.

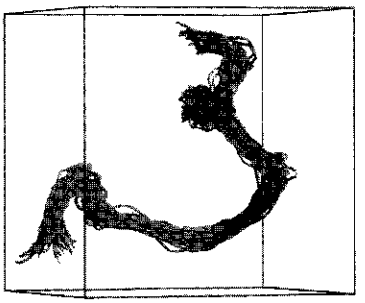

Fig. 9.29
Molecular dynamics simulation of a chain with $N = 400$ monomers in an entangled polymer melt. Forty configurations of the chain are shown at equally spaced time intervals up to the Rouse time of the chain. Picture courtesy of G. S. Grest based on data from K. Kremer and G. S. Grest, *J. Chem. Phys.* **92**, 5057 (1990).

9.6.2 Monte Carlo

Random sampling of different possible states of the system is called a Monte Carlo simulation technique. Starting from an arbitrary initial state of the system, a transition into another state is attempted following a certain set of transition rules. In the simplest cases, this transition corresponds to a random jump of a particle or several particles.[9] If different states of a system have different energies, the probability P_i of the system to be found in a state i with energy E_i is proportional to its statistical weight. For systems with constant volume, temperature, and number of particles, the statistical weight of a state is given by the Boltzmann factor:

$$P_i \sim \exp\left(-\frac{E_i}{kT}\right). \tag{9.103}$$

In equilibrium, a detailed balance must be satisfied, meaning that the number of transitions per unit time from any state i to any state j is on average equal to the number of transitions per unit time from j to i. Then, the number of transitions from any state i to any state j is proportional to the product of the probability P_i of being in state i, the probability $g_{i\to j}$ of making an attempt to move from state i to state j and the probability $p_{i\to j}$ of accepting this attempted transition. Therefore, detailed balance can be written as a simple equation:

$$P_i g_{i\to j} p_{i\to j} = P_j g_{j\to i} p_{j\to i}. \tag{9.104}$$

The condition of detailed balance can be solved for the ratio of acceptance probabilities of forward and backward transitions between states i and j.

$$\frac{p_{i\to j}}{p_{j\to i}} = \frac{P_j g_{j\to i}}{P_i g_{i\to j}}. \tag{9.105}$$

9.6.2.1 Metropolis algorithm

In the simplest Monte Carlo methods, such as the **Metropolis algorithm**, the probability of attempting to move to state j from state i is the same as the probability of attempting to move to state i from state j:

$$g_{j\to i} = g_{i\to j}. \tag{9.106}$$

[9] In practicce, the transitions often do not correspond to realistic moves, in an attempt to sample all of phase space as rapidly as possible.

In this case, the ratio of acceptance probabilities for attempted moves between states i and j depends on the energy difference $E_j - E_i$ between these states:

$$\frac{p_{i\to j}}{p_{j\to i}} = \frac{P_j}{P_i} = \exp\left(-\frac{E_j - E_i}{kT}\right). \tag{9.107}$$

In the Metropolis algorithm an attempted transition into a state with lower energy is always accepted:

$$p_{i\to j} = 1 \quad \text{if } E_j \leq E_i. \tag{9.108}$$

If the energy of the final state E_j is higher than the energy of the initial state E_i, the attempted transition is accepted with probability

$$p_{i\to j} = \exp\left(-\frac{E_j - E_i}{kT}\right) \quad \text{if } E_j > E_i, \tag{9.109}$$

thereby automatically satisfying detailed balance at equilibrium. If the transition is not accepted, the old state counts one more time for any quantity to be calculated in the Monte Carlo simulation. For example, the average of any quantity over a large number K of Monte Carlo steps (after a large number J of equilibration steps) includes multiple terms with the same value whenever attempted moves were not accepted:

$$\langle A \rangle = \frac{1}{K}\sum_{i=J+1}^{J+K} A_i. \tag{9.110}$$

The Metropolis set of transition rates [Eqs (9.108) and (9.109)] satisfies the detailed balance [Eq. (9.107)] at equilibrium and the average over a long Monte Carlo run approximates the thermodynamic average. The detailed balance is also satisfied and thermodynamic equilibrium is approached in more sophisticated biased Monte Carlo algorithms with the probability of attempting to move to state j from state i not equal to the probability of attempting to move to state i from state $j (g_{j\to i} \neq g_{i\to j})$. These algorithms are used to enhance sampling of highly improbable states. Below, we outline several examples of lattice Monte Carlo models in which the states are either allowed and have equal energies and equal probabilities or forbidden with infinite energies and zero probabilities.

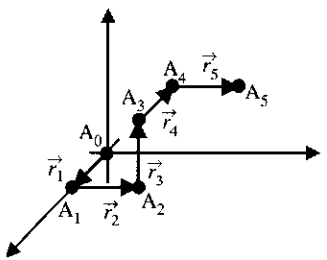

Fig. 9.30
Random walk on a cubic lattice.

9.6.2.2 Random walk

For a chain modeled by an ideal N-step random walk on a cubic lattice there are 6^N different states with a fixed position of one end (see Fig. 9.30). It is impossible to sample all of these states for large N. Therefore, the simulation is restricted to a smaller, but still representative, subset of all allowed states for long polymers. There are many different methods of generating this subset of states. For example, the first monomer A_0 can be placed at the origin and the bonds of the chain are placed sequentially with their bond directions determined by a random number generator.

The random number generator produces random numbers in the interval between 0 and 1. For a random walk on a cubic lattice, there are six possible directions. If the first random number is less than 1/6, the first bond is chosen to be directed to the right. If it is between 1/6 and 1/3, the bond $\vec{r}_1$ is directed up. If the random number is between 1/3 and 1/2, the bond is directed to the left. If the random number is between 1/2 and 2/3, the bond is directed down. If the random number is between 2/3 and 5/6, the bond is directed forward (out of the page). If the random number is greater than 5/6, the bond $\vec{r}_1$ between A_0 and A_1 is directed backward (into the page). The same procedure (with different random numbers) is repeated for the remaining $N-1$ bonds of the N-step random walk generating one possible conformation of the chain. Repeating the same procedure many times produces a large number of conformations of ideal random walks. The resulting random walks satisfy the ideal chain statistics of Chapter 2.

9.6.2.3 Self-avoiding walk

Monte Carlo simulations of a polymer in an athermal solvent are more difficult. In order to satisfy the excluded volume requirements in a lattice simulation, no lattice site can be occupied by more than one monomer. The simplest sampling technique is based on the algorithm described above for an ideal random walk. The only modification is that whenever an attempted new bond runs into an already occupied site, the whole chain is thrown away and a new chain is grown from the very beginning. The success rate for growing a self-avoiding N-mer by this simple algorithm rapidly decreases with N. In order to simulate long self-avoiding walks, alternative Monte Carlo algorithms have been developed. These alternative approaches include biased sampling (checking one step ahead to avoid self-intersection), dimerization (attempting to connect two shorter self-avoiding chains of $N/2$ monomers each), and the pivot algorithm (rotating sections of a self-avoiding chain by a lattice angle). Similar methods are also used for off-lattice simulations.

9.6.2.4 Verdier–Stockmayer model of unentangled chain dynamics

Verdier and Stockmayer used Monte Carlo simulations to study polymer dynamics using the bond moves shown in Fig. 9.31. The Monte Carlo simulation proceeds by randomly choosing one of the $N+1$ monomers of the chain by a procedure similar to choosing a random direction for a bond (multiplying a random number from an interval between 0 and 1 by $N+1$ and taking an integer part of the product). Next, an attempt is made to move the chosen monomer by selecting the type of move from the set shown in Fig. 9.31 and randomly picking the new potential location for the monomer. Moves 1, 2, and 3 in Fig. 9.31 are used for random walks, while moves 1, 2 and 4 are used for self-avoiding walks.

For example, if the end monomer is chosen to be moved by an end flip (move 1 in Fig. 9.31), its new possible position is selected in a way identical to choosing a random bond vector for a random walk (by choosing one of

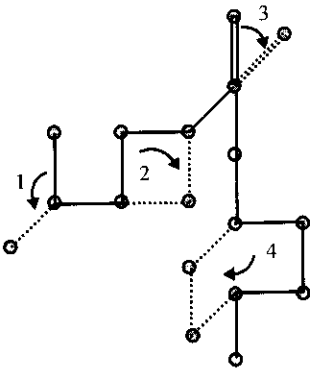

Fig. 9.31
Typical moves in a dynamic Monte Carlo simulation: (1) end flip, (2) corner move, (3) kink jump, and (4) crankshaft move. The solid lines are bonds in one of many possible configurations and the dotted lines are potential new bond positions.

six possible directions for the bond). The final step is to determine whether the move is accepted or not by checking whether it satisfies the conditions of the problem. For example, for self-avoiding walks the move is not accepted if there is an overlap between monomers. Whether the move is accepted or not, the clock of the simulation is moved forward by $1/(N+1)$ time units. A unit time in a Monte Carlo simulation corresponds to $N+1$ such attempted moves (an average of one attempt per monomer). All of the Monte Carlo moves (Fig. 9.31) are local and not directly correlated with each other. They can be thought of as representing uncorrelated monomer displacements of the Rouse model. On larger length and time scales the chain follows Rouse dynamics. The Monte Carlo time unit is shorter than, but proportional to, the monomer relaxation time τ_0.

In the random walk and self-avoiding walk models, described above, all energies are either zero (no interactions) or infinite (complete exclusion for overlapping monomers). In a more general case, finite, but non-zero interaction energies could be considered. In this case, different states (different polymer conformations) would have different energies and therefore different statistical weights. Monte Carlo moves are accepted or rejected according to an algorithm satisfying detailed balance [such as the Metropolis algorithm of Eqs (9.108) and (9.109)]. Some results of off-lattice Monte Carlo simulations of isolated chains in implicit solvents of different quality were presented in Fig. 3.16.

9.6.2.5 Evans–Edwards model of entangled chain dynamics

The dynamics of an entangled chain in an array of fixed obstacles can also be studied by Monte Carlo simulations. An initial unrestricted random walk conformation of a chain on a lattice (representing a chain in a melt) could be obtained using the method of section 9.6.2.2. The topological entanglement net of surrounding chains is represented by obstacles, sketched as solid circles in the middle of each elementary cell in Fig. 9.32.

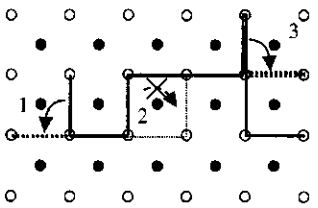

Fig. 9.32
Evans–Edwards model on a two-dimensional square lattice. Corner flips (move 2) cross obstacles and are forbidden. End flips (move 1) and kink flips (move 3) satisfy topological constraints and are allowed.

Motion of the chain, represented by a random walk on a lattice, is defined by the set of allowed elementary moves of monomers between neighbouring sites that preserve chain connectivity and do not allow the chain to cross obstacles. Moves 1, 2, and 3 for an unrestricted two-dimensional random walk on a square lattice are sketched in Fig. 9.32. The corner flip (move 2) crosses obstacles and is therefore forbidden. The two remaining moves (end flips and kink jumps) satisfy topological constraints and therefore are allowed. The Monte Carlo model of chain motion by end flips and kink jumps is called the Evans–Edwards model. Forbidding corner flips leads to a dramatic change of polymer dynamics from free Rouse motion to Rouse motion of a chain confined in a tube (reptation with tube length fluctuations). The only allowed moves for a monomer in the middle of an entangled Evans–Edwards chain are the kink jumps that represent the diffusion of loops in the reptation model (Fig. 9.1). The time in a Monte Carlo simulation is defined by the average number of attempted moves per monomer.

The diffusion coefficient D of the chain [Eq. (8.1)] is calculated by averaging the square of the displacement of the centre of mass of the chain $\langle(\vec{r}_{cm}(t) - \vec{r}_{cm}(0))^2\rangle$ during some long time t over many independent runs and taking its ratio to $6t$ in a three-dimensional simulation ($4t$ in a two-dimensional simulation):

$$D = \lim_{t \gg \tau} \frac{\langle(\vec{r}_{cm}(t) - \vec{r}_{cm}(0))^2\rangle}{6t}. \tag{9.111}$$

The limit in front of the ratio means that the time t has to be much longer than the longest relaxation time of the chain. The resulting diffusion coefficients obtained by Monte Carlo simulation of the Evans–Edwards model of entangled polymers are presented in Fig. 9.33(a). The diffusion coefficient decreases with the number of monomers in the chain. Another quantity that can be extracted from the Monte Carlo simulations of the Evans–Edwards model is the relaxation time of the chain. It can be defined as the characteristic decay time of the time correlation function of the end-to-end vector $\langle R(t)R(0)\rangle \sim \exp(-t/\tau_{rep})$. Figure 9.33(b) presents the results of such simulations.

Both diffusion coefficient and relaxation time obey stronger power laws in chain length than predicted by the simple reptation model [Eqs (9.8) and (9.12)].

$$D \sim N^{-2.5\pm0.1} \quad \tau_{rep} \sim N^{3.5\pm0.1}. \tag{9.112}$$

These stronger molar mass dependences are in excellent agreement with experiments on entangled polymer liquids and the Doi fluctuation model. The important modes missing in the simple reptation model (that uses only the centre of mass diffusion along the contour of the tube) are already included in the Evans–Edwards model. It is important to emphasize that no assumptions about the existence of a confining tube or a primitive path was made in the Evans–Edwards model. The chain knows nothing about such definitions and moves the best way it can within the established rules. In order to verify that the missing modes are indeed related to tube length fluctuations, an even simpler model is discussed next.

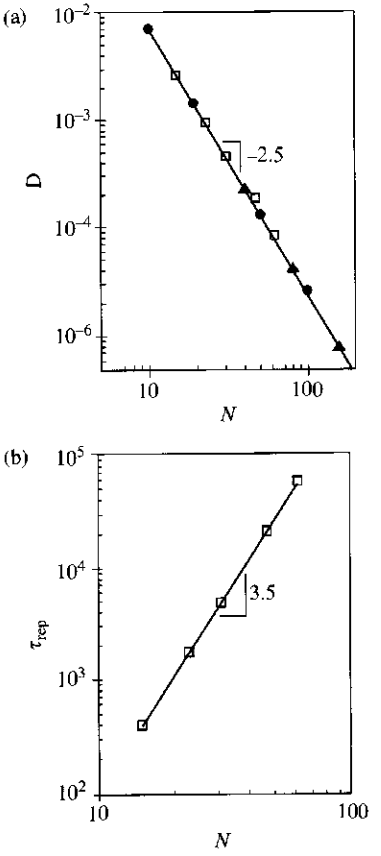

Fig. 9.33
Chain length dependence of diffusion coefficient and relaxation time from Monte Carlo simulations of the Evans–Edwards model. Filled circles are from J. M. Deutsch and T. L. Madden, *J. Chem Phys.* **91**, 3252 (1989). Open squares are from J. Reiter, *J. Chem. Phys.* **94**, 3222 (1991). Filled triangles are from A. Baumgartner *et al.*, *J. Stat. Phys.* **90**, 1375 (1998).

9.6.2.6 Repton model of chain motion in a confining tube

The original reptation model of de Gennes assumes that loops diffuse randomly along the tube. The cumulative effect of the diffusion of loops is the reptation motion. A discretized version of the reptation model is the **repton model** that follows the diffusion of loops along the contour of the tube. The confining tube is represented by a set of neighbouring sites on a one-dimensional lattice. The chain in its tube is coarse-grained to a cluster of reptons on these lattice sites. Each tube section must have at least one repton. Longer loops are represented by additional reptons assigned to the section of the tube from which the loop emanates.

Figure 9.34 displays the mapping of a chain in an array of fixed obstacles to the repton model. Topological obstacles form a lattice with cell size equal to the tube diameter. Roughly N_r monomers are in cell I, between the end of the chain A and the point B where the chain finally leaves cell I for

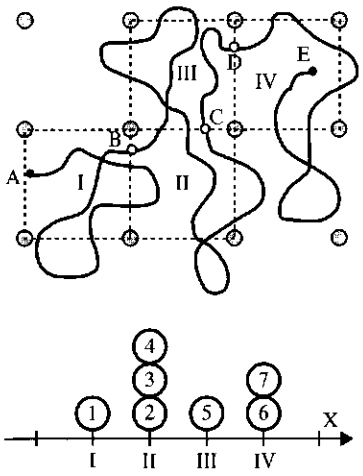

Fig. 9.34
Mapping of a chain in an array of topological entanglements (grey circles) onto a repton model. Cells of the entanglement net, numbered I–IV, are outlined by dotted lines and are mapped onto a one-dimensional lattice. Unentangled loops corresponding to these cells are mapped onto reptons, numbered 1–7, on the lattice sites.

cell II. This is mapped into a single repton at site I of the one-dimensional lattice. The number of monomers assigned to one repton N_r is proportional to, but smaller than, the number of monomers per entanglement strand N_e [see Eq. (9.114)]. Cell II has roughly $3N_r$ monomers in the chain section between points B and C, thereby placing three reptons at site II of the repton model. Similarly, cell III has roughly N_r monomers and cell IV has roughly $2N_r$ monomers, making the number of reptons 1 and 2 at sites III and IV of the one-dimensional lattice, respectively. In this manner, the chain of N monomers in Fig. 9.34 is mapped onto a sequence of $n=7$ reptons that are placed on $K=4$ sites of a one-dimensional lattice. This mapping effectively coarsens the chain to an integer number of connected reptons that each represents a section of the chain with N_r monomers.

The dynamics of a single chain in a tube is mapped onto the dynamics of the cluster of reptons along the one-dimensional lattice. To properly describe chain motion along the tube, the motion of reptons must obey a specific set of rules. The reptons can never vacate a site in the middle of the cluster because the real chain always stays connected. This means that repton 5 cannot move at the particular time step shown in Fig. 9.34 and that repton 1 cannot move to a site to the left of site I (but could move to site II). The order of the reptons must always be preserved, since they represent sequential sections of the chain along the confining tube. Hence, repton 2 could move to site I but not to site III, repton 3 cannot move[10] and repton 4 can move to site III, but not to site I.

At each time step, a repton and the direction of its motion (+ or −) are randomly selected. If the move obeys the simple rules described above (preserving connectivity and order) the move is actually made with probability p. For a chain segment of N_r monomers in Fig. 9.34, corresponding to one repton, there are z possible directions to move, where z is the number of faces in each cell ($z=4$ for a square lattice and $z=6$ for a cubic lattice). For a move between neighbouring occupied sites, there is one and only one direction of motion that will move the repton to a new site, making $p=1/z$. For example, there is one face between cells II and III in Fig. 9.34 for the chain segment, corresponding to repton 4, to go through. All of the other $z-1$ directions effectively do not move the repton because these moves keep the chain in loops associated with the original cell. However, the reptons at the ends of the chain are different. The end sections of the chain have $z-1$ ways to move to new cells, making the probability $p=(z-1)/z$ for a repton to move to an empty site. For example, the last section of the chain, corresponding to repton 7, has $z-1=3$ new cells to choose from on the square lattice ($z=4$) in Fig. 9.34. The relative probability $p=(z-1)/z$ for a repton to move to an empty site controls the average number of occupied sites $\langle K\rangle$ for a cluster of N/N_r reptons:

$$\langle K\rangle = \left(\frac{z-1}{z}\right)\frac{N}{N_r} = \frac{N}{N_e}. \tag{9.113}$$

[10] The chain segments corresponding to repton 3 could be in cell II or in any cell adjacent to cell II, but the mapping to reptons always places repton 3 in cell II.

Thus, each repton contains slightly fewer than N_e monomers:

$$N_r = \frac{z-1}{z} N_e. \tag{9.114}$$

These simple rules for connectivity, order, and motion allow the repton model to be analysed analytically and easily solved numerically. The time dependence of such motion is shown in Fig. 9.35(a) for the extremities of the repton chain. The repton model allows direct visualization of tube length fluctuations.

The stress relaxation modulus is determined by the set of sites on the one-dimensional lattice (cells of the confining tube) that have not been vacated between time 0 (the moment of the step strain) and time t. The number of these 'still occupied' sites is the difference between the furthest propagation of the right end of the cluster to the left $x_R(t)$ (the upper dashed curve in Fig. 9.35(a)) and the furthest propagation of the left end of the cluster to the right $x_L(t)$ (the lower dashed curve in Fig. 9.35(a)). The stress relaxation modulus is proportional to the number of unrelaxed modes of the chain, equal to the number of cells of the original confining tube that have never been vacated. The stress relaxation modulus is proportional to the average fraction of still occupied sites in the repton model:

$$G(t) = G_e \frac{\langle x_R(t) - x_L(t) \rangle}{\langle K \rangle}. \tag{9.115}$$

The ensemble average utilizes only positive values of $x_R(t) - x_L(t)$, and averages over many different chains. All negative values of $x_R(t) - x_L(t)$ are replaced by zeroes. The stress relaxation modulus for a chain of 80 reptons is shown in Fig. 9.35(b).

Viscosity is determined by integration of the stress relaxation modulus [Eq. (7.117)] $\eta = \int G(t)\,dt$. The numerically calculated dependence of viscosity on the number of reptons (for the coordination number $z = 6$) is

$$\eta \sim N^{3.3} \tag{9.116}$$

for the entire range of repton numbers N studied (more than two decades), as shown in Fig. 9.36. Analogous results were obtained in Monte Carlo simulations of the Evans–Edwards model. The fact that the results of the Evans–Edwards model that does not assume the existence of the tube agree with the results of the repton model validates the concept of the confining tube.

The simple reptation model that takes into account only the centre of mass motion along the contour of the tube, but ignores tube length fluctuations, predicts different results than what are obtained from the Evans–Edwards and repton models, as well as from experiments. This implies that tube length fluctuations lead to important corrections to the simple reptation dynamics of the chain in its confining tube. The apparent molar mass exponent in the Evans–Edwards and repton models (as well as in experiments) is larger than the 'pure' reptation value of 3 because real chains abandon their tube *faster* through fluctuations in tube length and

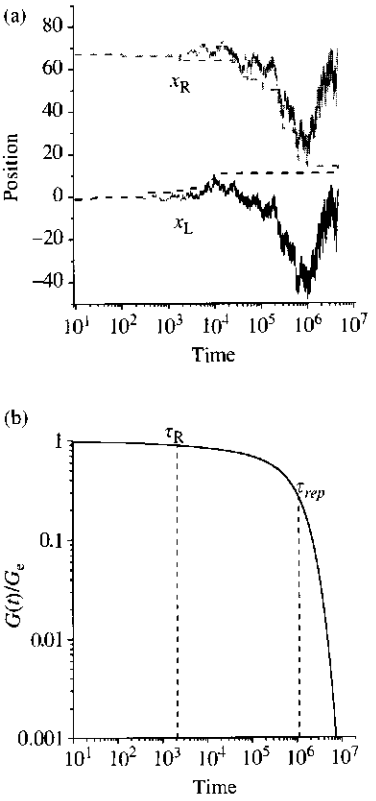

Fig. 9.35
Repton model results for a chain of 80 reptons, courtesy of D. Shirvanyants. (a) Tube length fluctuations represented by the coordinates of the first (lower curve) and the last (upper curve) reptons. The interval $x_R(t) - x_L(t)$ between the dashed lines has always been occupied between times 0 and t. (b) The stress relaxation modulus calculated from ensemble averaging information from part (a) for many runs.

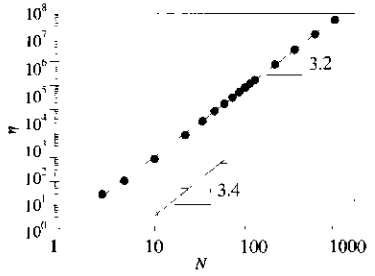

Fig. 9.36
Viscosity of linear polymer calculated from Monte Carlo simulations. Filled circles are repton model data from M. Rubinstein, *Phys. Rev. Lett.* **59**, 1946 (1987), with data range extended by D. Shirvanyants and open squares are Evans–Edwards model data from J. M. Deutsch and T. L. Madden, *J. Chem Phys.* **91**, 3252 (1989).

the effect gets stronger as the chains get shorter. The tube length fluctuations that are evident in Fig. 9.35(a) directly result in the stronger molar mass dependence of viscosity observed in Fig. 9.36.

9.7 Summary of entangled dynamics

Topological constraints, called entanglements, are manifestations of the fact that chains cannot cross one another. There is no first-principles microscopic model of chain entanglements. The most successful existing model of entangled polymers is the Edwards tube model. This model postulates that topological constraints of surrounding chains confine the motion of any long chain to a tube-like region. This postulate separates the complicated many-chain problem of entangled polymer solutions and melts into two simpler problems: the motion of a single chain in its tube and the motion of the tube due to motion of surrounding chains.

The main parameter of the tube model is the tube diameter a, determined by the amplitude of fluctuations that are restricted by the surrounding chains. The tube diameter is related to the number of monomers in an entanglement strand N_e:

$$a \approx b\sqrt{N_e}. \tag{9.117}$$

The tube diameter in an athermal solvent is proportional to, but larger than, the correlation length ξ

$$a(\phi) \approx a(1)\phi^{-0.76} \quad \text{for an athermal solvent.} \tag{9.118}$$

The tube diameter in a θ-solvent is proportional to, but larger than, the distance between binary contacts

$$a(\phi) \approx a(1)\phi^{-2/3} \quad \text{for a } \theta\text{-solvent.} \tag{9.119}$$

The number of monomers in an entanglement strand has practically the same concentration dependence in all solvents $N_e \sim \phi^{-1.3}$. The number of monomers in an entanglement strand is usually determined from the plateau modulus G_e (the value of the stress relaxation modulus at the relaxation time of an entanglement strand τ_e):

$$G_e \approx \frac{kT}{v_0 N_e} \quad \text{for polymer melts.} \tag{9.120}$$

The plateau modulus in entangled polymer solutions has practically the same concentration dependence in all solvents, $G_e \sim \phi^{2.3}$.

The primary mode of motion of a linear chain along its confining tube is reptation, first proposed by de Gennes. Reptation is a snake-like diffusion of a chain, as a whole, along the contour of its tube, with a Rouse curvilinear diffusion coefficient. The relaxation time of the melt is the time it takes the chain to reptate out of its original tube, called the reptation time τ_{rep}. The reptation time and the viscosity of entangled polymers are

predicted by the simple reptation model to be proportional to the cube of polymer molar mass

$$\tau_{rep} \sim \eta \sim M^3. \tag{9.121}$$

The three-dimensional diffusion coefficient is predicted by the simple reptation model to be reciprocally proportional to the square of polymer molar mass:

$$D \sim M^{-2}. \tag{9.122}$$

The probability distribution function of the tube length L for a chain with N monomers is approximately Gaussian, with mean-square fluctuation of the order of the mean-square end-to-end distance of the chain. The tube length fluctuates in time, leading to stronger molar mass dependences of relaxation time, viscosity, and diffusion coefficient resembling experimental observations over some range of molar masses:

$$\tau_{rep} \sim \eta \sim M^{3.4}, \tag{9.123}$$

$$D \sim M^{-2.4}. \tag{9.124}$$

Tube length fluctuations modify the rheological response of entangled polymers. Reptation dynamics adds a $t^{1/4}$ regime to the mean-square monomer displacement that was not present in the free Rouse model. This extra regime is a characteristic signature of Rouse motion of a chain confined to a tube.

Entangled star polymers relax by arm retractions with relaxation times and viscosities exponentially large in the number of entanglements per arm N_a/N_e [Eqs (9.58) and (9.61)]. This leads to exponentially small diffusion coefficients [Eq. (9.62)] for entangled star polymers.

Reptation and tube length fluctuations of surrounding chains release some of the entanglement constraints they impose on a given chain and lead to Rouse-like motion of its tube, called constraint release. Constraint release modes are important for stress relaxation, especially in polydisperse entangled solutions and melts.

Problems

Section 9.1

9.1 The molar mass of an entanglement strand in a PDMS melt at 25 °C is $M_e \cong 12\,000\,\text{g mol}^{-1}$. Estimate the plateau modulus G_e if the density of the PDMS melt at 25 °C is $\rho = 0.97\,\text{g cm}^{-3}$.

9.2 Consider a poly(methyl methacrylate) melt at 140 °C.

(i) Use the information in Table 2.1 to estimate the volume v_0 of a Kuhn monomer at 140 °C.

(ii) Calculate the number of Kuhn monomers per entanglement strand N_e and the molar mass M_e of an entanglement strand, assuming the number of entanglements strands $P_e = 20$ per confinement volume a^3 and compare your estimate with the experimental value $M_e \cong 10\,000\,\text{g mol}^{-1}$.

(iii) What is the tube diameter a of PMMA at 140 °C?

(iv) Calculate the plateau modulus G_e of poly(methyl methacrylate) melt at 140 °C and compare it with the experimental value $G_e \cong 3.1 \times 10^5$ Pa.

Section 9.2

9.3 Consider a PDMS melt with molar mass $M = 6 \times 10^5$ g mol^{-1}. The relaxation time of a Kuhn monomer is $\tau_0 = 10^{-10}$ s. The molar mass of a Kuhn monomer is $M_0 \cong 381$ g mol^{-1} and the molar mass of an entanglement strand is $M_e \cong 12\,000$ g mol^{-1}.

(i) Estimate the reptation time τ_{rep} of chains. How much longer is it than the Rouse time τ_R of the chains?

(ii) Estimate the diffusion coefficient D of these chains if the Kuhn length is $b = 1.3$ nm.

(iii) Estimate the melt viscosity if the plateau modulus of a PDMS melt is $G_e = 2.0 \times 10^5$ Pa.

9.4 Consider a polystyrene melt with molar mass $M = 10^6$ g mol^{-1}.

(i) Estimate the width of the rubbery plateau (τ_{rep}/τ_e) if the molar mass of an entanglement strand $M_e \cong 17\,000$ g mol^{-1} assuming the cubic dependence of the reptation time on the molar mass [Eq. (9.121)].

(ii) Repeat the calculation of (i) using the 3.4 power law dependence of reptation time on the molar mass [Eq. (9.123)].

9.5 Consider an entangled polymer melt of N-mers with monomeric friction coefficient ζ, monomer size b, and tube diameter $a \approx bN_e^{1/2}$ under steady shear with shear rate $\dot{\gamma}$.

(i) Show that the relative three-dimensional velocity of two typical overlapping chains of size $R \approx b\sqrt{N}$ is $v \approx \dot{\gamma}R$.

In order for one chain to move a distance of the order of the tube diameter a, the other chain must move out of its way by the curvilinear distance of the order of the tube length $\langle L \rangle$.

(ii) Demonstrate that the relative velocity of the monomers of two overlapping chains is

$$v_c \approx \dot{\gamma} R \frac{N}{N_e}.$$

The rate of energy dissipation per unit volume $\eta\dot{\gamma}^2$ defines the viscosity η of the melt.

(iii) Calculate the viscosity of an entangled melt using the energy dissipation rate per monomer ζv_c^2.

9.6 Consider a segment s of the tube of an entangled N-mer at time $t = 0$. Assume that the chain moves along its tube by simple diffusion with curvilinear diffusion coefficient D_c.

(i) Show that the probability $\Psi(\xi, t; s)$ that the primitive path of the chain moves the distance ξ during time t, while its ends have not yet reached a segment s of the original tube is

$$\Psi(\xi, t; s) = \frac{2}{\langle L \rangle} \sum_{p=1}^{\infty} \sin\left(\frac{\pi s}{\langle L \rangle} p\right) \sin\left(\frac{\pi(s-\xi)}{\langle L \rangle} p\right) \exp\left(-\frac{p^2 t}{\tau_{rep}}\right), \quad (9.125)$$

where the reptation time is

$$\tau_{rep} = \frac{\langle L \rangle^2}{\pi^2 D_c}.$$

Hint: The probability $\Psi(\xi, t; s)$ is the solution of the diffusion equation

$$\frac{\partial \Psi}{\partial t} = D_c \frac{\partial^2 \Psi}{\partial \xi^2},$$

with initial condition $\Psi(s - \langle L \rangle, 0; s) = \delta(\xi)$ and two boundary conditions $\Psi(s, t; s) = 0 = \Psi(s - \langle L \rangle, t; s)$.

(ii) Show that the probability of the segment s of the original tube (at time $t = 0$) to still be the part of the tube at time t is

$$\psi(s, t) = \sum_{\text{odd } p} \frac{4}{\pi p} \sin\left(\frac{\pi s}{\langle L \rangle} p\right) \exp\left(-\frac{p^2 t}{\tau_{\text{rep}}}\right). \tag{9.126}$$

Hint: In order for segment s to still be part of the tube at time t is should not be reached by the ends of the tube. Therefore, the displacement ξ of the tube during time t should be between $s - \langle L \rangle$ and s. This means that

$$\psi(s, t) = \int_{s-\langle L \rangle}^{s} d\xi \Psi(\xi, t; s).$$

(iii) The normalized stress relaxation modulus for reptation is the fraction of original tube segments that have not been vacated between times 0 and t. Demonstrate that this normalized stress relaxation modulus is

$$\frac{G(t)}{G_e} = \frac{8}{\pi^2} \sum_{\text{odd } p} \frac{1}{p^2} \exp\left(-\frac{p^2 t}{\tau_{\text{rep}}}\right). \tag{9.127}$$

Hint: Note that the normalized stress relaxation modulus for reptation is the probability $\psi(s, t)$ that a segment s is still a part of the tube after time t averaged over all segments s:

$$\frac{G(t)}{G_e} = \frac{1}{\langle L \rangle} \int_0^{\langle L \rangle} ds \, \psi(s, t).$$

9.7 (i) Calculate the upper bound on the error made in replacing the reptation stress relaxation modulus [Eq. (9.20)] by a single exponential:

$$G(t) \cong G_e \exp\left(-\frac{t}{\tau_{\text{rep}}}\right).$$

Hint: The largest error arising from neglecting any term $p = 3, 5, 7, \ldots$ in Eq. (9.20) occurs at $t = 0$.

(ii) Calculate the upper bound on the error made in replacing the reptation stress relaxation modulus [Eq. (9.21)] by a sum of two exponentials:

$$G(t) \cong \frac{9}{10} G_e \left[\exp\left(-\frac{t}{\tau_{\text{rep}}}\right) + \frac{1}{9} \exp\left(-\frac{9t}{\tau_{\text{rep}}}\right)\right].$$

9.8 (i) Demonstrate that the storage modulus of the Doi–Edwards reptation model with stress relaxation modulus given by Eq. (9.20) is

$$G'(\omega) = \frac{8}{\pi^2} G_e \sum_{\text{odd } p} \frac{\omega^2 \tau_{rep}^2}{p^2 (p^4 + \omega^2 \tau_{rep}^2)}, \tag{9.128}$$

while the loss modulus is

$$G''(\omega) = \frac{8}{\pi^2} G_e \sum_{\text{odd } p} \frac{\omega \tau_{rep}}{p^4 + (\omega \tau_{rep})^2}. \tag{9.129}$$

(ii) Calculate the low frequency limiting behaviour of G' and G''.
(iii) Estimate the longest relaxation time as the reciprocal of the frequency at which the low-frequency power laws of G' and G'' cross.
(iv) What is the error in assuming this estimate of the longest relaxation time is τ_{rep}?

Section 9.3

9.9 Determine the number of other chains P_c in the entanglement volume a^3 as a function of concentration in semidilute solution for

(i) an athermal solvent;
(ii) a θ-solvent;
(iii) what happens at low concentrations in a θ-solvent?

9.10 Consider a semidilute polymer solution in a good solvent with excluded volume v. At different length scales an entanglement strand can be viewed as (see Figs 5.5 and 5.6) an ideal chain of g_T monomers in a thermal blob; a self-avoiding walk of g/g_T thermal blobs up to correlation length ξ, where g is the number of monomers in a correlation volume; and an ideal chain of N_e/g correlation blobs on the largest length scale, where N_e is the number of monomers in an entanglement strand. Assume that a certain fixed number of binary contacts is required in a confinement volume a^3.

(i) Estimate the number of binary contacts between two overlapping thermal blobs.
(ii) Assume that the number of binary contacts between two neighbouring correlation volumes is the same as between two overlapping thermal blobs. Estimate the number of monomers in an entanglement strand N_e from the assumption that the total number of contacts between monomers on different chains in the confinement volume a^3 is constant and equal to $(a(1)/b)^3$. Demonstrate that the number of monomers in an entanglement strand N_e in the concentration interval $\phi_e < \phi < \phi^{**}$ is

$$N_e(\phi) \approx N_e(1) \left(\frac{\phi^{**}}{\phi}\right)^{1/(3\nu-1)} (\phi^{**})^{-4/3}. \tag{9.130}$$

(iii) Estimate the entanglement concentration ϕ_e as a function of excluded volume v for the case with $\phi_e < \phi^{**}$. How does the width of unentangled semidilute regime ϕ_e/ϕ^* depend on the excluded volume v?
(iv) How does the number of monomers in an entanglement strand N_e depend on concentration at higher concentrations $\phi > \phi^{**}$?

(v) Determine the condition at which the entanglement concentration is in the concentrated regime $\phi_e > \phi^{**}$?
(vi) Estimate the width of the unentangled semidilute regime for the case with $\phi^{**} < \phi_e$.

9.11 (i) Consider long polystyrene chains in carbon disulphide at 25 °C (athermal solvent). Estimate the correlation length ξ and tube diameter a at volume fractions $\phi = 0.1$ and $\phi = 0.02$.
(ii) Consider long polystyrene chains in cyclohexane at 35 °C (θ-solvent). Estimate the correlation length ξ and tube diameter a at volume fractions $\phi = 0.1$ and $\phi = 0.02$.
(iii) What are the entanglement concentrations ϕ_e of polystyrene with molar mass $M = 500\,000$ in carbon disulphide at 25 °C (athermal solvent) and in cyclohexane at 35 °C (θ-solvent)?

9.12 Explain the length scales over which the reptation, Rouse, and Zimm models describe dynamics in semidilute entangled solutions of linear polymers.

9.13 Consider an entangled solution of N-mers in a good solvent with excluded volume v and Kuhn monomer length b, in a solvent with viscosity η_s at volume fraction $\phi_e < \phi < \phi^{**}$ and derive the following results for

(i) the relaxation time τ_ξ of the polymer strand of size equal to the correlation blob

$$\tau_\xi \approx \frac{\eta_s b^3}{kT}\left(\frac{b^3}{\mathrm{v}}\right)^{3(2\nu-1)/(3\nu-1)} \phi^{-3\nu(3\nu-1)}; \tag{9.131}$$

(ii) the reptation time of the chain

$$\tau_{\mathrm{rep}} \approx \frac{\eta_s b^3}{kT}\frac{N^3}{N_e(1)}\left(\frac{\mathrm{v}}{b^3}\right)^{2/3} \phi^{3(1-\nu)/(3\nu-1)}; \tag{9.132}$$

(iii) the diffusion coefficient of the chain

$$D \approx \frac{kT}{\eta_s b}\frac{N_e(1)}{N^2}\left(\frac{b^3}{\mathrm{v}}\right)^{1/[3(3\nu-1)]} \phi^{-(2-\nu)/(3\nu-1)}; \tag{9.133}$$

(iv) the specific viscosity of the solution

$$\eta_{sp} \approx \left(\frac{\mathrm{v}}{b^3}\right)^{3(2\nu-1)/(3\nu-1)} \frac{N^3}{[N_e(1)]^2}\phi^{3/(3\nu-1)}. \tag{9.134}$$

9.14 Repeat the calculations of Section 9.3 using the dependence of reptation time τ_{rep} on molar mass with power 3.4 instead of 3 and using the values of the scaling exponent $\nu \cong 0.588$ for athermal solvent and $\nu = 1/2$ for a θ-solvent.

(i) Derive the following results for the concentration dependence of the reptation time in athermal solvent and in θ-solvent:

$$\tau_{\mathrm{rep}} \sim \phi^{2.1} \quad \text{for an athermal solvent;} \tag{9.135}$$

$$\tau_{\mathrm{rep}} \sim \phi^{2.9} \quad \text{for a } \theta\text{-solvent.} \tag{9.136}$$

(ii) Derive the following results for the concentration dependence of the diffusion coefficient in athermal solvent and in θ-solvent:

$$D \sim \phi^{-2.4} \quad \text{for an athermal solvent;} \tag{9.137}$$
$$D \sim \phi^{-2.9} \quad \text{for a } \theta\text{-solvent.} \tag{9.138}$$

(iii) Derive the following results for the concentration dependence of viscosity in athermal solvent and in θ-solvent:

$$\eta \sim \phi^{4.5} \quad \text{for an athermal solvent;} \tag{9.139}$$
$$\eta \sim \phi^{5.2} \quad \text{for a } \theta\text{-solvent.} \tag{9.140}$$

9.15 Consider a solution of DNA with molar mass $M = 1.1 \times 10^8$ g mol^{-1} corresponding to $n = 1.64 \times 10^5$ base pairs. Assume that the ionic strength is high enough to ignore excluded volume interactions.

(i) What is the contour length R_{max} of this DNA if $l = 3.4$ Å per base pair?
(ii) What is the overlap concentration if the Kuhn length is $b = 100$ nm (approximately 300 base pairs).
(iii) Assuming that the entanglement concentration $c_e \approx 10c^*$ estimate the contour length of an entanglement strand at $c = 0.5$ mg mL^{-1}. What is the molar mass of an entanglement strand at this concentration?
(iv) Estimate the plateau modulus at the concentration 0.5 mg mL^{-1} at 30 °C.
(v) Estimate the relaxation time and the viscosity of the DNA solution at the concentration 0.5 mg mL^{-1} at 30 °C. Assume the solvent viscosity is $\eta_s = 10^{-3}$ Pa s.

9.16 Consider a solution of polystyrene with molar mass $M = 10^6$ g mol^{-1} in cyclohexane at 35 °C (θ-solvent with viscosity $\eta_s = 7.6 \times 10^{-4}$ Pa s). Estimate the relaxation time, plateau modulus, viscosity, and diffusion coefficient as functions of concentration in semidilute solution.

9.17 Demonstrate that the specific viscosity η_{sp} of entangled solutions in a good solvent can be expressed as a universal function (independent of molar mass and polymer species) of the ratio ϕ/ϕ^* and the number of Kuhn monomers in an entanglement strand in the melt.

9.18 Demonstrate that the ratio of specific viscosity η_{sp} and the 2/3 power of degree of polymerization N of entangled solutions in a$^*\theta$-solvent can be expressed as a universal function of the ratio ϕ/ϕ^* and the number of Kuhn monomers in an entanglement strand in the melt.

9.19 How does the width of the plateau region of the stress relaxation modulus of entangled polymer solutions (the ratio of reptation time τ_{rep} to the Rouse time τ_e of a strand between entanglements) increase with concentration:

(i) for athermal solutions;
(ii) for θ-solutions.

9.20 Consider a linear chain of N Kuhn monomers of length b and monomer volume v_0 in a θ-solvent confined to an infinite cylindrical pore with diameter a and impenetrable walls. What average length $\langle L \rangle$ of the pore is occupied by the chain? Is this average length the same or different for the confining tube of diameter a in a semidilute entangled solution in a θ-solvent? Explain your answer.

9.21 Consider a linear chain of N monomers in a good solvent with excluded volume v.

(i) Find the condition on N for which the onset of entanglement concentration ϕ_e is in concentrated regime above ϕ^{**} if the number of monomers per entanglement strand in a melt is $N_e(1)$.

(ii) What is the concentration dependence of the diffusion coefficient for the case with $\phi_e > \phi^{**}$ in the three different concentration regimes: $\phi^* < \phi < \phi^{**}$; $\phi^{**} < \phi < \phi_e$; $\phi_e < \phi < 1$.

9.22 Consider a small non-adsorbing spherical particle of diameter d diffusing in an entangled polymer solution of linear chains with N Kuhn monomers of length b, with volume fraction ϕ in an athermal solvent with solvent viscosity η_s. Calculate the diffusion coefficient of the particle if its diameter is:

(i) smaller than the correlation length ξ of the solution ($d < \xi$);
(ii) larger than ξ but smaller than the tube diameter a ($\xi < d < a$);
(iii) larger than the diameter a of the confining tube ($d > a$).

Section 9.4

9.23 The primitive path is defined as the shortest line with the same topology as the original chain. Provide a precise definition of what is meant by the 'same topology'.

9.24 The confining tube can be visualized by a long-exposure photograph of a wiggling chain (see Fig. 9.29). What is the shortest time for this photograph to clearly show the entire volume of the tube?

9.25 Consider a chain represented by an unrestricted random walk of N steps on a square lattice, as sketched in Fig. 9.37. Topological constraints are represented by obstacles placed in the middle of each cell. The chain is not allowed to cross any of these obstacles. The primitive path (thick line in Fig. 9.37) is then defined as the shortest walk on the lattice with the same end points and the same topology as the original walk with respect to obstacles.

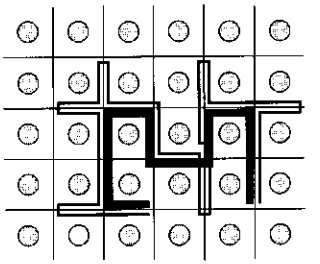

Fig. 9.37
Lattice model of a chain in an array of fixed topological obstacles. Thick line—primitive path.

(i) Show that the average number of segments in a primitive path $\langle K \rangle$ for a N-step random walk on a square lattice (Fig. 9.37) is

$$\langle K \rangle = \frac{N}{2}. \tag{9.141}$$

(ii) Generalize this result to the N-step random walk on a cubic lattice (with coordination number $z = 6$) and show that the average number of segments in a primitive path $\langle K \rangle$ is

$$\langle K \rangle = \left(\frac{z-2}{z}\right) N = \frac{2}{3} N. \tag{9.142}$$

Hint: Note that the primitive path is a non-reversible random walk (with no direct back-folding).

9.26 Imagine that one traditional student and another adventurous student are sent to randomly wander in two different cities (Fig. 9.38). The traditional student is sent to the city, called Squaros with a simple square grid of streets. The adventurous student is sent to a city, called Betheus on a high dimensional planet Cayleus in a recently discovered Universe. The streets in the city Betheus form a Bethe lattice with coordination number $z = 4$. The reason for this layout of streets is to avoid arguments about the shortest way of getting between any two locations in the city (there is only one path).

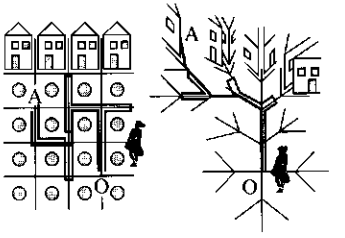

Fig. 9.38
Mapping of a primitive path onto a Cayley tree.

(i) Demonstrate that any sequence of loops and primitive path steps for a random walk in Squaros can be mapped onto a simple random walk in the streets of Betheus.

(ii) Show that loops formed by these two walks are identical, while the length of the primitive path of the walk in Squaros corresponds to the shortest path between the beginning and the end of the walk in Betheus.

9.27 Estimate the probability distribution for an N-step walk of the adventurous student on the streets of Betheus (each step corresponds to a block) with end-to-end distance of K blocks (see Fig. 9.38 and Problem 9.26).

(i) Show that for an arbitrary coordination number z this probability distribution function is

$$p(N,K) \cong \frac{1}{2}\left(\frac{1}{z}\right)^{(N-K)/2}\left(\frac{z-1}{z}\right)^{(N+K)/2}\frac{N!}{((N-K)/2)!((N+K)/2)!}. \tag{9.143}$$

(ii) Derive an approximate expression for the probability distribution function

$$p(N,K) = \sqrt{\frac{\gamma}{2\pi\langle K\rangle}}\exp\left[-\frac{\gamma}{2\langle K\rangle}(K-\langle K\rangle)^2\right], \tag{9.144}$$

where the average end-to-end distance (see Problem 9.25)

$$\langle K\rangle = \frac{z-2}{z}N$$

and the coefficient

$$\gamma = \frac{z(z-2)}{4(z-1)}. \tag{9.145}$$

Hint: Use Stirling's approximation [Eq. (2.75)] and see Section 2.5.

Note that Eq. (9.144) is a probability distribution for a primitive path of an N-step walk to consist of K steps and is an approximate expression for tube length fluctuations.

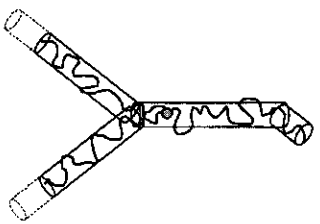

Fig. 9.39
Junction displacement mechanism of star dynamics.

9.28 Consider an alternative mechanism for relaxation of entangled star polymers, studied by Klein. This relaxation process is analogous to reptation of linear chains with the branch point of a star moving up the tube of one of its f arms. All remaining arms follow the branch point along the primitive path of the chosen arm (Fig. 9.39). The tube length for each arm stays close to the equilibrium length.

(i) Show that the free energy cost of the branch point displacement by s/a primitive path steps is

$$F(s) \approx kT(f-2)\frac{s}{a}. \tag{9.146}$$

(ii) Compare this free energy cost with tube length fluctuations and estimate its importance for star polymers with different numbers of arms f.

9.29* Stress relaxation for polydisperse linear chains

Assume that the distribution of relaxation rates $P(\varepsilon)$ in Eq. (8.184) has a sharp cutoff at some characteristic lowest rate ε^* in the form of a stretched exponential with some exponent x. $A(\varepsilon)$ is a weaker pre-exponential function (such as a power law):

$$P(\varepsilon) = A(\varepsilon)\ \exp\left[-(\varepsilon^*/\varepsilon)^x\right].$$

(i) Show that the integral in Eq. (8.184) is dominated by the maximum of the exponential with

$$\varepsilon \approx \left[x\frac{(\varepsilon^*)^x}{t}\right]^{1/(x+1)} \approx \varepsilon^*(\varepsilon^* t)^{-1/(x+1)}$$

with the value of the exponent at this maximum

$$\varepsilon t \approx (\varepsilon^* t)^{x/(x+1)}.$$

Thus, the stress relaxation function can be approximated by a stretched exponential form

$$G(t) = B(t)\exp\left[-(\varepsilon_n t)^{x/(x+1)}\right], \tag{9.147}$$

where $B(t)$ is a slowly varying function and $\varepsilon_n \approx \varepsilon^*$.

(ii) Consider the distribution of chains obtained in a linear condensation polymerization [Eq. (1.66)].

$$n_N \cong \frac{1}{N_n}\exp(-N/N_n).$$

In an unentangled melt, the number density of modes relaxing with rate ε corresponds to the number of chain sections containing K Kuhn segments such that

$$\frac{1}{\varepsilon} = \tau_0 K^2$$

Show that the number density of these sections of K monomers is

$$\left(\frac{N_n}{K}+1\right)\exp(-K/N_n)$$

and therefore the spectrum of relaxation rates for an unentangled melt can be represented by

$$P(\varepsilon)|d\varepsilon| = \left(\sqrt{\varepsilon/\varepsilon_n}+1\right)\exp\left(-\sqrt{\varepsilon_n/\varepsilon}\right)\frac{|d\varepsilon|}{2\tau_0^{1/2}\varepsilon^{3/2}},$$

where the relaxation rate of the N_n-mer is

$$\varepsilon_n = \frac{1}{\tau_0 N_n^2}.$$

(iii) Note that this distribution is of the stretched exponential form $P(\varepsilon) = A(\varepsilon)\ \exp(-(\varepsilon^*/\varepsilon)^x)$ with exponent $x = 1/2$. Show that the exponent in the stretched exponential form of $G(t)$ is 1/3.

9.30* Consider a regular g-generation dendrimer entangled in an array of fixed obstacles. The functionality of each junction point is f and the number of

Kuhn monomers in each linear section N_a is sufficiently large that these sections overlap with many obstacles and entangle extensively. Describe the hierarchy of the relaxation processes of this entangled dendrimer. Estimate the relaxation time and the diffusion coefficient. Assume a harmonic arm retraction potential [Eq. (9.54)].

9.31* Entangled rings

Consider the dynamics of an entangled ring polymer in an array of fixed obstacles [Fig. 9.40(a)]. The ring is not permanently trapped by the obstacles, but is able to diffuse. The ring does not have free ends and, therefore, 'classical' snake-like reptation is not expected for it. An ideal untrapped ring polymer in an array of fixed topological obstacles is an unentangled loop formed by double-folded strands of N_e monomers each, similar to an arm of a star at the moment of complete retraction.

(i) Show that the size of an ideal entangled untrapped ring polymer is

$$R_{ring} \approx b\sqrt[4]{NN_e}. \tag{9.148}$$

Even though the conformation of entangled ring polymers is similar to that of branched polymers, they do not have fixed branch points and therefore rings do not need to invoke the exponentially slow arm retraction process to change their conformations. The reason the arm retraction of branched polymers is an exponentially slow process is that they have to reduce their entropy to form exponentially unlikely unentangled loops. This high price was already paid when the ring polymer was squeezed into the array of fixed topological obstacles and formed conformations with double-folded strands. Motion of the ring polymer from one such conformation to another one does not carry any entropic penalty.

The dynamics of rings is qualitatively different from that of linear chains and branched polymers. Consider any section of a ring, such as the lower part between points A and B [Fig. 9.40(a)]: this section can be treated as a linear polymer consisting of a primitive path and several loops. The corresponding part AB of the branched polymer representation of the ring consists of a trunk [thick line in Fig. 9.40(b)], corresponding to the primitive path of the section, and side branches, corresponding to unentangled loops.

(ii) Demonstrate that the number of monomers n_l along the linear section (trunk) of a ring is proportional to the square root of the total number of monomers n in the section:

$$n_l \approx \sqrt{nN_e}.$$

Thus, most of the monomers are in the side branches, corresponding to the unentangled loops.

Consider the diffusion of kinks (small unentangled loops containing N_e monomers) along the portion AB of the molecule. Diffusion of kinks along large unentangled loops [branches of the equivalent tree in Fig. 9.41(b)] changes the conformation of these loops, but does not contribute significantly to the overall transport of the AB section. Mass transport, corresponding to this diffusion stays within larger unentangled loops, represented by circles in Fig. 9.40(c). These larger unentangled loops act as a reservoir of kinks that move along the primitive path (trunk) of the section AB [shown by arrows in Fig. 9.40(c)].

(iii) Prove that the mean-square displacement of the centre of mass of the section AB along the primitive path during the relaxation time τ_e of an entangled strand is

$$\Delta s_{cm}^2 \approx a^2\left(\frac{N_e}{n}\right)^{3/2}$$

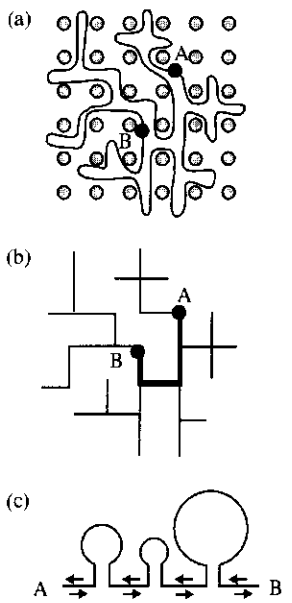

Fig. 9.40
(a) Ring polymer in an array of fixed topological obstacles. (b) Equivalent branched polymer with the 'trunk' of the branched tree between points A and B marked in bold. (c) Branches of the tree of the section AB, represented by circles of different size, act as reservoirs of kinks. Kinks diffuse between these reservoirs along the trunk, as indicated by arrows.

and the curvilinear diffusion coefficient of section AB along its primitive path is

$$D_c(n) \approx \frac{D_0}{N_e}\left(\frac{N_e}{n}\right)^{3/2},$$

where the monomeric diffusion coefficient is $D_0 \approx b^2/\tau_0$.

(iv) Show that the relaxation time of section AB is

$$\tau(n) \approx \tau_e\left(\frac{n}{N_e}\right)^{5/2}.$$

(v) Prove that the relaxation time of the whole ring with N monomers is

$$\tau_{ring} = \tau_e\left(\frac{N}{N_e}\right)^{5/2}. \tag{9.149}$$

(vi) Demonstrate that the diffusion coefficient of an ideal entangled untrapped ring is

$$D \approx D_0\frac{N_e}{N^2}. \tag{9.150}$$

9.32 Show that a stress relaxation modulus of an entangled but non-concatenated melt of rings on the basis of the single chain dynamic modes described in Problem 9.31 is

$$G(t) \approx G_e\left(\frac{t}{\tau_e}\right)^{-2/5}\exp(-t/\tau_{ring}), \tag{9.151}$$

where the relaxation time of a ring is given by Eq. (9.149).

9.33 What is the mean-square curvilinear displacement of monomers in an entangled melt along the confining tube on time scales between the relaxation time of an entanglement strand τ_ξ and the reptation time τ_{rep}? Sketch this time dependence of $\langle[s(t)-s(0)]\rangle^2$.

9.34 Estimate the time dependence of the mean-square displacement of the *centre of mass* of an entangled linear chain in a melt on time scales: (i) $t < \tau_e$; (ii) $\tau_e < t < \tau_R$; (iii) $\tau_R < t < \tau_{rep}$; (iv) $t > \tau_{rep}$.

9.35 Estimate the time dependence of the mean-square displacement of a monomer in an entangled polymer solution.

(i) On time scales $t < \tau_\xi$, where τ_ξ is the relaxation time of a chain section with size equal to the correlation length.
(ii) On time scales $\tau_\xi < t < \tau_e$, where τ_e is the relaxation time of a strand between entanglements.
(iii) On time scales $\tau_e < t < \tau_R$, where τ_R is the Rouse time of the polymer.
(iv) On time scales $\tau_R < t < \tau_{rep}$, where τ_{rep} is the reptation time of the polymer.
(v) On time scales $t > \tau_{rep}$.

9.36 Demonstrate that the loss modulus is predicted to have the following high-frequency behaviour for various models:

(i) $G''(\omega) \sim \omega^{-1}$ for the Maxwell model (if $\omega\tau \gg 1$);
(ii) $G''(\omega) \sim \omega^{-1,4}$ for the Doi fluctuation model (if $1/\tau_R \ll \omega \ll 1/\tau_e$);
(iii) $G''(\omega) \sim \omega^{-1/2}$ for the reptation model (if $\omega\tau_{rep} \gg 1$).

9.37* Calculate the storage and loss moduli corresponding to the Doi fluctuation model with stress relaxation modulus

$$G(t) = G_N^0 \int_0^{2\mu\sqrt{N_e/N}} d\xi \exp\left[-\frac{16\mu^2 N_e}{\xi^4 \tau_{rep} N} t\right] + G_N^0 \int_{2\mu\sqrt{N_e/N}}^1 d\xi \exp\left\{-\frac{t}{[\tau_{rep}(\xi - \mu\sqrt{N_e/N})^2]}\right\}. \quad (9.152)$$

9.38*

(i) Use the approximate expression for the time $\tau(s)$ for retraction of an arm of the entangled star polymer down to length s

$$\tau(s) \approx \tau_{arm} \exp\left[\frac{\gamma'}{2}\left(\frac{s^2}{N_a b^2} - \frac{N_a}{N_e}\right)\right] \quad (9.153)$$

to obtain a simple estimate of the stress relaxation modulus of a star polymer:

$$G(t) \approx G_N^0 \left(1 - \sqrt{1 - \frac{N_e}{N_a}\frac{2}{\gamma'}\ln\frac{\tau_{arm}}{t}}\right) \quad \text{for } t < \tau_{arm} \quad (9.154)$$

(ii) A simple way to obtain the storage modulus of star polymers is to replace t in the stress relaxation modulus by $1/\omega$. Show that the storage modulus is

$$G'(\omega) \approx G_N^0 \left(1 - \sqrt{1 - \frac{N_e}{N_a}\frac{2}{\gamma'}\ln \omega\tau_{arm}}\right).$$

9.39 Consider an entangled monodisperse melt of H-polymers with N_{bb} Kuhn monomers in the central backbone and N_a monomers in each of the four arms, with N_e monomers between entanglements.

(i) Estimate the terminal relaxation time of the H-polymer considering exclusively single-chain modes. Express this terminal time in terms of the single arm retraction time τ_{arm}.
(ii) What is the diffusion coefficient of the H-polymer? Ignore multi-chain contributions to dynamics.
(iii) What is the single-chain expression of the stress relaxation modulus of the H-polymer melt in terms of stress relaxation modulus $G_s(t)$ of individual arms and the reptation contribution of the central backbone?

9.40 Consider a molecule made out of two f-arm stars with N_a Kuhn segments per arm with junction points connected by a central linear strand of N_{bb} Kuhn monomers. This molecule is called a pom-pom polymer. If $f = 1$, this molecule is linear, while the H-polymer corresponds to $f = 2$. Estimate the f-dependence of relaxation time and diffusion coefficient of a melt of monodisperse pom-pom polymers for $f > 1$. Consider only single-chain modes and assume that the coordination number of an entanglement network is z.

9.41 Consider an asymmetric star with one short and two long arms in an array of fixed topological obstacles. The short arm contains N_S Kuhn monomers. The long arms contain N_L Kuhn monomers and the number of Kuhn monomers between entanglements is N_e.

(i) Estimate the relaxation time τ_S of the short arm.
(ii) How many entanglements of the long arms do not have time to disentangle during the relaxation time of the short arm τ_S.

(iii) Estimate the relaxation time of the asymmetric entangled star assuming that the junction point moves along the contour of the tubes of long arms with curvilinear diffusion constant $D_c \approx a^2/\tau_S$.

(iv) What is the diffusion coefficient of this asymmetric star in an array of fixed obstacles?

9.42 Ignoring many-chain effects, relate the stress relaxation modulus $G(t)$ of a comb polymer consisting of q branches with N_a monomers and backbone with N_{bb} monomers to the stress relaxation modulus of a star with N_a monomers per arm.

9.43 Curro–Pincus relaxation in networks

The stress relaxation of polymer networks on long time scales is believed to be due to arm retraction of dangling ends (Fig. 7.7). The polydispersity of dangling ends is determined during crosslinking. Assume the number fraction distribution of linear dangling ends [Eq. (1.52)]

$$n_N = p^N(1-p)$$

with the number-average number of monomers in a dangling end of the order of that of a network strand [Eq. (1.51)] $N_n = 1/(1-p)$. Assume that the contribution of dangling ends to the stress relaxation modulus is proportional to the unretracted part of these chains (similar to star polymers)

$$G(t) - G_\infty \sim \sum_{N=K(t)}^{\infty} \left(\frac{N}{N_e} - \frac{s(t)}{a}\right) n_N.$$

In the above equation, $a \approx bN_e^{1/2}$ is the tube diameter with N_e monomers between entanglements, $K(t)$ is the number of monomers in the dangling chain with retraction time equal to t

$$K(t) = \frac{2}{\gamma'} N_e \ln(t/\tau_1),$$

where we ignore weak (logarithmic) dependence of τ_1 on K [Eq. (9.58)]. All shorter dangling ends have already relaxed by time t. The sum in the equation above is only over longer dangling ends with $s(t)$ the length of the tube that has already been vacated by time t.

(i) Assume a simple logarithmic time dependence of the relaxed part of dangling ends $s(t) \approx a \ln(t/\tau_1)$ and show that the contribution of dangling ends to the stress relaxation modulus of the network decays as a power law in time.

(ii) What is wrong with the assumed time dependence of the relaxed part of dangling ends $s(t)$? What should be the corrected time dependence of the relaxed part of dangling ends? *Hint*: Is it consistent with a parabolic retraction potential [Eq. (9.56)]?

9.44 Entanglement during gelation

Consider vulcanization of a melt of N-mers. At some extent of reaction $\varepsilon = (p - p_c)/p_c$ above the gel point and beyond the Ginzburg point (in the mean-field regime) the network strands become entangled with each other.

(i) Show that the size of the network strand's linear backbone is

$$R_{bb} \approx bN^{1/2}\varepsilon^{-1/2}.$$

Hint: Remember that every network strand is branched, with structure similar to the characteristic polymer at each extent of reaction.

(ii) Elastically effective linear backbones of these network strands are random walks. Show that these linear backbones contain $N_{bb} \approx N/\varepsilon$ monomers.

(iii) In the mean-field region of the gelation transition, the gel fraction is $P_{gel} \approx \varepsilon$ and the number of monomers in a characteristic strand is $N^* \approx N/\varepsilon^2$ including both backbone and side branches. Show that the volume fraction of the backbone is $\phi_{bb} \approx \varepsilon^2$.

(iv) The confining tube diameter in the melt of N-mers before the vulcanization reaction was $a(1)$. Demonstrate that the tube diameter, due exclusively to entanglements between the backbones of the gel, is

$$a \approx a(1)\varepsilon^{-4/3} \tag{9.155}$$

assuming all elastically ineffective side branches act as θ-solvent.

(v) Show that the number of monomers in the linear part of an entanglement strand is

$$N_e \approx \left(\frac{a(1)}{b}\right)^2 \varepsilon^{-8/3}. \tag{9.156}$$

(vi) Demonstrate that the modulus of the network is

$$G \approx \frac{kT}{b[a(1)]^2}\varepsilon^{14/3}. \tag{9.157}$$

Section 9.5

9.45 Tube dilation for a binary blend

Consider a melt consisting of a mixture of entangled long and short chains with degrees of polymerization $N_L \gg N_S > N_e$. Long chains are assumed to be entangled with each other and with short chains. The distance between entanglements of long chains a_L (if short chains are replaced by a θ-solvent) is larger than the average distance between all entanglements in the melt (tube length a_0). Ignore tube length fluctuations and consider only reptation of chains in their tubes with a single mode.

(i) Show the constraint release process for long chains due to motion of short chains takes place on time scale

$$\tau_S \approx \tau_{e0}\left(\frac{N_S}{N_{e0}}\right)^3$$

and the relaxation time of a long-chain strand between neighbouring entanglements with other long chains is

$$\tau_{eL} \approx \tau_S\left(\frac{N_{eL}}{N_{e0}}\right)^2 \approx \tau_S\left(\frac{a_L}{a_0}\right)^4.$$

(ii) Demonstrate that the average number of long-chain entanglements with other long chains is

$$\frac{N_L}{N_{eL}} \approx \frac{N_L}{N_{e0}}\left(\frac{a_0}{a_L}\right)^2$$

and the reptation time of a long chain in a dilated tube of diameter a_L with elementary friction due to constraint release is

$$\tau_{\text{dilated}} \approx \tau_{e0}\left(\frac{N_S}{N_{e0}}\right)^3\left(\frac{N_L}{N_{e0}}\right)^3\left(\frac{a}{a_L}\right)^2.$$

(iii) Prove that this reptation of long chains in dilated tubes is faster than their reptation τ_L in thin (original) tubes for relatively short surrounding chains

$$\frac{N_S}{N_{e0}} < \left(\frac{a_L}{a_0}\right)^{2/3}.$$

(iv) Recall the dependence of the number of monomers in an entanglement strand N_e on polymer concentration ϕ [Eq. (9.36)]:

$$N_e \sim \phi^{-\alpha},$$

where $\alpha = 4/3$ in θ-solvents. Polymer concentration ϕ is replaced in the tube dilation models by the fraction of unrelaxed chains. Show that the ratio of dilated and bare tube diameters is

$$\frac{a_L}{a_0} \approx \phi_L^{-\alpha/2}$$

and reptation in the dilated tubes is effective for small numbers of entanglements in the short chains:

$$\frac{N_S}{N_{e0}} < \phi_L^{-\alpha/3}.$$

(v) Demonstrate that for this inequality to be valid and for the volume fraction of long chains to be above the entanglement onset of long chains, it is necessary that the number of entanglements in the long chains is larger than the cube of the number of entanglements in the short chains:

$$\frac{N_L}{N_{e0}} > \left(\frac{N_S}{N_{e0}}\right)^3. \tag{9.158}$$

(vi) The dilated tube is effective as long as the lifetime of the corresponding constraint (the reptation time of the long chains) is longer than the Rouse time of constraint release of the corresponding entanglement strands $\tau_{eL} < \tau_L$. Prove that tube dilation can be observed for intermediate volume fraction ϕ_L of long chains in the melt:

$$\left(\frac{N_L}{N_{e0}}\right)^{-1/\alpha} < \phi_L < \left(\frac{N_S}{N_{e0}}\right)^{-3/\alpha}.$$

(vii) Estimate the composition range for the tube dilation approximation for a binary blend of long chains containing $N_L/N_e = 300$ entanglements and short chains containing $N_s/N_e = 5$ entanglements. Assume that the number of monomers in an entanglement strand N_e decreases with volume fraction ϕ as $N_e \sim \phi^{-4/3}$.

9.46 Tube dilation for a power law polydispersity

For a chain to be confined to a dilated tube, the mean-square displacement $\langle [r_\perp(t) - r_\perp(0)]^2 \rangle$ of its monomers in the direction perpendicular to the contour of the tube has to be restricted by the mean-square tube diameter $[a(t)]^2$.

Consider a melt with volume fraction of N-mers described by a power law distribution

$$\phi(N) \approx N^{-\beta} \quad \text{for } N > N_{e0}$$

with $\beta > 2$. Assume single-mode reptation of chains in their tubes.

(i) Show that polymers relaxing at time t have degree of polymerization

$$N(t) \approx N_e \left(\frac{t}{\tau_e}\right)^{1/3}.$$

Assume that all shorter chains with $N < N(t)$ have already relaxed, while all longer chains with $N > N(t)$ have not relaxed yet.

(ii) Show that the volume fraction of unrelaxed chains decreases with time as

$$\mu(t) \approx \left(\frac{t}{\tau_e}\right)^{(1-\beta)/3}.$$

(iii) Demonstrate that the mean-square diameter of dilated tubes grows with time as

$$\left(\frac{a(t)}{a_0}\right)^2 \approx \frac{N_e(t)}{N_e(0)} \approx \left(\frac{t}{\tau_e}\right)^{\alpha(\beta-1)/3}$$

assuming that all relaxed chains no longer constrain the unrelaxed chains.

(iv) Explain why the Rouse friction of the constraint release process at an entanglement with an N-mer with lifetime $\tau(N)$ is

$$\zeta(N) \approx \frac{kT}{a^2}\tau(N).$$

Prove that the average Rouse friction of the constraint release process at time t due to short N-mers with $N < N(t)$ is

$$\langle \zeta(t) \rangle \approx \begin{cases} kT/a^2[N(t)]^{4-\beta} & \text{for } \beta < 4, \\ \zeta_0 & \text{for } \beta > 4. \end{cases}$$

Hint: Assume that the probability of entanglement with an N-mer is proportional to its volume fraction $\phi(N)$.

(v) Demonstrate that the time dependence of the average friction coefficient is

$$\langle \zeta(t) \rangle \sim \begin{cases} t^{(4-\beta)/3} & \text{for } \beta < 4, \\ t^0 & \text{for } \beta > 4. \end{cases}$$

(vi) Show that the subdiffusive mean-square monomer displacement due to constraint release increases with time as

$$\langle (r(t) - r(0))^2 \rangle \sim \begin{cases} t^{(\beta-1)/6} & \text{for } \beta < 4 \\ t^{1/2} & \text{for } \beta > 4 \end{cases}$$

and therefore the diluting tube is not effective in constraining the chain at all times and for all values of distribution exponent $\beta > 2$.

9.47 Stress relaxation modulus in tube dilation models

There is a conceptual difference between tube dilation and constraint release. The motion of the tube in *constraint release* does not affect single-chain modes inside the tube (reptation and tube length fluctuation). The tube diameter for these single chains in a tube processes is, on average, constant. In contrast, the tube diameter increases with time in the *tube dilation* process and dramatically affects the chain motion within the tube.

(i) Explain why the stress relaxation modulus in tube dilation models can be written as the product of the time-dependent modulus $G_e(t)$ times the single chain in a dilated tube relaxation function $\mu(t)$:

$$G(t) = G_e(t)\mu(t). \tag{9.159}$$

(ii) Demonstrate that the time-dependent modulus can be expressed in terms of the time-dependent number of monomers in an entanglement strand $N_e(t)$ of the dilated tube:

$$G_e(t) \approx \frac{kT}{b^3 N_e(t)}.$$

(iii) Use the dependence of the number of monomers in an entanglement strand $N_e(t)$ on the volume fraction of unrelaxed chains $\mu(t)$ to derive the stress relaxation modulus

$$G(t) \approx G_e(0)[\mu(t)]^{\alpha+1}$$

(iv) The double reptation model assumes that the stress relaxation modulus is

$$G(t) \approx G_e(0)[\mu(t)]^2.$$

What value of α corresponds to the double reptation model? In Section 9.3, we have presented theoretical arguments and experimental data supporting the value $\alpha = 4/3$ in θ-solvents (and melts with ideal chain statistics). What is the expression of the stress relaxation modulus of tube dilation models corresponding to $\alpha = 4/3$?

9.48 Constraint release vs. tube dilation

Consider an isolated long probe P-mer entangled in a melt of shorter N-mers. Tube dilation assumes that as soon as short chains relax, stress in the long P-mer drops to zero. In particular, a version of tube dilation called double reptation imposes an exact symmetry between single chains in a tube and multi-chain processes. As one chain reptates away, stress at a common entanglement (stress point) is relaxed *completely*. In constraint release models, this stress relaxes only partially due to connectivity of the P-mer.

(i) What is the relaxation time of a P-mer in the constraint release models if the reptation time of N-mers is $\tau_{rep}(N)$ and the number of monomers in an entanglement strand in the melt is N_e?
(ii) What is the relaxation time of an isolated long P-mer in the tube dilation model?

9.49 Consider a comb polymer consisting of a backbone with N_{bb} monomers and q branches with N_a monomers and arm retraction time τ_{arm}. Assume that backbones reptate along a dilated tube with entanglements only due to other backbones. Use θ-solvent scaling of the tube diameter with concentration of entangled polymers.

(i) Estimate the stress relaxation time of a comb.
(ii) What is the diffusion coefficient of a comb?
(iii) Relate the stress relaxation modulus $G(t)$ of a comb to the stress relaxation modulus $G_s(t)$ of a star with N_a monomers per arm.

9.50* Enormously long linear chains may have a many-chain effect that retards their reptation. The plateau modulus of an entanglement network is given by Eq. (9.18). In equilibrium there are small fluctuations of stress $\Delta\sigma(r)$

and strain $\Delta\varepsilon(r)$ in entanglement networks with elastic energy of order kT stored in these fluctuations on all length scales r.

(i) If the energy per unit volume due to strain $\Delta\epsilon(r)$ is $G_e[\Delta\epsilon(r)]^2$ show that a typical thermal fluctuation of stress is

$$\Delta\sigma(r) \approx \frac{kT}{\sqrt{v_0 N_e r^3}}.$$

(ii) A polymer segment with n monomers and size $r \approx bn^{1/2}$ entering this pre-stressed network will induce additional strain with energy

$$\Delta F(n) \approx v_0 n \Delta\sigma(r).$$

As long as this energy is less than the thermal energy kT, the segment will average over the whole volume r^3. Show that the largest unperturbed segment has degree of polymerization

$$n^* \approx \frac{b^6}{v_0^2} N_e^2.$$

(iii) Demonstrate that for smaller unperturbed segments the strain energy is

$$\Delta F(n) \approx kT\sqrt{\frac{v_0}{b^3}}\left(\frac{n}{N_e^2}\right)^{1/4} \quad \text{for } n < n^* \approx \frac{b^6}{v_0^2} N_e^2.$$

(iv) Longer segments $n > n^* \approx (b^6/v_0^2)N_e^2$ cause strain energy larger than kT and tend to localize in regions of lower stress with elastic energy proportional to the number of these localization blobs. Show that the strain energy of larger segments is

$$\Delta F(n) \approx kT\frac{n}{n^*} \approx kT\frac{v_0^2}{b^6}\frac{n}{N_e^2} \quad \text{for } n > n^* \approx \frac{b^6}{v_0^2} N_e^2.$$

(v) For a melt of very long chains with degree of polymerization N, the distance between chain ends is large ($r \approx bN^{1/3}$). The section of polymer that needs to penetrate the region devoid of chain ends of size r has a large number of monomers $n \approx N^{2/3}$. Using this result in the strain energy of part (iv) and assuming motion requires overcoming this potenial barrier, derive the following relation for the relaxation time of extremely long linear chains:

$$\tau \sim \exp\left(\text{const.}\frac{v_0^2}{b^6}\frac{N^{2/3}}{N_e^2}\right) \quad \text{for } N/N_e > \frac{b^9}{v_0^3} N_e^2. \tag{9.160}$$

Section 9.6

9.51 In a molecular dynamics simulation, the average value of any quantity A is estimated by averaging over a large number X of molecular dynamics time steps of length δt after a long initial equilibration of the system during Y molecular dynamics time steps:

$$\langle A \rangle = \frac{1}{X}\sum_{k=1}^{X} A(Y+k)\delta t.$$

Is the relative error of this estimate $1/\sqrt{X}$?

9.52 Which of the two computer simulation methods is more efficient in accurately simulating (i) static and (ii) dynamic properties of a single polymer chain in dilute solution: molecular dynamics with explicit solvent or Brownian dynamics without explicit solvent?

9.53 Determine the fraction of attempted moves of an entangled Evans–Edwards chain that actually move a monomer to a new lattice site for the:

(i) square lattice;
(ii) simple cubic lattice;
(iii) repeat both calculations for an unentangled Verdier–Stockmayer chain.

Hint: Write the final answers as functions of N.

9.54 Determine the assignment of reptons by starting at the opposite end of the chain in Fig. 9.34. Explain the differences between these assignments and the original assignments. Will they affect the diffusion coefficient?

9.55 Show that the minimum of the Lennard-Jones potential [Eq. (9.94)] is at $r = 2^{1/6}\sigma$. Find the value of the potential at the minimum.

9.56 (i) Consider particles of mass m interacting via a Lennard-Jones potential with energy parameter ε and distance parameter σ. Construct a time scale out of these parameters, called the Lennard-Jones time τ_{LJ}. What is the physical significance of this time scale?

(ii) Consider an example of a bead representing a Kuhn segment of polystyrene with $m = M_0 = 740\,\mathrm{g\,mol^{-1}}$, $\varepsilon = kT/2$, $\sigma = 18\,\text{Å}$, at temperature $T = 300\,\mathrm{K}$. Calculate the corresponding Lennard-Jones time τ_{LJ} and the molecular dynamics time step $\delta t = 0.01\tau_{LJ}$, thereby taking it to be much smaller than the Lennard-Jones time.

(iii) Estimate the Einstein frequency of a Lennard-Jones crystal by approximating the Lennard-Jones potential near its minimum by a harmonic potential.

9.57 Consider a molecular dynamics simulation of a polymer system consisting of 20 chains, each with 100 Lennard-Jones monomers. Let us assume that the molecular dynamics step $\delta t = 0.01\tau_{LJ}$ takes 10 ms of CPU time, where τ_{LJ} is the Lennard-Jones time (corresponding to the monomeric relaxation time):

(i) How long will it take to relax the system if we assume it is unentangled (obeying Rouse dynamics)?
(ii) How long would it take to obtain a 10% accuracy on an average quantity, such as the longest relaxation time.

9.58 Show that the Metropolis algorithm satisfies detailed balance.

9.59 Estimate the N-dependence of the success rate of a simple Monte Carlo simulation of a self-avoiding walk with $N = 100$ steps. Assume that random walks are generated on a cubic lattice. Each step of the walk is not allowed to step back (they can only go forward, up, down, turn left, or right with equal probability of 1/5). Walks that intersect themselves are discarded.

(i) Make a mean-field estimate of the N-dependence of the success rate.
(ii) Use the number of N-step self-avoiding walks

$$W_{sa}(N) \approx \bar{z}^N N^{\gamma-1},$$

where $\gamma = 7/6$ and $\bar{z} = 4.68$ for a three-dimensional simple cubic lattice, to obtain a better estimate of the success rate. How does this success rate compare with the mean-field estimate?

9.60 Does the probability of successfully overlapping two independent three-dimensional self-avoiding walks increase or decrease with the number of steps N in these walks? Successful overlap of self-avoiding walks avoids direct overlap of any monomers. Answer this question for two different methods of overlapping walks:

(i) Dimerization—the end of one walk is adjacent (or coincides) with the end of the other walk.
(ii) Shared pervaded volume. The centres of mass of the two walks coincide.

Bibliography

Berry, G. C. and Fox, T. G. The viscosity of polymers and their concentrated solutions, *Adv. Polym. Sci.* **5**, 261 (1968).

Binder, K. *Monte Carlo Simulation in Statistical Physics*, 4th edition (Springer, New York, 2002).

Doi, M. *Introduction to Polymer Physics* (Clarendon Press, Oxford, 1996).

Doi, M. and Edwards, S. F. *The Theory of Polymer Dynamics* (Clarendon Press, Oxford, 1986).

Ferry, J. D. *Viscoelastic Properties of Polymers*, 3rd edition (Wiley, New York, 1980).

Graessley, W. W. The entanglement concept in polymer rheology, *Adv. Polym. Sci.* **16**, 1 (1974).

Graessley, W. W. Viscoelasticity and flow in polymer melts and concentrated solutions. In: *Physical Properties of Polymers* (American Chemical Society, Washington, 1984).

McLeish, T. C. B. and Milner, S. T. Entangled dynamics and melt flow of branched polymers, *Adv. Polym. Sci.* **143**, 195 (1999).

Pearson, D. S. Recent advances in the molecular aspects of polymer viscoelasticity, *Rubber Chem. Technol.* **60**, 439 (1987).

$\cong$ numerical approximation, e.g. $\pi \cong 3.14$
$\approx$ approximately equal, e.g. $R \approx bN^{0.588}$
$\sim$ proportional, e.g. $R \sim N^{1/2}$
$\langle \ldots \rangle$ ensemble average, p. 51
! factorial $N! = 1 \times 2 \times 3 \times \ldots \times N$
A entropic part of Flory interaction parameter χ, [dimensionless], p. 145
A_2 second virial coefficient, [m^3 kg^{-2} mol], p. 28
$A_{2,w}$ weight-average second virial coefficient, [m^3 kg^{-2} mol], p. 28
$A_{2,z}$ z-average second virial coefficient, [m^3 kg^{-2} mol], p. 33
A_{ij} second virial coefficient between species i and j, [m^3 kg^{-2} mol], p. 28
a Mark-Houwink exponent, [dimensionless], p. 34
a tube diameter, [m], p. 265
a_n degeneracy, [dimensionless], p. 206
a_T time scale multiplicative shift factor, [dimensionless], p. 335
B coefficient in enthalpic part of Flory interaction parameter χ, [K], p. 145
b Kuhn length, [m], p. 54
b_T modulus scale multiplicative shift factor, [dimensionless], p. 335
C coefficient of molar mass dependence of glass transition, [kg K mol^{-1}], p. 340
C_1, C_2 Mooney-Rivlin coefficients, [kg m^{-1} s^{-2}], pp. 268–269
C_r, C_m scaling factors, [dimensionless], p. 11
C_n, C_∞ Flory's characteristic ratio, [dimensionless], p. 53
c polymer mass concentration, [kg m^{-3}], p. 13
$\mathbf{c}$ speed of light, [m s^{-1}], p. 30
c^* overlap concentration, [kg m^{-3}], p. 13
c_N mass concentration of N-mers, [kg m^{-3}], p. 16
c_n monomer number density, [m^{-3}], p. 100
D size of compression blob, [m], p. 108
D diffusion coefficient, [m^2 s^{-1}], p. 309
$\mathcal{D}$ fractal dimension, [dimensionless], p. 10
D_c curvilinear diffusion coefficient, [m^2 s^{-1}], p. 363
D_R Rouse diffusion coefficient, [m^2 s^{-1}], p. 311
D_Z Zimm diffusion coefficient, [m^2 s^{-1}], p. 313
d space dimension, [dimensionless], p. 9
d diameter of a cylindrical monomer, [m], p. 99
$\vec{E}$ electric field, [$cm^{-1/2}$ $g^{1/2}$ s^{-1}], p. 30

E	monomer-surface interaction energy, [kg m^2 s^{-2}], p. 112
E	Young's modulus, [kg m^{-1} s^{-2}], p. 296
E_a	activation energy for flow, [kg m^2 s^{-2}], p. 337
E_{cr}	critical adsorption energy per monomer, [kg m^2 s^{-2}], p. 112
E_i	incident electric field, [cm$^{-1/2}$ g$^{1/2}$ s^{-1}], p. 30
E_s	scattered electric field, [cm$^{-1/2}$ g$^{1/2}$ s^{-1}], p. 30
E_λ	Young's modulus due to wavelength λ, [kg m^{-1} s^{-2}], p. 334
ΔE	energy of vaporization, [kg m^2 s^{-2}], p. 143
ΔE	energy barrier between trans and gauche minima, [kg m^2 s^{-2}], p. 50
ΔE_A, ΔE_B	energy of vaporization for a molecule of species A or B, [kg m^2 s^{-2}], p. 144
e	elementary charge, [cm$^{3/2}$g$^{1/2}$s^{-1}]
F	Helmholtz free energy, [kg m^2 s^{-2}], p. 71
$\Delta \bar{F}_{mix}$	free energy of mixing per site, [kg m^2 s^{-2}], p. 140
ΔF_{mix}	free energy of mixing, [kg m^2 s^{-2}], p. 164
F_{conf}	confinement free energy, [kg m^2 s^{-2}], p. 108
F_{el}	elastic part of the free energy, [kg m^2 s^{-2}], p. 275
F_{ent}	entropic part of the free energy, [kg m^2 s^{-2}], p. 116
F_{int}	interaction part of the free energy, [kg m^2 s^{-2}], p. 100
$\vec{f}$	force, [kg m s^{-2}], p. 72
f	magnitude of force, [kg m s^{-2}], p. 72
f	functionality, [dimensionless], p. 206
f	free volume, [m^3], p. 337
$f_{j\alpha}$	α-component of the force acting on bead j, [kg m s^{-2}], p. 359
$f(r)$	Mayer f-function, [dimensionless], p. 99
$f_+(N/N^*)$	cutoff function above the gel point, [dimensionless], p. 227
$f_-(N/N^*)$	cutoff function below the gel point, [dimensionless], p. 227
f_E	energetic part of the force, [kg m s^{-2}], p. 254
f_g	free volume at the glass transition, [m^3], p. 338
f_S	entropic part of the force, [kg m s^{-2}], p. 255
G	shear modulus, [kg m^{-1} s^{-2}], p. 259, 282
$G(t)$	stress relaxation modulus, [kg m^{-1} s^{-2}], p. 284
$G'(\omega)$	storage modulus, [kg m^{-1} s^{-2}], p. 291
$G''(\omega)$	loss modulus, [kg m^{-1} s^{-2}], p. 291
$G^*(\omega)$	complex modulus, [kg m^{-1} s^{-2}], p. 292
G_0	Kuhn modulus, [kg m^{-1} s^{-2}], p. 364
G_e	plateau modulus, [kg m^{-1} s^{-2}], p. 266
G_{eq}	equilibrium shear modulus, [kg m^{-1} s^{-2}], p. 284
G_g	glassy modulus, [kg m^{-1} s^{-2}], p. 336
G_M	modulus in the Maxwell model, [kg m^{-1} s^{-2}], p. 283

G_x crosslink contribution to the modulus, [kg m^{-1} s^{-2}], p. 263
g number of monomers in a chain section, [dimensionless], p. 12
g exponent of the end-to-end distribution function, [dimensionless], p. 122
$g(r)$ pair correlation function, [m^{-3}], p. 78
$g_{i\to j}$ probability of attempting a transition between states i and j, [dimensionless], p. 395
g_T number of monomers in a thermal blob, [dimensionless], p. 113
H diameter of a wire, [m], pp. 9, 10
H height of the brush, [m], p. 187
$\bar{I}$ intensity scattered by molecules in a unit volume, [kg m^{-3} s^{-3}], p. 31
I_1, I_2, I_3 strain invariants, [dimensionless], p. 268
I_i intensity of incident wave, [kg s^{-3}], p. 30
I_s intensity of scattered wave, [kg s^{-3}], p. 30
$J(t)$ creep compliance, [kg^{-1} m s^2], p. 288
J_{eq} steady state compliance, [kg^{-1} m s^2], p. 288
$J_R(t)$ recoverable compliance, [kg^{-1} m s^2], p. 290
K optical constant, [m^2 kg^{-2} mol], p. 32
K Mark-Houwink coefficient, [m^3 kg^{-1} (mol kg^{-1})^a], p. 34
K number of chains in the scattering volume [dimensionless], p. 189
K bulk modulus, [kg m^{-1} s^{-2}], p. 296
K number of particles in a simulation box, [dimensionless], p. 392
k Boltzmann constant, [kg m^2 s^{-2} K^{-1}], p. 27
k_p spring constant of mode p, [kg s^{-2}], p. 359
k_H Huggins coefficient, [dimensionless], p. 34
$\mathcal{L}$ Langevin function, [dimensionless], p. 76
L contour length of the primitive path, [m], p. 361
L_a contour length of a tube of an arm, [m], p. 377
L_x, L_y, L_z dimensions of deformed network, [m], p. 256
L_{x0}, L_{y0}, L_{z0} dimensions of undeformed network, [m], p. 256
l length of a bond, [m], pp. 8, 12
l_0 scattering length of solvent, [m], p. 196
l_B Bjerrum length, [m], p. 129
l_D scattering length of deuterated monomers, [m], p. 196
l_H scattering length of hydrogenated monomers, [m], p. 196
l_p persistence length, [m], p. 57
M molar mass, [kg mol^{-1}], p. 2
M_0 molar mass of a Kuhn monomer, [kg mol^{-1}], p. 54
M_e molar mass of an entanglement strand, [kg mol^{-1}], p. 266

M_{mon}	molar mass of a chemical monomer, [kg mol^{-1}], p. 3
M_N	molar mass of N-mer, [kg mol^{-1}], p. 16
M_n	number-average molar mass, [kg mol^{-1}], p. 17
M_s	number-average molar mass of a network strand, [kg mol^{-1}], p. 259
M_w	weight-average molar mass, [kg mol^{-1}], p. 18
M_x	apparent molar mass of a network strand, [kg mol^{-1}], p. 263
M_z	z-average molar mass, [kg mol^{-1}], p. 18
M_{z+k}	$(z+k)$-average molar mass, [kg mol^{-1}], p. 18
m	mass of an object, [kg], pp. 9, 10
m	number of monomers in a chain section [dimensionless], p. 78
m_k	k-th moment of the number fraction distribution, [kg^k mol^{-k}], p. 17
N	degree of polymerization, [dimensionless], p. 2
N^*	characteristic degree of polymerization, [dimensionless], p. 210
N_a	number of Kuhn monomers in an arm of a star, [dimensionless], p. 377
N_A, N_B	number of lattice sites occupied by a molecule A and a molecule B, [dimensionless], p. 138
N_{bb}	number of monomers in a reptating backbone, [dimensionless], p. 381
N_e	number of monomers in an entanglement strand, [dimensionless], p. 266
N_n	number average degree of polymerization, [dimensionless], p. 17
$\mathcal{N}_{Av}$	Avogadro's number, [mol^{-1}], p. 3
N_{comb}	number of monomers in a combined chain, [dimensionless], p. 262
n	number of backbone bonds, [dimensionless], p. 3
n	refractive index of the medium, [dimensionless], p. 31
n	number of scatterers in the scattering volume, [dimensionless], p. 123
n	number of lattice sites in a mixture, [dimensionless], p. 138
n	number of strands in a network, [dimensionless], p. 257
n_0	refractive index of a solvent, [dimensionless], p. 31
$n(p, N)$	number of N-mers per monomer at extent of reaction p, [dimensionless], p. 21
n_A, n_B	number of molecules of species A and B in a mixture, [dimensionless], p. 139
n_N	number fraction of N-mers, [dimensionless], p. 16
$n_{tot}(p)$	number density of molecules, [dimensionless], p. 205
P	overlap parameter, [dimensionless], p. 14
$P(\vec{q})$	form factor, [dimensionless], p. 82

$P_{1d}(N, x)$ 1-dimensional probability distribution function for the N-step walk, [m^{-1}], pp. 69–70

$P_{3d}(N, x)$ 3-dimensional probability distribution function for the N-step walk, [m^{-3}], pp. 69–70

$P_{gel}(p)$ gel fraction, [dimensionless], p. 214

P_e number of overlapping strands in an entanglement volume, [dimensionless], p. 362

P_i probability of being in state i in a Monte Carlo simulation, [dimensionless], p. 395

$P_{sol}(p)$ sol fraction, [dimensionless], p. 214

p extent of reaction, [dimensionless], pp. 20, 213

p dipole moment, [$cm^{5/2}\ g^{1/2}\ s^{-1}$], p. 30

p bond probability, [dimensionless], p. 203

p_c percolation threshold, [dimensionless], p. 203

$p_{i\to j}$ probability of accepting an attempted transition between states i and j, [dimensionless], p. 395

p_ξ crossover mode index in semidilute solutions, [dimensionless], p. 328

Q equilibrium swelling ratio, [dimensionless], p. 275

$Q(\vec{q})$ intermolecular contribution to scattering, [dimensionless], p. 195

q charge, [$cm^{3/2}\ g^{1/2}\ s^{-1}$], p. 74

q magnitude of the scattering wavevector, [m^{-1}], p. 81

$\vec{q}$ scattering wavevector, [m^{-1}], p. 81

$\vec{q}_i$ incident wavevector, [m^{-1}], p. 80

$\vec{q}_s$ scattered wavevector, [m^{-1}], p. 80

R chain size, [m], pp. 8, 11, 13

R ball radius, [m], p. 9

$R_\parallel$ longitudinal size of a chain, [m], p. 108

R_0 root-mean-square end-to-end distance of an ideal chain, [m], p. 54

R_θ Rayleigh ratio, [m^{-1}], p. 31

R_g radius of gyration, [m], p. 60

R_{gl} size of a globule, [m], p. 114

R_h hydrodynamic radius, [m], p. 311

$\vec{R}_i$ position vector of the i-th monomer, [m], p. 60

$\vec{R}_{ij}$ vector connecting monomers i and j, [m], p. 82

$R_{j\alpha}$ α-component of the position vector of monomer j, [m], p. 359

R_{max} contour length, [m], p. 50

$\vec{R}_n$ end-to-end vector, [m], p. 51

$\vec{R}_{cm}$ center of mass position vector, [m], p. 60

R_{ref} reference size of a network strand, [m], p. 275

$\mathcal{R}$ gas constant $\mathcal{R} = \mathcal{N}_A k$, [$kg\ m^2\ s^{-2}\ K^{-1}\ mol^{-1}$], p. 27

r radius of a sphere enclosing an object, [m], pp. 9, 10

r size of a chain section, [m], p. 12

r_{bond}	maximum bond extension in a FENE potential, [m], p. 394
r_{cut}	cut-off distance for the interaction potential, [m], p. 392
$\vec{r}_i$	bond vector, [m], p. 50
S	entropy, [kg m^2 s^{-2} K^{-1}], p. 70
ΔS_A, ΔS_B	entropy change on mixing of a molecule A and a molecule B, [kg m^2 s^{-2} K^{-1}], p. 138
$S_{DD}(\vec{q})$	labeled monomer pair contribution to scattering, [dimensionless], p. 196
$S_{HD}(\vec{q})$	labeled-unlabeled pair contribution to scattering, [dimensionless], p. 196
$S_{HH}(\vec{q})$	unlabeled monomer pair contribution to scattering, [dimensionless], p. 196
ΔS_{mix}	entropy of mixing, [kg m^2 s^{-2} K^{-1}], p. 139
$\Delta \bar{S}_{mix}$	entropy of mixing per site, [kg m^2 s^{-2} K^{-1}], p. 139
$S(\vec{q})$	scattering function, [dimensionless], p. 123
$S(\vec{q}, t)$	dynamic structure factor, [dimensionless], p. 348
s	curvilinear coordinate along the tube, [m], pp. 377, 382
s_p	number of main chain bonds in a persistence segment, [dimensionless], p. 56
T	absolute temperature, [K], p. 27
T_0	reference temperature, [K], p. 335
T_∞	Vogel temperature, [K], p. 338
T_b	temperature of a binodal, [K], p. 150
T_c	critical temperature, [K], p. 152
T_e	entanglement trapping factor, [dimensionless], p. 281
T_g	glass transition temperature, [K], p. 15
$T_{g\infty}$	glass transition temperature of high molar mass polymer, [K], p. 340
T_m	melting temperature, [K], p. 15
T_s	temperature of a spinodal, [K], p. 151
t	time, [s]
U	energy, [kg m^2 s^{-2}], p. 71
$U(r)$	effective interaction potential between a pair of monomers, [kg m^2 s^{-2}], p. 98
U_A	average interaction of an A monomer with one of its neighbors, [kg m^2 s^{-2}], p. 141
U_B	average interaction of a B monomer with one of its neighbors, [kg m^2 s^{-2}], p. 141
$\Delta \bar{U}_{mix}$	energy change on mixing per site, [kg m^2 s^{-2}], p. 142
U_λ	energy of a mode with wavelength λ, [kg m^2 s^{-2}], p. 332
$\vec{u}_i$, $\vec{u}_s$	unit vectors along incident and scattered directions, [dimensionless], p. 80
u_{AA}, u_{AB}, u_{BB}	pairwise interaction energies between adjacent lattice sites, [kg m^2 s^{-2}], p. 141
V	ball volume, [m^3], p. 9

V pervaded volume, [m^3], p. 13
V scattering volume, [m^3], p. 29
V_{dry} network volume in a dry state, [m^3], p. 275
V_{eq} volume of the equilibrium swollen state, [m^3], p. 275
v excluded volume, [m^3], pp. 99, 156–157
v velocity [m s^{-1}]
v_0 lattice site volume, [m^3], p. 137
v_A, v_B molecular volume of species A and B, [m^3], p. 138
v_c relative velocity of two overlapping chains, [m s^{-1}], p. 404
v_{mon} occupied volume of a single chemical monomer, [m^3], p. 13
$W(N, x)$ number of N-step walks with displacement x, [dimensionless], p. 66
w three-body interaction parameter, [m^6], pp. 100, 156
w_N weight fraction of N-mers, [dimensionless], p. 16
$w(p, N)$ weight density of n-mers (per monomer), [dimensionless], p. 214
$\vec{X}_p$ normal mode p, [m], p. 359
$X_{p\alpha}$ α-component of normal mode p, [m], p. 359
x fraction of labeled chains, [dimensionless], p. 189
Z partition function, [dimensionless], p. 75
z chain interaction parameter, [dimensionless], p. 103
z coordination number, [dimensionless], p. 141
Γ adsorbed amount per unit surface area, [m^{-2}], p. 188
Γ decay rate, [s^{-1}], p. 349
$\Lambda_L(t)$ constraint release contribution to stress relaxation modulus of long chains, [dimensionless], p. 390
$\Lambda_S(t)$ constraint release contribution to stress relaxation modulus of short chains, [dimensionless], p. 390
Π osmotic pressure, [kg m^{-1} s^{-2}], pp. 26, 155
$\Delta\varepsilon$ energy difference between trans and gauche minima, [kg m^2 s^{-2}], p. 50
Σ_k k-th moment of the sum, [dimensionless], p. 208
Υ numerical prefactor, [dimensionless], p. 375
Φ Fox-Flory constant, [mol^{-1}], p. 316
$\Psi(\xi, t; s)$ probability for primitive path to move distance ξ in time t, while its end has not reached s, [m^{-1}], p. 404
Ω number of states, [dimensionless], p. 70, 138
Ω_A number of states of a molecule A in a pure A state, [dimensionless], p. 138
Ω_{AB} number of states of a molecule in a homogeneous AB mixture, [dimensionless], p. 138
$\Omega(N, \vec{R})$ number of conformations of N-mer with end-to-end vector $\vec{R}$, [dimensionless], p. 70
α polarizability, [cm^3], p. 30
α angle between scattering wavevector and vector between monomers, [rad], p. 83

α_f thermal expansion coefficient of the free volume, [$m^3\ K^{-1}$], p. 338
γ shear strain, [dimensionless], p. 282
γ, γ' effective dimensionless spring constants, [dimensionless], pp. 375, 377
$\dot{\gamma}$ shear rate, [s^{-1}], p. 283
γ_0 strain amplitude, [dimensionless], p. 290
γ_e, γ_v elastic and viscous shear strains in the Maxwell model, [dimensionless], p. 283
δ dimensionless adsorption energy per monomer, [dimensionless], p. 110
δ exponent of the end-to-end distribution function, [dimensionless], p. 121
δ phase angle, [rad], p. 291
δ, δ_A, δ_B solubility parameter, [$kg^{1/2}\ m^{-1/2}\ s^{-1}$], p. 143
$\delta_{\alpha\beta}$ Kronecker delta, [dimensionless], p. 359
$\delta(t-t')$ Dirac delta function, [dimensionless], p. 359
δt integration time step in a molecular dynamics simulation, [s], p. 393
$\delta\phi$ composition fluctuation, [dimensionless], p. 159
ϵ dielectric constant, [dimensionless], p. 94
ϵ Lennard-Jones interaction parameter, [$kg\ m^2\ s^{-2}$], pp. 118 and 392
ε relative extent of reaction, [dimensionless], p. 209
ε_G Ginzburg relative extent of reaction, [dimensionless], p. 239
ζ friction coefficient, [$kg\ s^{-1}$], p. 309
ζ_0 friction coefficient at the reference temperature T_0, [$kg\ s^{-1}$], p. 335
ζ_{br} effective friction of a branch point, [$kg\ s^{-1}$], p. 381
ζ_p friction coefficient of normal mode p, [$kg\ s^{-1}$], p. 359
ζ_R Rouse friction coefficient of a chain, [$kg\ s^{-1}$], p. 311
ζ_Z Zimm friction coefficient of a chain, [$kg\ s^{-1}$], p. 313
η viscosity, [$kg\ m^{-1}\ s^{-1}$], p. 33
η_M viscosity in the Maxwell model, [$kg\ m^{-1}\ s^{-1}$], p. 283
η_r relative viscosity, [dimensionless], p. 314
η_s solvent viscosity, [$kg\ m^{-1}\ s^{-1}$], p. 33
η_{sp} specific viscosity, [dimensionless], p. 315
$[\eta]$ intrinsic viscosity, [$m^3\ kg^{-1}$], p. 34
θ scattering angle, [rad], p. 29
θ tertahedral angle, [rad], p. 49
θ bending angle, [rad], p. 330
κ exponent of the time dependence of stress relaxation modulus, [dimensionless], p. 351
κ bond strength of the FENE potential, [$kg\ s^{-2}$], p. 394
κ_λ spring constant due to mode with wavelength λ, [$kg\ s^{-2}$], p. 333
λ wavelength of light, [m], p. 29

λ wavelength of mode, [m], p. 331
λ_x, λ_y, λ_z deformation factors, [dimensionless], p. 256
μ number density of elastically effective crosslinks, [m^{-3}], p. 263
μ coefficient in Doi fluctuation model, [dimensionless], p. 384
ν frequency of light, [s^{-1}], p. 30
ν scaling exponent, [dimensionless], p. 104
ν number density of molecules, [m^{-3}], p. 156
ν number density of elastically effective network strands, [m^{-3}], p. 259
ν Poisson's ratio, [dimensionless], p. 296
ξ blob size, [m], p. 72
ξ correlation length, [m], p. 162
ξ_{ads} adsorption blob size, [m], p. 110
ξ_h hydrodynamic screening length, [m], p. 325
ξ_T thermal blob size, [m], p. 113
ρ polymer density, [kg m^{-3}], p. 13
σ grafting density of a brush, [m^{-2}], p. 186
σ shear stress, [kg m^{-1} s^{-2}], p. 282
σ Lennard-Jones length, [m], pp. 118 and 392
σ_{ij} stress tensor, [kg m^{-1} s^{-2}], p. 258
σ_{true} true stress, [kg m^{-1} s^{-2}], p. 258
σ_{eng} engineering stress, [kg m^{-1} s^{-2}], p. 259
σ_λ stress due to mode with wavelength λ, [kg m^{-1} s^{-2}], p. 333
τ turbidity, [m^{-1}], p. 45
τ^* relaxation time of a characteristic cluster, [s], p. 342
τ_0 Kuhn monomer relaxation time, [s], p. 312
τ_{arm} retraction time of an arm, [s], pp. 378, 381
τ_{chain} relaxation time of a chain, [s], p. 327
τ_e Rouse time of an entanglement strand, [s], p. 363
τ_g relaxation time of the fastest stiff mode, [s], p. 334
τ_M relaxation time in the Maxwell model, [s], p. 283
τ_p relaxation time of the p-th mode, [s], p. 319
τ_R Rouse time, [s], p. 311
τ_{rep} reptation time, [s], p. 363
τ_{tube} constraint release relaxation time of the confining tube, [s], p. 388
τ_Z Zimm time, [s], p. 313
φ torsion angle, [rad], p. 49
φ phase difference, [rad], p. 80
ϕ volume fraction, [dimensionless], p. 13
ϕ_0 volume fraction of a gel in a preparation state, [dimensionless], p. 274
$\bar{\phi}$ average volume fraction, [dimensionless], p. 159
ϕ_A, ϕ_B volume fractions of components A and B of the mixture, [dimensionless], p. 137
ϕ_c critical volume fraction, [dimensionless], p. 152

ϕ_e entanglement volume fraction, [dimensionless], p. 369
ϕ_L volume fraction of long chains, [dimensionless], p. 390
ϕ_S volume fraction of short chains, [dimensionless], p. 390
ϕ^* overlap volume fraction, [dimensionless], p. 13
ϕ_θ^* overlap volume fraction for θ-solvents, [dimensionless], p. 172
ϕ^{**} semidilute-concentrated crossover volume fraction, [dimensionless], p. 180
ϕ_{2body} crossover volume fraction in mean-field theory, [dimensionless], p. 181
$\psi(s, t)$ probability for segment s to still be part of the tube at time t, [dimensionless], p. 405
χ Flory interaction parameter, [dimensionless], p. 142
χ_b Flory interaction parameter for a binodal, [dimensionless], p. 150
χ_c critical interaction parameter, [dimensionless], p. 152
χ_s Flory interaction parameter for a spinodal, [dimensionless], p. 151
ω angular frequency, [rad s^{-1}], p. 291

Index

Bold page numbers refer to bold entries in the text, where terms are first introduced. Italic page numbers refer to homework problems.